Spin-charge gauge approach to HTS cuprates: Theory versus Experiments

Thesis submitted for the degree of

Doctor Philosophiæ

Candidate:
Giuliano Orso

Supervisors:
P.A. Marchetti and L. Yu

October 2003

Contents

Introduction

High temperature superconductivity was discovered by Bednorz and Muller (1986) in a complex oxide containing quasi-two dimensional copper-oxygen planes. These CuO_2 sheets are surrounded by layers of other atoms which play the role of charge reservoirs.

Undoped cuprates are well understood half-filled Mott-Hubbard insulators with long range antiferromagnetic order. By chemical substitutions in the charge reservoirs one can add or remove electrons from the CuO_2 planes. This introduces charge carriers into the planes which can delocalize quantum-mechanically.

The interesting point is that this delocalization is a highly collective phenomenon: the moving holes disturb the spin order and as a result the antiferromagnet "distorts" locally and the holes are surrounded by a droplet of quantum spin liquid.

Even in the absence of superconductivity, this new quantum state of matter has little to do with the traditional Fermi-liquid. Detailed experimental investigations in cuprates have shown that the temperature dependences of a variety of physical observables *deviate strongly* from the corresponding Fermi-liquid predictions.

Understanding the normal state properties of these materials is a great challenge for theorists and it may also shed light on the mechanism of High T_c superconductivity.

From the theoretical front there has been several attempts to derive the low-energy properties of cuprates in a unifying frame, but we are far from a theory that is consistent with all the experimental data. It is generally accepted that the $t - J$ model or the Hubbard model (at large U) contain the relevant physics for cuprates.

The main difficulty is that these models are not integrable in two-dimensions so one has to resort to a mean field approximation or other approximation schemes. Since we are interested in energy scales much smaller than the on-site Coulomb repulsion U, the constraint of no doubly occupied sites must be implemented exactly, beyond a mean field approximation.

The gauge theory approach followed in this thesis is an attempt to implement the

Gutzwiller projection in a non perturbative way. Said in words, the idea is that if we "detach" the spin from the electron creating a spinless fermion $\tilde{c}_j$ (holon) and a neutral boson doublet Σ_α (spinon):

$$c_{\alpha j} = \tilde{c}_j \Sigma_{\alpha j} \tag{1}$$

the Pauli principle no longer sees the spin of the particle and it *automatically forbids* any double occupation of a given site.

A useful tool to separate formally the charge from the spin degrees of freedom of the electron comes from Mathematical Physics and is the so called Chern-Simons bosonization. This technique allows one to write action and partition function for the $t - J$ model in a path integral formalism in terms of holon and spinon fields. The price you pay is that $\tilde{c}_j$ and Σ_α appear minimally coupled to additional statistical fields, gauging the global symmetries of the model.

The Chern-Simon representation is *exact* but apparently more complicated than the original one. One hopes nevertheless that the new version is more suitable for a Mean Field approximation, as it already contains the germ of spin-charge separation.

Another important point is that decomposition (1) introduces a fictitious U(1) local symmetry so the ultimate picture is that of holons and spinons scattering against a U(1) gauge field. Following Nagaosa and Lee[41], we assume that this scattering is the main source of dissipation at low energy.

According to the above picture, the role of the gauge field is to *destroy the Luttinger liquid excitations* which means that spin-charge separation is not "complete" in 2D.

It is fair to say that there is no small parameter in the problem, so we must proceed by intuition and test the relevance of the theory *a posteriori* by making some explicit prediction for a given observable and comparing it with experimental data.

In Chapter 1 we discuss the generic (T, δ) phase diagram for hole-doped cuprates, where T is the temperature and δ the density of holes. We focus our attention on the normal, i.e. non superconducting, phase where we identify *two non-Fermi liquid regions* separated by a crossover temperature T^*.

Optimally doped samples and underdoped samples at $T > T^*$ belong to the "Strange Metal phase"; this phase is metallic in nature with the in-plane and out-of-plane resistivities showing linear-in-T behaviour.[1]

---

[1] Also overdoped samples at high temperatures enter this phase.

By decreasing the temperature below T^*, underdoped samples enter the "Pseudogap phase" characterized by a suppression of the density of state near the Fermi level.

The reduction of the scattering rate due to the pseudogap opening affects the in-plane resistivity which becomes *sublinear*. At sufficiently low temperature and in the absence of superconductivity a striking *Metal Insulator Crossover* (MIC) is observed in these samples. On the basis of the experimental data, we reject the interpretation of the MIC as due to disorder-induced localization and we assume that *the MIC is a hallmark of the Pseudogap*.

In the remaining part of this chapter we briefly review some of the anomalies of the normal state of cuprates superconductors.

The spin-charge gauge approach to the $t - J$ model for the "Pseudogap phase" is presented with enough details in Chapter 2. The spinon dynamics is described by a non-linear σ-model with a theoretically derived mass gap $m_s \sim J(\delta|\ln \delta|)^{1/2}$, where J is the exchange integral.

The holon is fermionic with "small" Fermi surfaces ($\epsilon_F \sim t\delta$) (with t as the hopping integral) centered around $(\pm\pi/2, \pm\pi/2)$ in the Brillouin zone and a reduced spectral weight outside the reduced Brillouin Zone. The small Fermi surface picture is due to the presence of a strong *statistical* magnetic field which frustrates the charge motion.

The low energy dynamics for the gauge field is obtained from holon integration and, due to the finite Fermi surface, the propagator for the transverse component A^T exhibits a *Reizer singularity*.

The analogies and differences with respect to the corresponding one-dimensional problem are explicitly quoted.

Chapter 3 is more technical in nature. In the spin-charge approach both holon and spinon are coupled with the gauge field and the in-plane resistivity is controlled by the particle having the shortest scattering time (Ioffe-Larkin rule), the spinon in our case. In order to apply Kubo formula, we evaluate the *spinon current-current correlation function*, averaged over gauge fluctuations.

The out-of-plane motion is a totally different story: only the electron is gauge invariant and hops between the layers, so holon and spinon should recombine first, as first suggested by Anderson[1]. The Green's function for the physical electron, needed to calculate the $c-$axis resistivity and compare with the ARPES data, is given by the product of holon and spinon propagators, averaged over gauge fluctuations. We find that gauge fluctuations are sufficient to bind holon and spinon into a *resonance*

near the Fermi level.

In the evaluation of physical correlators, we use path-integral methods and eikonal approximation, strictly preserving gauge invariance.

Chapter 4 *is the core of this thesis*. The results obtained in the previous chapter are systematically used here to calculate a variety of observables.

The MIC for the in-plane resistivity ρ_{ab} is explained[48] in terms of the competition, in the spinon sector, between the mass gap m_s and gauge fluctuations which account for the dissipative motion of charge carriers. This competition explains also the broad peak found in the spin-lattice relaxation rate for many underdoped samples.

The emergence of a MIC for underdoped superconducting cuprates ($\delta \gtrsim 0.06$) when a strong magnetic field is applied along the $c-$axis to destroy superconductivity, is the key to interpret the *large positive* in-plane magnetoresistance measured in these materials.[50] *These results were derived previously and are reported here for completeness.*

We have subsequently extended our analysis to account for other peculiar properties of the "Pseudogap"[59][60].

The universality curve for the normalised resistivity ρ_n (see Sect. 4.2) noticed in a variety of cuprates (YBCO, LSCO, BSCO, etc.) is a natural consequence of our formula.

Following the approach of Kumar et al.[39], we calculate the thermal behaviour of the out-of-plane resistivity ρ_c in the Pseudogap finding a very good agreement. In particular the theory predicts a marked *roundeed knee* that is indeed seen in the experimental data[17]. We interpret it as due to a change in the temperature dependence of the *electron recombination time*.

Motivated by a very recent experiment [53], we generalize the approach to frequency dependent phenomena and we calculate the (Far Infrared) dynamical in-plane conductivity for strongly underdoped cuprates. We show that at low temperatures the *Drude response disappears* and a *broad peak* emerges at finite frequencies ($\omega \sim 100$ cm^{-1}) which is the analogue of the peak found in temperature dependent DC conductivity for the same sample. The anisotropy in the MIC temperatures along the a and b plane directions found in both the DC [54] and AC [53] conductivities data, is almost certainly related to a corresponding anisotropy in the antiferromagnetic correlation lengths. Neutron scattering experiments[56] have indeed revealed that the magnetic correlation lengths are strongly anisotropic, with $\xi_a > \xi_b$.

In Chapter 5 we extend the gauge approach to describe the "Strange Metal phase". This phase differs from the Pseudogap by the fact that there is no *statistical* magnetic

flux per plaquette so charge carriers delocalize more easily. This causes a change in the dispersion relation which in the absence of gauge fluctuations is simply given by the usual tight binding expression and one finds a *large* Fermi surface, as predicted by electronic structure studies at high temperatures.

The role of holon-induced gauge fluctuations *strengthen up* and leads to metallic resistivities, with ρ_{ab} and ρ_c both *linear-in-T* at high temperatures.

Moreover, the calculated spin lattice relaxation rate at the Cu sites $\left(\frac{1}{T_1 T}\right)$ has the same temperature dependence of the in-plane conductivity. All these features are well supported by experimental data.

Finally, in view of the technical details, the procedures followed to find the optimal spinon configuration for a given holon background in both the Pseudogap and Strange Metal phases are outlined in the Appendix.

Chapter 1

Phenomenology of HTS cuprates

1.1 Introduction and Model Hamiltonian

Cuprate compounds are a class of layered materials sharing the same Perovskite-like structure: the basic unit cell is made up of one or few planes of CuO_2 atoms on top of which there are layers of other atoms (O,Ba,La,Ca, etc.). A typical single layer reference compound is La_2CuO_4 (LSCO) whose simplified unit cell is sketched in Fig. (1.1).

Transport experiments have shown that cuprates are quasi two dimensional systems with the relevant physics taking place in the CuO_2 sheets. The surrounding layers play a secondary role acting as charge reservoirs that control the carriers concentration in the sheets.

The undoped compounds have one hole per Cu atom, occupying the hybridized O-$2p$ and Cu-$3d_{x^2-y^2}$ orbitals. These materials are charge transfer insulators with long range antiferromagnetic order. The insulating nature clearly indicates that electrons in the CuO_2 planes are strongly correlated: the on site Coulomb repulsion freezes completely the charge degrees of freedom and the system becomes purely magnetic.

Doping is obtained via chemical substitution of atoms from the charge reservoirs with other atoms having a different ionization state. In order for the Copper to achieve shell completeness, electrons are then taken out of the CuO_2 planes (hole doping) or donated to them (electron doping). For instance, La_2CuO_4 can be hole-doped by substituting the trivalent La atom in the reservoir with the divalent Sr atom while Nd_2CuO_4 is electron-doped by replacing Nd^{3+} by Ce^{4+} in the charge reservoirs.

Injecting holes, i.e. empty sites, in the CuO_2 sheets we allow electrons to delocalize in order to decrease their kinetic energy and for a given temperature, this determines the metallic or insulating state of the material.
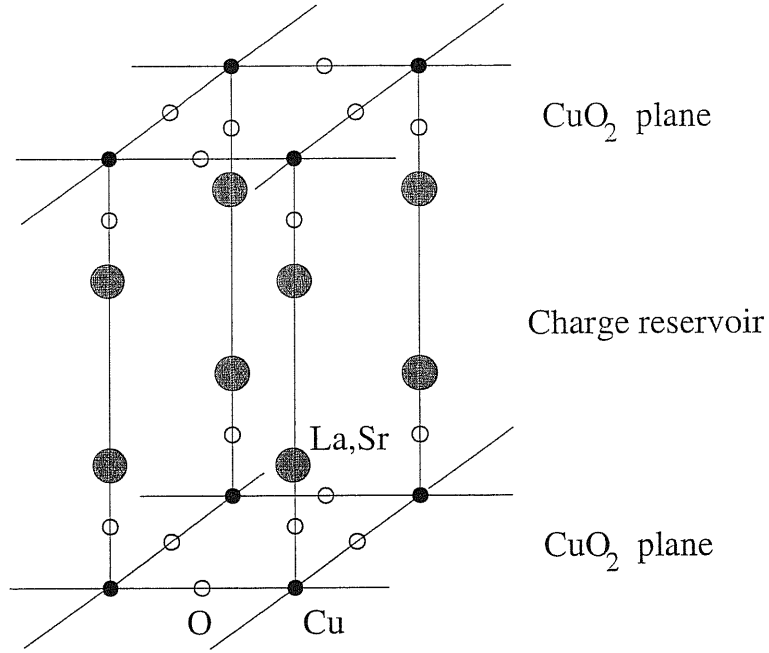
Figure 1.1: Simplified unit cell of the $La_{2-x}Sr_xCuO_4$ crystal.

The simplest model consistent with the above phenomenology is the one band Hubbard model defined in a square lattice:

$$H_{Hubb} = \sum_{<ij>\alpha} -tc^{\dagger}_{i\alpha}c_{j\alpha} + h.c. + U\sum_i n_{i\uparrow} \cdot n_{i\downarrow}, \qquad (1.1)$$

in the strong coupling limit $t \ll U$.

According to this picture, undoped compounds are simply half-filled Mott-Hubbard insulators. This is due to the fact that, to first order in U^{-1}, the Hubbard model becomes equivalent to a Heisenberg model with the spins given by the localized electrons and a (super-)exchange coupling constant $J = 4t^2/U$, leading to a Neel ground state with small quantum fluctuations.

The strong coupling limit of the Hubbard model at finite holes density is the so called $t - J$ model:

$$H_{t-J} = \sum_{<ij>,\alpha} \hat{P}_G(-tc^{\dagger}_{i\alpha}c_{j\alpha} + h.c.)\hat{P}_G + J\sum_{<ij>} (\vec{S}_i \cdot \vec{S}_j - \frac{1}{4}n_i n_j), \qquad (1.2)$$

where $\hat{P}_G$ is the Gutzwiller projector enforcing the constraint of no double occupation of a given site. The relevant parameter for cuprates is $J/t \simeq 0.3$, well inside the strong

correlation regime. This model has been suggested to be relevant for high T_c cuprates by Anderson, in a seminal paper [1] in 1987.

The $t - J$ model is particularly appealing because it emphasizes the competition between the hopping term favoring delocalization and the spin term working against it, because the charge motion anavoidably frustrates the spin background. The need to implement $\hat{P}_G$ in a non perturbative way is at the basis of our approach.

For real materials an additional term $t' \sim 0.2t$ describing hopping between next to nearest neighbor sites is usually added to the effective models (1.1) or (1.2). For simplicity, we omit this term. This approximation should be acceptable if we are mainly concerned with the anomalous thermal properties of cuprates, but of course properties depending on the details of the Fermi surface are completely lost.

1.2   Phase Diagram

Experimentally, all hole-doped High T_c cuprates adhere to the same schematic phase diagram, shown in Fig. (1.2), the interesting parameters being the hole concentration δ measured from half-filling ($\delta = 0$) and the temperature T. This diagram is known to be extremely rich and it's microscopic explanation is one of the most challenging open problems for physicists.

At very low doping $\delta \lesssim 0.02$, the material retains the properties of the parent compound, i.e. it is an insulator with long range antiferromagnetic (AF) order with small quantum fluctuations; this phase is theoretically well understood. The super-conducting phase (SC) occurs in a range of doping roughly given by $0.05 \lesssim \delta \lesssim 0.3$ with T_c reaching a maximum at the optimal doping $\delta = \delta_{opt} \simeq 0.16$.

The boundaries of these two phases are marked with thick lines to emphasize that they should correspond to real 3D phase transitions. The dashed lines, however, represent crossovers from different regimes inside the normal state. In particular the first two regimes dubbed Pseudogap (PG) and Strange Metal (SM) show a variety of observables (resistivity, spin lattice relaxation rate, Hall constant, bulk magnetic susceptibility, etc.) whose temperature dependences deviate strongly from standard Landau Fermi liquid predictions.

Below, we shall review experimental data for a variety of physical observables, putting special emphasis on the anomalous thermal behaviour. The "Pseudogap" is certainly the most interesting region of the phase diagram showing peaks, minima and inflection points at will. For a recent and thorough experimental survey on the Pseudogap please consult the review paper by Timusk and Bratt [2].
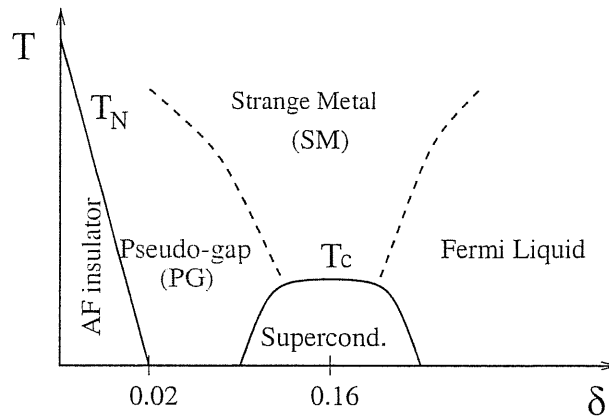
Figure 1.2: Schematic phase diagram of hole-doped cuprates.

Theoretical models attempting to interpret the Pseudogap are very much diversified. Basically, there are two schools of thought.

According to one school, the pseudogap is a "precursor" to superconductivity, i.e., the superconducting state is more fundamental. The other school emphasizes the proximity to the Mott insulating state, considering the pseudogap phase as nothing but doped Mott insulators. Therefore, the normal state is more fundamental, while the superconduting state is derived from this anomalous normal state, as the BCS superconductivity appears when a pairing force is present in the Landau Fermi liquid.

There were several early proposal on the first approach, assuming preformed pairs in the normal state.[3] The underlying idea is that above T_c, the phase of the super-conducting order parameter is no longer rigid which means that coherence and off-diagonal long-range order of the superconductor are lost[4].

The other school of thought was pioneered by P.W. Anderson and collaborators [1][5] leading to the RVB theory. To implement the single occupancy constraint in the frame of spin-charge separation, a gauge theory approach was developed by many authors.[6, 38, 41]

In recent years, new alternative theories emerged such as the quantum critical point scenario[7, 8] and the Z_2 gauge theory of electron fractionalization by Senthil and Fisher et al.[9]

1.3 Outline of Normal State Properties

After more than a decade of intense experimental investigations of high quality materials, we know by now that the anomalous T-dependences of many observables such as resistivities, spin susceptibilities, etc. are quite universal at least in the class of hole-doped cuprates.

Before reviewing some of the peculiar properties of cuprates in the normal state, it may be useful to recall the corresponding Landau Fermi Liquid (LFL) predictions.

Properties of the normal LFL follow from the one-to-one mapping of the low energy eigenstates of the interacting electrons with those of a free Fermi gas. The prerequisite of this assumption is that the volume of the Fermi Surface is conserved and that low energy quasiparticles are sufficiently well defined (both these assumptions are questionable in cuprates).

Direct consequences are the linear specific heat $C_V = \gamma T$ and the temperature independent spin susceptibility χ.

The resistivity is of the form $\rho(T) = a + bT^2$ where the constant term is due to impurities or imperfections always present in a metal and the second term comes from electron-electron scattering which cause quasiparticles to decay with life-time proportional to T^{-2}.

The Hall constant R_H is temperature independent and inversely proportional to the carriers concentration.

1.3.1 In-plane Resistivity

The phase diagram of High T_c cuprate has been largely inspired by the anomalous T dependence of the in plane resistivity.

In Fig. (1.3) we report data of Takagi et al. [10] for LSCO high quality samples. One of the most striking feature is the linear in T behaviour for optimally doped samples over a remarkably wide range of temperatures from just above T_c to near 1000K.

In underdoped and overdoped samples, however, the resistivity at low T is far from linear. A remarkable yet universal feature appearing in strongly underdoped samples is the existence of a minimum in ρ_{ab}, with T_{MIC} located around $50 - 100$K, corresponding to a Metal-Insulator crossover (MIC).[1] It should be noted that for these samples, the estimated $k_F l \lesssim 0.1$ at the MIC, that is the in-plane resistivity is well

---

[1]This crossover has been observed in non-superconducting $Bi_{2+x}Sr_{2-y}CuO_{6\pm\delta}$,[11] and non-superconducting $YBa_2Cu_3O_{7-\delta}$(YBCO)[12, 13] and La-doped Bi-2201.[14].

above the Mott-Regel limit. This means that the MIC cannot be explained in terms of disorder induced localization.

By increasing the Sr content x, the MIC shifts to lower temperature and eventually disappears near T_c, where the resistivity drops abruptly.[2]

According to our interpretation of the phase diagram, *the MIC in ρ_{ab} is the hallmark of the "Pseudogap".*

Another characteristic feature of in-plane resistivity which appear quite universal in underdoped samples is an inflection point, i.e. a maximum of $d\rho/dT$ at $T^* \sim 100 - 200K$; this maximum disappear for higher dopings. At even higher temperature the resistivity exhibits a linear in T behaviour approached from below.

At very low temperature many samples exhibit a second inflection point below which the resistivity diverges approximately logarithmically in T.[15] These two inflection points as a function of the holes content δ limit a portion of the (δ, T) phase diagram that we identify as the "Pseudogap phase"; the temperature T^* then corresponds to the crossover to the "Strange Metal phase" of the diagram.

In overdoped samples ρ_{ab} is always metallic and the linear in T behaviour at large temperatures is instead reached from above, suggesting a possible Fermi Liquid regime with $\rho_{ab}(T) \sim T^\alpha$, $\alpha > 1$ at low T.

---

[2]By applying a strong magnetic field to suppress superconductivity, a MIC has been observed in a number of superconducting samples. In LSCO samples, using a 60 T pulsed magnetic field, the metal to insulator crossover persists up to optimal doping.[15, 16]
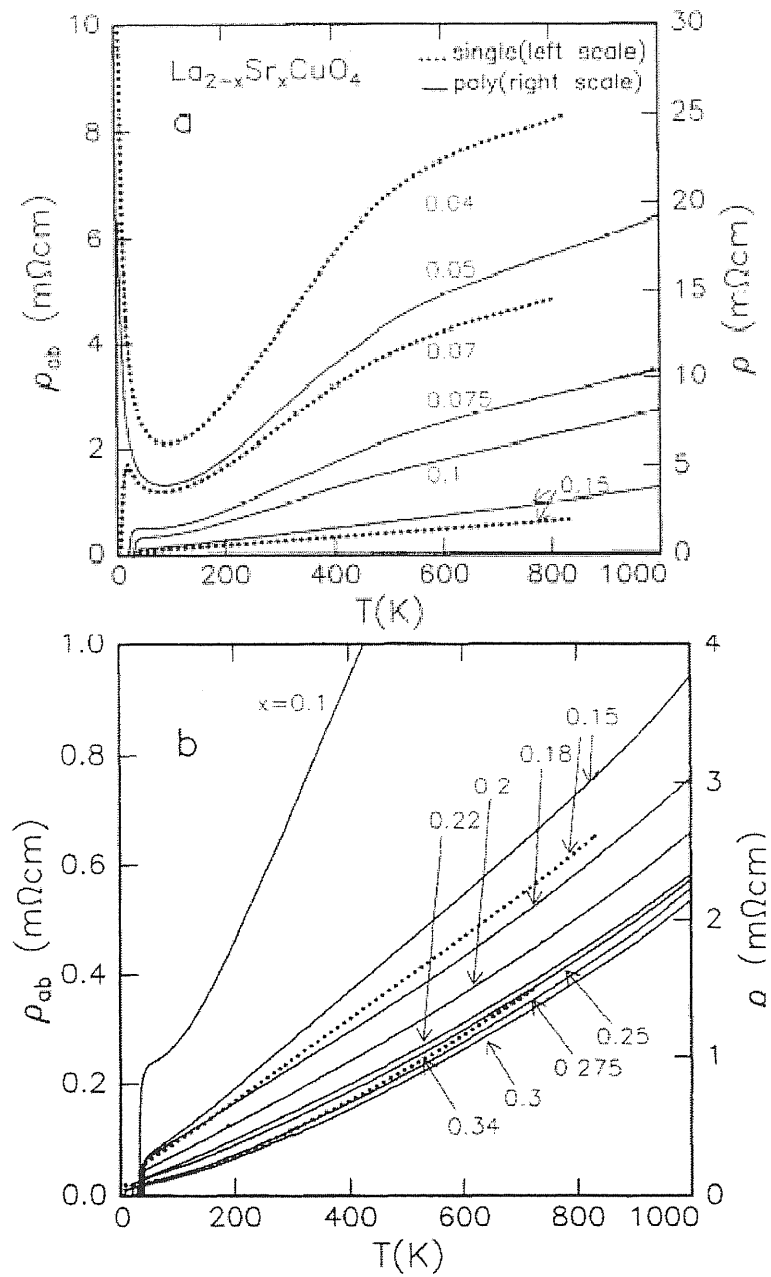
Figure 1.3: In-plane resistivity vs T for LSCO samples with different Sr content x. From Ref.[10]

1.3.2 Out-of-plane Resistivity

The strong anisotropy of cuprate compound is suggested by the c-axis resistivity ρ_c which can be from two to three order of magnitude larger than ρ_{ab}. In particular ρ_c is well above the Mott-Ioffe-Regel limit $(10m\Omega \cdot cm)$.

The out-of-plane motion is incoherent, i.e. the mean free path of charge carriers moving orthogonally to the CuO_2 planes is much smaller than the interlayer distance, suggesting that conductivity along the c-axis in cuprates occurs by interplanar tunneling processes.

The remarkable temperature dependence $\rho_c(T)$ found in cuprate compounds is shown in Fig (1.4). At low temperatures in the "Pseudogap phase" $\rho_c(T)$ is insulating, behaving like T^{-1} with a coefficient essentially material independent. At higher temperatures, it typically develops a *rounded knee* followed by a much slower decrease. Eventually a minimum is reached after which $\rho_c(T)$ grows linearly in T like the in-plane resistivity.

We shall interpret the $T-$linearity of both $\rho_c(T)$ and $\rho_{ab}(T)$ as a hallmark of the "Strange Metal phase". The MIC in the out-of-plane resistivity then arises because ρ_c is insulating in the "Pseudogap" and metallic in the "Strange Metal". The MIC in ρ_{ab}, however, is an intrinsic feature of the Pseudogap.

The coexistence in the PG of metallic in-plane and insulating out-of-plane resistivities is hard to explain within Fermi Liquids theory.

1.3.3 Anisotropy Ratio

The resistivity anisotropy ratio $\rho_c(T)/\rho_{ab}(T)$ increases as T decreases in the "Pseudogap" and tends asymptotically to a doping dependent constant at high temperatures, as shown in Fig. (1.5).

At very low doping and temperature, the system enters a new phase and the anisotropy ratio goes through a maximum and decreases for $T \to 0$.

We also mention that, if superconductivity is suppressed by a sufficiently strong magnetic field, the anisotropy ratio for $x \gtrsim 0.06$ remains finite for vanishing temperatures as shown for instance by Boebinger et al. [16].
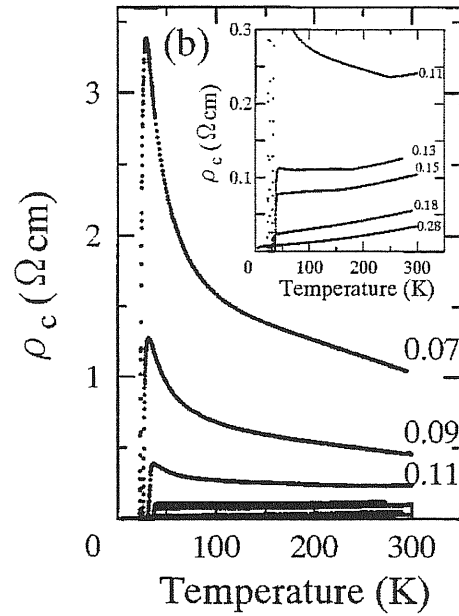
Figure 1.4: Temperature dependence of the out-of-plane resistivity of LSCO single crystals at different Sr content. From Ref.[17]
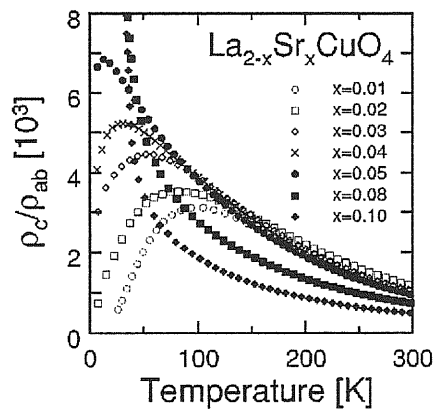
Figure 1.5: Resistivity anisotropy ratio of LSCO single crystals. From Ref.[18]
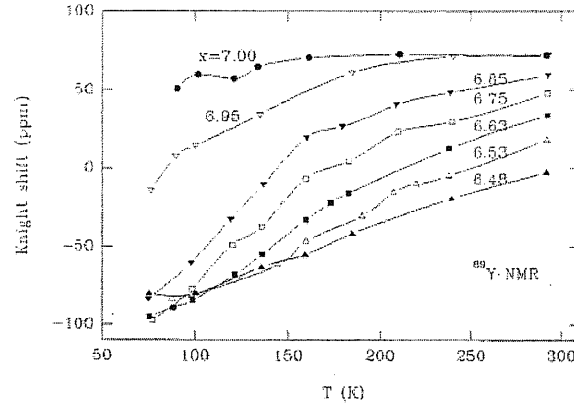
Figure 1.6: Temperature dependence of the ^{89}Y knight shift ΔK for a series of YBCO samples with different oxigen contents x. From Ref.[19]

1.3.4 Knight Shift

The Knight shift K is determined by the real part of the static magnetic susceptibility χ' (at a given nucleus) as the response to an applied magnetic field:

$$K = A\chi'(\omega = 0, \vec{q} = 0), \tag{1.3}$$

where A is the hyperfine constant.

In an ordinary Fermi Liquid K is temperature independent.

Fig. (1.6) shows the planar ^{89}Y Knight shift for a series of YBCO samples with different oxigen contents. We see that $K(T)$ is depressed at low T in underdoped samples due to the opening of a spin gap at $T < T^*$ while it is almost T-independent at optimally doped samples.

In overdoped cuprates $K(T)$ is known to decrease as the temperature increases.

Finally, it has recently been found experimentally by Tallon et al. [20] that the thermal dependence of ^{89}Y Knight shift for $Y_{1-x}Ca_xBa_2Cu_3O_{7-\delta}$ is a universal function of T/T^* up to an overall (doping dependent) scale.

Figure 1.7: Planar ^{63}Cu spin-lattice relaxation rate in optimally doped YBa$_2$Cu$_3$O$_{6.95}$ (squares) and underdoped YBa$_2$Cu$_3$O$_{6.64}$. The pseudogap causes a suppression in the relaxation rate well above T_c. From Ref.[21]

1.3.5 Spin-lattice Relaxation Rate

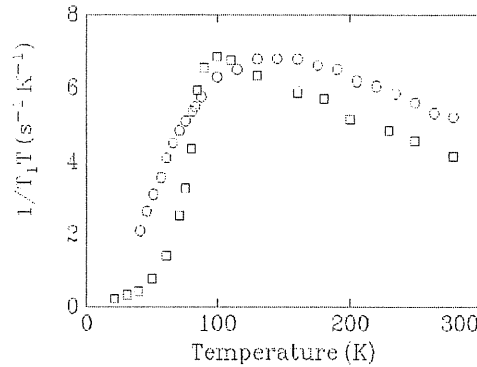The spin-lattice relaxation rate $T_1{}^{-1}$ measured the average spin fluctuation response at a given nucleus to a quasi static magnetic field. It is related to the imaginary part χ'' of the magnetic susceptibility

$$\frac{1}{T_1} = TA^2 \lim_{\omega \to 0} \sum_{\vec{q}} \frac{\chi''(\omega, \vec{q})}{\omega} F(\vec{q}),$$ (1.4)

where $F(\vec{q})$ is a form factor depending on the lattice geometry. Both the Knight shift and the spin relaxation rate are measured in NMR (Nuclear Magnetic Relaxation) experiments.

At the Cu sites, the form factor is strongly peaked around $\vec{q} = \vec{Q}_{AF}$ due to the short range AF order. For Fermi Liquids, the following Korringa law is valid: $T_1{}^{-1} \propto K^2 T$ which implies $\frac{1}{T_1 T}$ =constant.

In Fig. 1.7 we show the thermal dependence of the spin-lattice relaxation rate at ^{63}Cu nuclei for YBCO cuprate compound as found by Warren et al.[21] For optimally doped and slightly overdoped samples, $\frac{1}{T_1 T} \propto \frac{1}{T}$.

For underdoped compounds, this T^{-1} behaviour is reached at relatively high temperatures: by decreasing T, $\frac{1}{T_1 T}$ goes through a broad maximum and then decreases at low T. A curious feature emerging from the experimental data is that the spin-lattice rate $\frac{1}{T_1 T}$ share, qualitatively, the same temperature dependence with the in-plane conductivity $\sigma_{ab}(T)$ both in the Pseudogap and the Strange Metal phases.
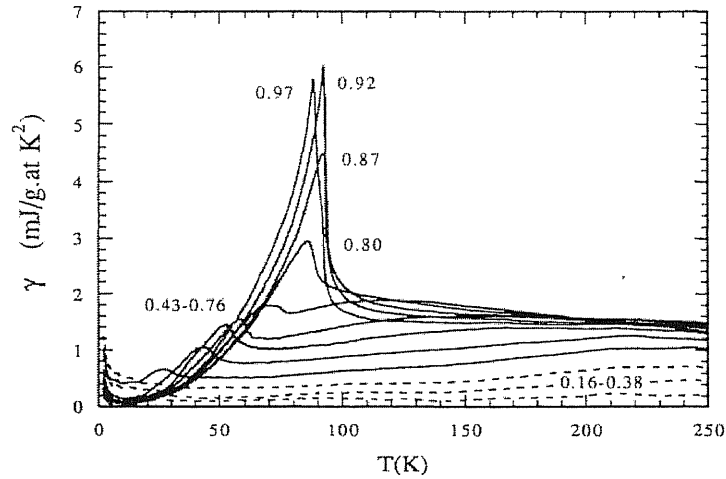
Figure 1.8: Temperature dependence of γ_{el} of $YBa_2Cu_3O_{6+x}$ for different oxigen content. From Ref.[22]

1.3.6 Electronic Specific Heat

The electronic specific heat C_{el} is a bulk thermodynamic quantity determined uniquely for a given material by its spectrum of low lying electronic excitations. It basically counts the number of degrees of freedom active at a given temperature and therefore is an important test for any effective theory for cuprates.

In a usual LFL, the specific heat coefficient $\gamma_{el} = \frac{C_{el}}{T}$ is T-independent and proportional to the density of state at the Fermi Surface. This is due to the fact that only the quasiparticles whose energy is within $k_B T$ from the FS are not frozen by Fermi statistics for $T \ll \epsilon_F$.

In Fig. (1.8) we show the electronic specific heat coefficient as a function of T for YBCO compounds taken from Loram et al.[22]. In the "Strange Metal phase", $\gamma_{el}(T)$ is almost flat with a sudden increase in corrispondence to T_c. It's doping dependence is also very weak.

At low temperatures in the "Pseudogap phase", $\gamma_{el}(T)$ decreases with T reaching a minimum at around $T \sim 50K$ and then increases with an inflection point somewhere between $100 - 200K$. It is important to note that this minimum is not due to superconducting fluctuations as it is present also for non superconducting samples such as LSCO with Sr content $x = 0.03$, see Ref.[23].
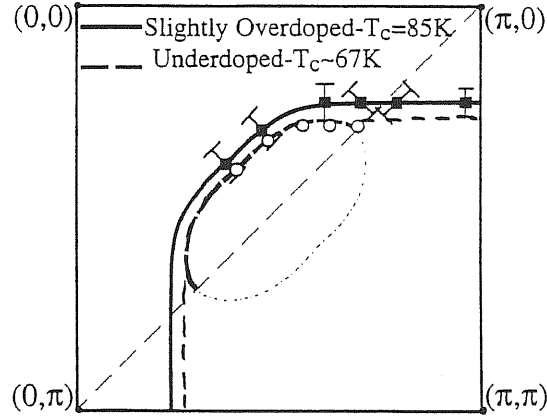
Figure 1.9: Fermi surface of nearly optimal and underdoped Bi-2212 samples. From Ref.[24]

1.3.7 Fermi Surface

Angle-resolved photoemission spectroscopy (ARPES) has been used extensively to obtain direct information about the Fermi Surface of cuprates. Fig. 1.9 shows the Fermi surface of two Bi-2212 samples as found by Marshall et al.[24]: the solid and dashed lines refer to the overdoped and underdoped samples, respectively.

We see that for optimal and overdoped cuprates, the Fermi surface is large, consistent with the Luttinger theorem and with predictions of electronic structure studies at high temperatures. For underdoped samples, the FS develops a a half-pocket like structure centered at the points $(\pm\pi/2, \pm\pi/2)$ in the Brillouin zone.

The current picture of the pseudogap opening leading to a small Fermi surface in underdoped cuprates is as follows[25]: by decreasing the temperature below T^*, a pseudogap first open near $(0,\pi)$ and equivalent points, it then gradually "eats" up the original large Fermi surface, converting it into "pseudogapped" part, eventually leaving only short disconnected arcs around $(\pi/2, \pi/2)$. Finally, these arcs shrink to nodal points of the gap function, and the pseudogap converges to the superconducting gap, with the same d-wave like symmetry. Meanwhile, the quasiparticle peak which is ill-defined in the normal-pseudogap state, becomes well-defined in the superconducting state, like in the typical BCS superconductors. This picture seems to be universal for all classes of cuprate superconductors, and is consistent with all available data on pseudogap phenomena.

Chapter 2

Chern-Simons Gauge Approach

2.1 Introduction

Gauge theories have been succesfully applied to describe the Fractional Quantum Hall Effect in two dimensional systems subject to a strong magnetic field.[26] The general idea is to attach magnetic flux quanta to the real electrons and to rewrite action and partition function for the model in terms of the new composite (fermion+gauge flux) fields. It is important to note that the new particles are anyons, i.e. they may obey a different statistics in virtue of the additional Aharonov-Bohm effect when two of them are interchanged.

The advantage in doing this is that the new action may be more suitable for a Mean Field Approximation, because it may naturally incorporate some non perturbative features.

In cuprates, gauge fields appear because of the locally constrained dynamics. A non perturbative way to implement the Gutzwiller projector $\hat{P}_G$ is through a formal spin-charge decomposition. Assume that the electron field operator on the lattice can be written as a product of a spinless fermion ($\tilde{c}_j$) and a boson spin doublet ($\Sigma_{j\alpha}$):

$$c_{j\alpha} = \tilde{c}_j \Sigma_{j\alpha}. \tag{2.1}$$

The no double occupation constraint is then satisfied by imposing at any site the condition

$$\Sigma_{j\alpha}^* \Sigma_{j\alpha} = 1, \tag{2.2}$$

which implies $c_{j\alpha}^\dagger c_{j\alpha} = \tilde{c}_j^\dagger \tilde{c}_j$. Therefore $\hat{P}_G$ is naturally taken into account by the Pauli principle applied to spinless fermions. Clearly a switch of statistics leading to a spinless boson and a fermion spin doublet (slave-boson theory) does not serve the cause, unless one imposes a hard-core exclusion on the bosons.

It is important to note that in slave-bosons and slave-fermion theories normalization (2.2) is usually replaced by condition $\tilde{c}_j^\dagger \tilde{c}_j + \Sigma_{j\alpha}^* \Sigma_{j\alpha} = 1$ and leads to different Mean field scheme.

Decomposition (2.1) introduces $6 - 4 = 2$ additional degrees of freedom per site; having already fix one by imposing (2.2), the spurious degree of freedom comes from the ambiguity in the spin-charge decomposition (2.1). The following h/s local transformation

$$\tilde{c}_j \rightarrow \tilde{c}_j e^{-i\lambda(j)}, \quad \Sigma_{j\alpha} \rightarrow \Sigma_{j\alpha} e^{i\lambda(j)} \tag{2.3}$$

affects both holon and spinon fields, but leaves the physical electron field c_j unchanged. As a result, the low energy effective actions for the charged fields $\tilde{c}_j$ and $\Sigma_{j\alpha}$ will ultimately describe particles coupled with a U(1) gauge field.

We shall assume that holons and spinons are true excitations and the main difference w.r.t. the 1D case is that such excitations interact strongly with the gauge field. The non trivial *working assumption* is that in Mean Field approximation any interaction non-mediated by the gauge field is neglected.

2.2 C-S Bosonization

A theoretical tool implementing decomposition (2.1) is the so called Chern-Simons bosonization. It basically consists in gauging a global symmetry of the model Hamiltonian by minimally coupling the conserved current to a statistical gauge field V whose dynamics is described by a Chern-Simons action which does not introduce spurious degrees of freedom. The global symmetries of the $t - J$ model (as inherited from the Hubbard model) are:

- U(1) $c_{j\alpha} \rightarrow e^{i\lambda_\alpha} c_{j\alpha}$ λ_α real   **Charge**

- SU(2) $c_{j\alpha} \rightarrow U_{\alpha\beta} c_{j\beta}$ $U \in SU(2)$ **Spin**

Early attempts based upon slave-boson and slave-fermion methods can be easily derived gauging only the U(1) symmetry[27]. Though relatively simple, these theories do not treat the spin degrees of freedom with enough accuracy.

We choose to gauge both charge U(1) and spin SU(2) degrees of freedom simultaneously. More precisely, our theoretical treatment of the t-J model is based on the following theorem[27, 28]:

If we couple the fermions of the t-J model to a $U(1)$ gauge field, B_μ, gauging the global charge symmetry, and to an $SU(2)$ gauge field, V_μ, gauging the global

spin symmetry of the model, and we assume that the dynamics of the gauge fields is described by the euclidean Chern-Simons actions:

$$S_{c.s.}(B) = -\frac{1}{2\pi i} \int d^3x \epsilon^{\mu\nu\rho} B_\mu \partial_\nu B_\rho$$

$$S_{c.s.}(V) = \frac{1}{4\pi i} \int d^3x Tr \epsilon^{\mu\nu\rho} [V_\mu \partial_\nu V_\rho + \frac{2}{3} V_\mu V_\nu V_\rho], \tag{2.4}$$

then the spin-charge gauged model so obtained is exactly equivalent to the original t-J model. In (2.2) $V_\mu = V_\mu^a \sigma_a/2$, $a = 1, 2, 3$, $\mu = 0, 1, 2$ with σ_a as Pauli matrices.

Let us give an idea of the proof of the above theorem for the partition function. We expand the partition function of the gauged model in the first-quantized formalism in terms of worldlines of the fermions. After integrating out the gauge fields, the effect of the coupling to $B_\mu (V_\mu)$ is only to give a factor $e^{-i\frac{\pi}{2}}$ ($e^{i\frac{\pi}{2}}$) for each exchange of the fermion worldlines, so that the two effects cancel each other exactly.

As a case test, this non-abelian bosonization scheme has been applied [29], via a dimensional reduction, to the $t - J$ model in 1D in the limit $J \ll t$: the exact critical exponents of spin and charge correlators, known from Bethe Ansatz and Conformal Field Theory techniques[30], are reproduced in a mean field approximation. The necessary ingredients were the semionic nature of the holon and spinon fields and the fact that the h/s gauge field has no transverse (physical) component in 1D which implies that the two excitations are effectively decoupled, leading to a complete Spin-Charge separation.

We believe that the present approach can be useful to treat the more interesting 2D case. In the remaining part of this chapter we presents the theory with enough details, along the lines of Ref. [28].

2.3   Implementation

We start by writing the grand canonical partition function $Z(\beta, \mu)$ for the $t - J$ model (1.2) in path integral representation:

$$Z(\beta, \mu) = \int \mathcal{D}\Psi \mathcal{D}\Psi^* e^{-S_{t-J}(\Psi, \Psi^*)}, \tag{2.5}$$

with

$$S_{t-J} = \int_0^\beta dx_0 \sum_i \Psi_{j\alpha}^*(\partial_0 - \mu)\Psi_{j\alpha} + \sum_{\langle i,j \rangle} (-t\Psi_{i\alpha}^* \Psi_{j\alpha} + h.c.)$$

$$- \frac{J}{2} \sum_{\langle i,j \rangle} |\Psi_{i\alpha}^* \Psi_{j\alpha}|^2 + \sum_{ij} u_{ij} \Psi_{i\alpha}^* \Psi_{j\beta}^* \Psi_{j\beta} \Psi_{i\alpha}. \tag{2.6}$$

The two body potential u_{ij} is given by:

$$u_{ij} = \begin{cases} \infty & i = j \\ -\frac{J}{4} & i,j \text{ nearest neighbors} \\ 0 & \text{otherwise} \end{cases}$$

with the Gutzwiller projector appearing as an infinite on-site repulsion.

In the Chern-Simons approach the Grassman field $\Psi_{i\alpha}$ representing the physical electron is written as a product of two gauge invariant objects:

$$\Psi_{i\alpha} = e^{-i\int_{\gamma_i} B} H_i^* (Pe^{i\int_{\gamma_j} V})\Sigma_j, \tag{2.7}$$

where H_i^* is a spinless fermion minimally coupled to the U(1) field B and and $\Sigma_{i\alpha}$ a boson spin doublet minimally coupled to the SU(2) field V.[1] In (2.7) the integration in the exponent is taken over an arbitrary path γ_i in the 2D plane, running from site i to a point at ∞ and P is the path ordering operator.

Applying the theorem mentioned in the previous section and taking into account the constraint (2.2), the grand canonical partition function $Z(\beta, \mu)$ can be rewritten as

$$Z(\beta, \mu) = \int \mathcal{D}H\mathcal{D}H^*\mathcal{D}\Sigma_\alpha\mathcal{D}\Sigma_\alpha^*\mathcal{D}B\mathcal{D}Ve^{-S(H,H^*,\Sigma,\Sigma^*,B,V)}\delta(\Sigma^*\Sigma - 1), \tag{2.8}$$

where the Euclidean action $S(H, H^*, \Sigma, \Sigma^*, B, V)$ is given by

$$S(H^*, H, \Sigma^*, \Sigma, B, V) = \int_0^\beta dx^0 \sum_j \left\{ H_j^* \left[\partial_0 - iB_0(j) - \mu \right] H_j + iB_0(j) + \right.$$

$$+(1 - H_j^* H_j)\Sigma_{j\alpha}^* \left[\partial_0 + iV_0(j) \right]_{\alpha\beta} \Sigma_{j\beta} \right\} +$$

$$+ \sum_{\langle ij \rangle} \left\{ \left[-tH_j^* e^{i\int_{\langle ij \rangle} B} H_i \Sigma_{i\alpha}^* \left(Pe^{i\int_{\langle ij \rangle} V} \right)_{\alpha\beta} \Sigma_{j\beta} + H.c. \right] + \right.$$

$$+ \frac{J}{2}(1 - H_i^* H_i)(1 - H_j^* H_j)\left(\left| \Sigma_{i\alpha}^* \left(Pe^{i\int_{\langle ij \rangle} V} \right)_{\alpha\beta} \Sigma_{j\beta} \right|^2 - \frac{1}{2} \right) \right\} -$$

$$+S_{c.s.}(B) + S_{c.s.}(V). \tag{2.9}$$

---

[1]With respect to (2.1) we have applied a particle-hole transformation to the spinless fermion.

By construction, the action (2.9) is invariant under U(1)×SU(2) gauge transformations and under the additional h/s gauge transformation. More explicitely, the U(1) symmetry is given by

$$H_j \rightarrow H_j e^{i\Lambda(j)}, \quad H_j^* \rightarrow H_j^* e^{-i\Lambda(j)}$$
$$B_\mu(x) \rightarrow B_\mu(x) + \partial_\mu \Lambda(x), \quad \Lambda(x) \in \mathbf{R} \tag{2.10}$$

while for the SU(2) spin symmetry we get

$$\Sigma_j \rightarrow g(j)\Sigma_j, \quad \Sigma_j^* \rightarrow \Sigma_j^* g^\dagger(j)$$

$$V_\mu(x) \rightarrow g(x)V_\mu(x)g^\dagger(x) - ig(x)\partial_\mu g^\dagger(x) \quad g(x) \in SU(2). \tag{2.11}$$

Finally, the h/s gauge invariance is given by

$$H_j \rightarrow H_j e^{i\zeta_j}, \quad H_j^* \rightarrow H_j^* e^{-i\zeta_j}$$

$$\Sigma_{j\alpha} \rightarrow \Sigma_{j\alpha} e^{i\zeta_j}, \quad \Sigma_{j\alpha}^* \rightarrow \Sigma_{j\alpha}^* e^{-i\zeta_j}, \quad \zeta_j \in \mathbf{R}. \tag{2.12}$$

2.4 Gauge Fixing

The grand canonical partition function in (2.8) is written as a functional integral over the composite fields and the statistical gauge fields. In order for this formula to make sense, i.e. to give a finite result, we need to gauge fix the U(1)×SU(2) symmetry before integrating over B_μ and V_μ^a and to gauge fix the h/s invariance before integrating over H and Σ_α fields.

Since our task is to find low energy effective actions for holon and spinon variables, we gauge fix the U(1)×SU(2) symmetry and postpone the h/s gauge fixing until integration over the composite fields is required. Our action will therefore possess an additional, fictitious degrees of freedom per site to be fixed.

The U(1) symmetry is gauge fixed by imposing a Coulomb condition on B (from now on $\mu = 1, 2$):

$$\partial_\mu B_\mu = 0. \tag{2.13}$$

To retain the bipartite lattice structure induced by the AF interactions, we gauge–fix the SU(2) symmetry by a "Néel gauge" condition:

$$\Sigma_j = \sigma_x^{|j|} \begin{pmatrix} 1 \\ 0 \end{pmatrix}, \quad \Sigma_j^* = (1, 0)\sigma_x^{|j|}, \tag{2.14}$$

where $|j| = j_1 + j_2$. Then we split the integration over V into an integration over a field $V^{(c)}$, satisfying the Coulomb condition:

$$\partial^\mu V_\mu^{(c)} = 0, \tag{2.15}$$

and its gauge transformations, expressed in terms of an SU(2) valued function $g(x)$

$$V = g^\dagger V^{(c)} g + g^\dagger \partial g. \tag{2.16}$$

The constrained integration over Σ_α, Σ_α^* is now replaced by integration over $g(x)^2$.

Integrating over B_0 which appears linearly in the action (2.9), we obtain

$$B_\mu = \bar{B}_\mu + \delta B_\mu, \quad \delta B_\mu(x) = \frac{1}{2} \sum_j H_j^* H_j \partial_\mu \arg(x - j), \tag{2.17}$$

where $\bar{B}_\mu$ gives rise to a π-flux phase, i.e., $e^{i \int_{\partial p} \bar{B}} = -1$ for every plaquette p.

Integrating over V_0, we find an explicit expression for V_μ^c:

$$V_\mu^{(c)} = \sum_j (1 - H_j^* H_j)(\sigma_x^{|j|} g_j^\dagger \frac{\sigma_a}{2} g_j \sigma_x^{|j|})_{11} \partial_\mu \arg (x - j) \sigma_a, \tag{2.18}$$

where σ_a, $a = x, y, z$ are the Pauli matrices. After the U(1)$\times$SU(2) field being gauge–fixed, the action (2.9) becomes $S = S_1 + S_2$ with

$$S_1(H, H^*, A, U) = \int_0^\beta dx^0 \left\{ \sum_j \left[H_j^* \left(\partial_0 - \mu \right) H_j + i(1 - H_j^* H_j) A_j \right] + \right.$$
$$\left. + \sum_{<ij>} (-t H_i U_{<ij>} H_j^* + h.c.) \right\} \tag{2.19}$$

$$S_2(H, H^*, U) = \int_0^\beta dx^0 \sum_{<ij>} \frac{J}{2}(1 - H_i^* H_i)(1 - H_j^* H_j) \left(|U_{<ij>}|^2 - \frac{1}{2} \right), \tag{2.20}$$

where the lattice gauge fields A_j, $U_{\langle ij \rangle}$ depends on spin and charge variables as:

$$iA_j \sim (\sigma_x^{|j|} g_j^\dagger \partial_0 g_j \sigma_x^{|j|})_{11},$$
$$U_{<ij>} \sim e^{i \int_{<ij>} (\bar{B} + \delta B)} (\sigma_x^{|i|} g_i^\dagger (P e^{i \int_{<ij>} V^{(c)}}) g_j \sigma_x^{|j|})_{11}. \tag{2.21}$$

It is easy to show that A_j is real while $U_{\langle ij \rangle}$ is complex with $|U_{\langle ij \rangle}| \leq 1$.

---

[2]This is consistent because an SU(2) matrix is determined by 3 real parameters and the degrees of freedom per site associated to Σ_α, Σ_α^* fields are exactly 4-1=3

In particular, action S_1 describes a gas of spinless fermions on a square lattice with hopping parameter on the link $\langle ij \rangle$ given by $t|U_{\langle ij \rangle}| \leq t$ in the presence of an e.m. field A_{em} given by

$$A_{em}^0(j) = A_j, \quad e^{i \int_{<ij>} \vec{A}_{em} d\vec{l}} = e^{i \, \mathrm{arg}(U_{\langle ij \rangle})}, \tag{2.22}$$

while action S_2 describes the Hamiltonian of a Heisenberg antiferromagnet with spins situated at the non-empty sites and with link dependent coupling constant $J_{\langle ij \rangle} = J(1 - |U_{<ij>}|^2) \leq J$.

2.5 Optimization

The Mean Field approach to an interacting "quartic" theory goes as follows. First the interacting term is rewritten via a Hubbard- Stratonovich tranformation introducing complex variables χ_{ij}, which play the role of order parameters for the system. The action is now quadratic in the matter fields and we integrate over them to obtain an effective action $S_{eff}(\chi_{ij}, \chi_{ij}{}^*)$.

Via a saddle point equation we find the configuration $\chi_{ij}^m(\chi_{ij}^{m*})$ that minimizes S_{eff}. The low energy action is then given by expanding quadratically S_{eff} around this optimal configuration and taking the continuum limit with the lattice spacing $a \rightarrow 0$.

Unfortunately, we cannot follow this route directly because the statistical gauge fields A_j, $U_{\langle ij \rangle}$ in (2.21) depend on both charge and spin degrees of freedom and no Hubbard-Stratonovich trick can make the actions (2.19) and (2.20) quadratic in H and g.

We can nevertheless calculate the holon dependent spinon configuration $g_j^m(H, H^*)$ which maximizes the action $S = S_1 + S_2$ for a given holon background $\{H_i\}$. We then make the assumption that the hole background is not significantly disturbed under small fluctuations of the spinon variables around the optimal configuration g^m.

This is reminescent of the Born-Oppenheimer approximation for molecules where nuclei are now represented by holons and electrons by spinons and can be justified because the dressed holes are quite heavy as a result of soft spinon fluctuations surrounding the hole in its motion. This is clearly different from the one dimensional case, where spin and charge propagate quite independently and no such screening effects take place.

The best configuration $g^m(\{H_i\})$ is found by a microscopic optimization process of the partition function $\Xi(A, U)$ of holons in a given g background, the latter being

defined as

$$\Xi(A,U) = \int \mathcal{D}H\mathcal{D}H^* e^{-S(H,H^*,A,U)}. \tag{2.23}$$

In order to keep this section readable, we defer the computation of g^m to the Appendix quoting here the result:

$$g_j^m = \bar{g}_j \tilde{g}_j = e^{-\frac{i}{2}\sum_{l\neq j}(-1)^l \sigma_z \arg(l-j)} e^{i\frac{\pi}{2}(-1)^j \sigma_y H_j^* H_j}. \tag{2.24}$$

We then trade the old spin variables g_j for new variables $R_j \in SU(2)$ measuring fluctuations around the optimal configuration through the definition

$$g_j = \bar{g}_j R_j \tilde{g}_j. \tag{2.25}$$

Plugging (2.25) in (2.19) and (2.20), the partition function for the $t - J$ model can be exactly written in terms of the euclidean action $S = S_h + S_s$,

$$S_h = \int_0^\beta dx^0 \Big\{ \sum_j H_j^*[\partial_0 - (\sigma_x^{|j|} R_j^\dagger \partial_0 R_j \sigma_x^{|j|})_{11} - \mu]H_j$$

$$+ \sum_{<ij>} [-tH_j^* e^{-i\int_{<ij>}(\bar{B}+\delta B)} H_i(\sigma_x^{|i|}\tilde{g}_i^\dagger R_i^\dagger P e^{i\int_{<ij>}(\bar{V}+\delta V)} R_j \tilde{g}_j \sigma_x^{|j|})_{11} + h.c.] \Big\} \tag{2.26}$$

$$S_s = \int_0^\beta dx^0 \Big\{ \sum_j (\sigma_x^{|j|} R_j^\dagger \partial_0 R_j \sigma_x^{|j|})_{11}$$

$$+ \sum_{<ij>} \frac{J}{2}(1 - H_i^* H_i)(1 - H_j^* H_j) \Big[|(\sigma_x^{|i|}\tilde{g}_i^\dagger R_i^\dagger P e^{i\int_{<ij>}(\bar{V}+\delta V)} R_j \tilde{g}_j \sigma_x^{|j|})_{11}|^2 - \frac{1}{2} \Big] \Big\}, \tag{2.27}$$

where $\bar{V} = V^{(c)}(g^m)$ is defined in Appendix A and $\delta V = V^{(c)} - \bar{V}$.

Remarks:

1. In (2.26) and (2.27) no approximations have been made. The point of the above analysis is that at low temperatures and near half filling, we expect that the typical spinon configurations are given by *small oscillations* R_j around the optimal distribution given by $R_j^{opt} = 1$.

2. We assume self-consistently that the variables R_j are the slowly varying components of g_j at the lattice scale.

3. The spin-charge separation is up to now only formal: it is imposed as *ansatz* in the Mean Field approximation.

4. The statistical field $\bar{V}$ coming from the SU(2) sector, and depending only on the istantaneous holes distribution, is the key and novel ingredient of our approach w.r.t. other slave boson/slave fermion theories.

2.6   "Improved" Mean Field Approximation

We recall that the electron field operator $\Psi_{i\alpha}$ is reconstructed out of two gauge invariant fields, a spinon field

$$(Pe^{i\int_{\gamma_j} V})\Sigma_j = e^{i\int_{\gamma_j}(\bar{V}^{(c)}+\delta V)}\bar{g}_j R_j \sigma_x^{|j|}\begin{pmatrix} 1 \\ 0 \end{pmatrix},$$

and a holon field

$$e^{-i\int_{\gamma_j}(\bar{B}+\delta B)} H_j.$$

We note that in C-S bosonization, the fields δV and δB appearing in the string γ_j are important to reproduce the semionic statistics of spin and charge gauge invariant fields.

In 1D, the proper account of the statistics of the holon and spinon field operators was crucial[29] for deriving (within the C-S approach) the correct physical properties of the model, known by Luttinger liquid and conformal field theory techniques. However, in 2D we believe the statistics of holons and spinons is less crucial because we expect that they form a bound state, as will be discussed later.

Before taking the continuum limit, we therefore assume $\delta V = 0$, $\delta B = 0$ which considerably simplify the actions (2.26) and (2.27). [3]

We write R_j in CP^1 form as

$$R_j = \begin{pmatrix} b_{j1} & -b_{j2}^* \\ b_{j2} & b_{j1}^* \end{pmatrix}, \qquad b_{j\alpha}^* b_{j\alpha} = 1, \tag{2.28}$$

where $b_{j\alpha}$ is a two component complex field and use it to compute the relevant link variable

$$R_i^\dagger e^{i\int_{<ij>}\bar{V}} R_j = \begin{pmatrix} \alpha_{<ij>}b_{i1}^* b_{j1} + \alpha_{<ij>}^* b_{i2}^* b_{j2} & -\alpha_{<ij>}b_{i1}^* b_{j2}^* + \alpha_{<ij>}^* b_{i2}^* b_{j1}^* \\ -\alpha_{<ij>}b_{i2} b_{j1} + \alpha_{<ij>}^* b_{i1} b_{j2} & \alpha_{<ij>}b_{i2} b_{j2}^* + \alpha_{<ij>}^* b_{i1} b_{j1}^* \end{pmatrix}$$

with $\alpha_{<ij>} = e^{\frac{i}{2}\int_{<ij>}\bar{V}_z}$.

Substituting $\tilde{g}_j$ by its expectation value found in first quantization (see the Appendix), the off-diagonal elements of (2.6) enter S_s through the Heisenberg term while the diagonal elements enter S_h via the hopping term.

---

[3]The first approximation ($\delta V = 0$) corresponds to neglect the spinon fluctuations R_j on the gauge field $V^{(c)}$ for small T, J/t; in order to reproduce the fermionic nature of the electron operator, we need to impose $\delta B = 0$.

2.7 Spinon Effective Action

In order to derive a low energy continuum effective action for spinons, we follow Haldane approach [see for instance [32]]: we introduce two order parameters $\vec{L}, \vec{\Omega}$ describing the ferromagnetic ($\vec{q} = 0$) and the antiferromagnetic ($\vec{q} = \vec{Q}_{AF}$) modes respectively

$$b_{j\alpha}^* \vec{\sigma}_{\alpha\rho} b_{j\beta} \sim \vec{\Omega}_j + (-1)^{|j|} \epsilon \vec{L}_j, \tag{2.29}$$

with $\vec{\Omega}^2 = f \leq 1$, $\vec{\Omega} \cdot \vec{L} = 0$, where $\vec{\Omega}, \vec{L}$ are defined on one of the two sublattices to mantain the correct number of degrees of freedom.

It is useful to rewrite $\vec{\Omega}$ in CP^1 form:

$$\vec{\Omega} = z_\alpha^* \vec{\sigma}_{\alpha\beta} z_\beta, \qquad z_\alpha^* z_\alpha = f, \tag{2.30}$$

where $z_\alpha, \alpha = 1, 2$ is a spin $\frac{1}{2}$ complex (hard-core) boson field.[4]

By writing

$$e^{-i \int_{<j\ell>} \vec{V}_z} \sim 1 + a(-i\vec{V}_z)(j) + O(a^2) \tag{2.31}$$

and treating the holon density in a mean field approximation ($H_i^* H_i \simeq \delta$), the Heisenberg term becomes, up to irrelevant constants

$$\frac{J}{2} \sum_{<ij>} \frac{|(\sigma_x^{|x|} R_i^\dagger e^{\frac{i}{2} \int_{<ij>} \vec{V}} R_j \sigma_x^{|j|})_{11}|^2 - \frac{1}{2}}{a^2}$$

$$= \frac{J}{2} \sum_{<ij>} \left\{ \frac{1}{2} \left(\frac{\vec{\Omega}_i - \vec{\Omega}_j}{a} \right)^2 + 2\vec{L}_j^2 + \vec{V}_z^2(j) \left[(\Omega_{jx})^2 + (\Omega_{jy})^2 \right] \right\} + O(a). \tag{2.32}$$

For the temporal term we obtain analogously

$$\sum_j (\sigma_x^{|j|} R_j^\dagger \partial_0 R_j \sigma_x^{|j|})_{11} = \sum_j [(-1)^{|j|} z_{j\alpha}^* \partial_0 z_{j\alpha} - i\frac{a}{2} \vec{L}_j \cdot (\vec{\Omega}_j \wedge \partial_0 \vec{\Omega}_j) + O(a^2).] \tag{2.33}$$

The first term in the r.h.s. of (2.33) is a topological Berry phase trivial in 2D[32] and can be safely neglected.

Integrating out $\vec{L}$ which appears quadratically in the action and taking the continuum limit, we obtain the massive NLσ model action for spinons[5]

$$S_s = \int d^3 x \frac{1}{g} [(\partial_0 \vec{\Omega})^2 + v_s^2 (\partial_\mu \vec{\Omega})^2 + \vec{V}_z^2 \Omega^2] \tag{2.34}$$

---

[4]These variables actually result from a coarse graining procedure, see for instance [31].

[5]The last term in the r.h.s. of (2.32) apparently breaks the spin rotational symmetry of the original Hamiltonian. We assume self-consistently that the system is in the unbroken phase and substitute $\Omega_x^2 + \Omega_y^2 \rightarrow \frac{2}{3}\Omega^2$. The remaining term is considered a small perturbation and is neglected.

with the coupling constant $g = \frac{8}{J}$ and the spin wave velocity $v_s = \sqrt{2}Ja$.

The $\bar{V}_z^2$ term in (2.34) acts as a *local, istantaneous mass for the spinon excitations*; in 1D no such non–trivial gauge field exists and the spinons are massless.

Since $\bar{V}_z$ is fixed for a given holon distribution, under the assumption that $\bar{V}_z^2$ varies slowly in space and time, we can replace it by an appropriate mean field value $\langle \bar{V}_z^2 \rangle$ by averaging over holon configurations with a given mean density δ. A detailed calculation [33][28] then yields

$$\langle \bar{V}_z^2 \rangle \sim -\delta \ln \delta. \tag{2.35}$$

Hence $\langle \bar{V}_z^2 \rangle$ drives the NLσ model from the symmetry broken Neel state to the disordered regime, with unbroken symmetry and correlation lenght $\xi_{AF} \simeq \frac{1}{(\delta|ln\delta|)^{1/2}} \propto \frac{1}{\sqrt{\delta}}$, fully consistent with neutron scattering data on underdoped cuprates[34].

The mass of the spinon with the specific doping dependence (2.35) is the key feature of our approach and does not appear in the other U(1)×SU(2) gauge field theory of P. Lee and collaborators[35], where the gauged SU(2) symmetry is an enlargement of the particle-hole symmetry at half-filling with switched statistics of holon and spinon w.r.t. ours.

Finally, we expect the constraint $\vec{\Omega}^2 = f$ to be relaxed at large scales for m_s not too small.[6]

We should also bear in mind that at very low doping the AF correlation length in real systems becomes strongly $T-$dependent as thermal spin fluctuations tend to destroy the antiferromagnetic 3D order.

Expressed in terms of $\vec{\Omega}$ the action S_s in (2.34) masks the coupling of the spinon variables to the h/s gauge field. To recover this gauge symmetry explicitely, we write S_s using the z_α fields defined in (2.30):

$$S_s = \int_{\mathbf{R}^2 \times [0,\beta]} d^3x \frac{1}{g} \left[v_s^{-2} \left| \left(\partial_0 - z_\beta^* \partial_0 z_\beta\right) z_\alpha \right|^2 + \left| \left(\partial_\mu - z_\beta^* \partial_\mu z_\beta\right) z_\alpha \right|^2 + m_s^2 z_\alpha^* z_\alpha \right]. \tag{2.36}$$

The quartic terms in z_α can be reexpressed via a Hubbard-Stratonovich tranformation introducing a self-generated U(1) lattice gauge field A_μ:

$$iA_\mu(x) = (-1)^{|j|} z_\alpha^*(x)\partial_\mu z_\alpha(x), \quad x = ja. \tag{2.37}$$

This field is indeed an internal variable over which we functionally integrate after the U(1) symmetry is gauge fixed.

---

[6]This constraint would typically generate short range interactions that we neglect in the scaling limit but it could in principle renormalize the spinon mass.
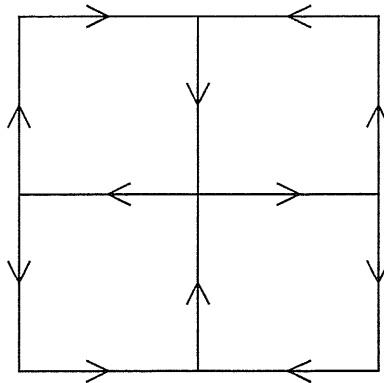
Figure 2.1: Distribution of phase factors for $\bar{B}$ on the lattice respecting $d-$wave symmetry.

2.8 Holon Effective Action

We now search a continuum limit for S_h. We see from (2.31) that the term linear in $\bar{V}$ is purely imaginary and does not contribute to the action. The first non vanishing contribution is given by the quadratic term $\bar{V}^2 a^2$ negligeable in the limit $a \to 0$.

For $\bar{B}$ we use a gauge choice that respects the π-flux per plaquette condition. Fig.(2.1) shows the corresponding distribution of phase factors on the lattice: for a given link $< ij >$ we have

$$\phi_{<ij>} = \pm\frac{\pi}{4}, \tag{2.38}$$

with the (+) sign if the line integral is calculated along the direction of the arrow on the link and the (-) sign in the opposite case. It is important to remark that any other consistent choice for $\bar{B}$ leads to the same effective action for holons.

To match the periodicity of $\phi_{<ij>}$, it is convenient to introduce 4 sublattices:

(1) for j_1, j_2 even

(2) for j_1 odd, j_2 even

(3) for j_1 even, j_2 odd

(4) for j_1, j_2 odd.

which can eventually be grouped into two sublattices A=$\{1, 4\}$ and B=$\{2, 3\}$ characterizing, respectively, the even and odd sites of the lattice.

Consistently we find useful to relabel the holon fields as

$$H_1 \to e^{-i\frac{\pi}{2}(j_x+j_y)}\tilde{H}_1$$
$$H_2 \to e^{-i\frac{\pi}{4}}e^{i\frac{\pi}{2}(j_x+j_y)}\tilde{H}_2$$
$$H_3 \to e^{-i\frac{3\pi}{4}}e^{i\frac{\pi}{2}(j_x+j_y)}\tilde{H}_3 \qquad (2.39)$$
$$H_4 \to e^{-i\frac{\pi}{2}}e^{i\frac{\pi}{2}(j_x+j_y)}\tilde{H}_4.$$

with $\tilde{H}_j$ playing the role of slowly varying field.

Taking into account the constraint $b_{i\alpha}^* b_{i\alpha} = 1$, the holon action S_h can be written as a bilinear form of $\tilde{H}_i^*$, $\tilde{H}_j$ with kernel $\hat{S}_{ij}$ given by

$$\begin{pmatrix} \partial_0 - z_\alpha^* \partial_0 z_\alpha - \mu & it(\partial_1 + z_\alpha^* \partial_1 z_\alpha) & -it(\partial_2 + z_\alpha^* \partial_2 z_\alpha) & 0 \\ it(\partial_1 - z_\alpha^* \partial_1 z_\alpha) & \partial_0 + z_\alpha^* \partial_0 z_\alpha - \mu & 0 & it(\partial_2 - z_\alpha^* \partial_2 z_\alpha) \\ -it(\partial_2 - z_\alpha^* \partial_2 z_\alpha) & 0 & \partial_0 + z_\alpha^* \partial_0 z_\alpha - \mu & it(\partial_1 - z_\alpha^* \partial_1 z_\alpha) \\ 0 & it(\partial_2 + z_\alpha^* \partial_2 z_\alpha) & it(\partial_1 + z_\alpha^* \partial_1 z_\alpha) & \partial_0 - z_\alpha^* \partial_0 z_\alpha - \mu \end{pmatrix}$$
$$(2.40)$$

The holon action can finally be cast in a more compact Dirac-like form by introducing the doublets Ψ_α, $\alpha = 1, 2$:[7]

$$\Psi_1 = \frac{1}{\sqrt{2}} \begin{pmatrix} \tilde{H}_1 + i\tilde{H}_4 \\ -\tilde{H}_2 - i\tilde{H}_3 \end{pmatrix}, \quad \Psi_2 = \frac{1}{\sqrt{2}} \begin{pmatrix} -\tilde{H}_2 + i\tilde{H}_3 \\ \tilde{H}_1 - i\tilde{H}_4 \end{pmatrix}.$$

Setting $\gamma_0 = \sigma_z, \gamma_\mu = (\sigma_y, \sigma_x)$ we find that the effective action for holes is given by

$$S_h = \int_{\mathbf{R}^2 \times [0,\beta]} d^3x \sum_{r=1}^{2} \bar{\Psi}_r \left[\gamma^0(\partial_0 - e_r z_\alpha^* \partial_0 z_\alpha - \mu) + v_F(\gamma^\mu \partial_\mu - z_\alpha^* \gamma^\mu \partial_\mu e_r z_\alpha) \right] \Psi_r$$
$$(2.41)$$

where $\bar{\Psi}_r = \Psi_r^\dagger \gamma^0$, $e_r = (-1)^r$ and $v_F = 2ta$.

Therefore the holes behave as massless dirac fermions coupled to the spinon-generated gauge field A_μ [see (2.37)]. The finite chemical potential $\mu \propto t\delta$ breaks the relativistic invariance and generates small Fermi surfaces of area $\sim \delta$ at the four nodes $(\pm\frac{\pi}{2}, \pm\frac{\pi}{2})$.

In conclusions, the full derived low energy effective action for spin and charge degrees of freedom in the "Pseudogap phase" is given by

$$S = \int_{\mathbf{R}^2 \times [0,\beta]} d^3x \left\{ \frac{1}{g} \left[v_s^{-2} |(\partial_0 - iA_0) z_\alpha|^2 + |(\partial_\mu - iA_\mu) z_\alpha|^2 + m_s^2 z_\alpha^* z_\alpha \right] + \right.$$

---

[7]Note that the two components of Ψ_α come from different sublattices A and B.

$$+ \sum_{r=1}^{2} \bar{\Psi}_r \left[\gamma^0 (\partial_0 - iA_0 - \mu) + v_F (\gamma^\mu \partial_\mu - \gamma^\mu iA_\mu) \right] \Psi_r \left. \right\} . \tag{2.42}$$

which clearly possesses the U(1) h/s symmetry as required from first principles.

2.9 Role of the Gauge Field

Before applying the theory to derive physically relevant observables, it is important to clarify the meaning of Spin-Charge separation in 2D and the role played in this respect by the gauge field.

In Section 2.1 we saw that a U(1) gauge field naturally appears because decomposition (2.1) contains an hidden local (h/s) symmetry.

In 1D the gauge field has no transverse component ($A^T = 0$), holons and spinons are *decoupled* and this yields a true spin-charge separation. In Mean Field approximation also the transverse component of the U(1) and SU(2) gauge fields vanish with the following effects:

- B_{MFA}^T =0, hence there is no Hofstatder mechanism and the holon has a quadratic dispersion;

- V_{MFA}^T=0, hence there is no spinon mass generation.

In 2D the gauge field has one physical transverse component A^T, which causes a finite magnetic flux per plaquette. This means that in 2D holon and spinon continue to "see" each other and this attractive interaction is mediated by the gauge field.

Said in other words, the hole to delocalize distorts severely the spin background, so the total magnetic energy raises and most of the phase space for the hole motion is energetically forbidden. As a result spin and charge degrees of freedom are strongly correlated and the gauge approach is one of the methods to treat such correlation.

A major consequence is that, in 2D, spin and charge sectors contribute *separately* to the evaluation of a given observable, the Ioffe-Larkin rule (see (3.1)) being a typical example.

As previously mentioned, the gauge field A is an internal variable over which we functionally integrate. Being a constraint, *it has no proper dynamics*: its low energy effective action comes enterely by integrating out holons and spinons.

We make the assumption that the scaling limit (large distance, long time) can be taken separately for the two subsystems. Then, using the techniques of Ref. [36], one can prove that in this scaling limit the action is *quadratic* in A. This conclusion follows from a derivative expansion for the spinon action, due to the presence of a mass scale, m_s, and from a tomographic decomposition along rays perpendicular to

the FS of holons, using the quadratic dependence on A of the scaling action for a single ray (Schwinger action). This result is valid only in the scaling limit when the high energy degrees of freedom are integrated out via a Renormalization Group scheme.

The term obtained from spinon (functional) integration is a 2D Maxwell-like action (as in quantum electrodynamics), because the spinons are massive and the spinon action is parity-invariant. The transverse component would then generate a logarithmic confining potential between spinons and anti-spinons. The longitudinal part is gapped due to the plasmon effect at finite T. This means that if only spinons were coupled to the gauge field, the renormalized gauge field would have confining dynamics.

However there are also fermions (holons) coupled to the gauge field: the presence of a finite Fermi Surface causes a Reizer-like contribution to $S_{eff}(A)$ when these degrees of freedom are integrated over. More precisely, the low–energy transverse component A^T of the gauge field in the limit $\omega \ll v_F|\vec{q}|$ is of the form[37]

$$\langle A^T A^T \rangle(\omega, \vec{q}) \sim (-\chi|\vec{q}|^2 + i\kappa\frac{\omega}{|\vec{q}|})^{-1}, \tag{2.43}$$

where χ is the diamagnetic susceptibility and κ the Landau damping.

This behavior dominates over the Maxwellian at large scales, destroying confinement. Nevertheless, as we shall see, the attraction generated by A^T in spinon-antispinon and spinon-holon pairs will be sufficient to produce resonances with the quantum numbers of the magnon and electron, respectively.

The mass of the spinons in our approach and its competition with dissipation of the gauge field due to coupling with holons have far-reaching consequences, and it will turn out to be responsible, in our scheme, for phenomena like the MIC, the low-T positive transverse in-plane magnetoresistance, the peak in the AC conductivity and in the Cu spin-lattice relaxation rate, hence for many experimental signatures of the "Pseudogap phase".

Chapter 3

Gauge fluctuations Effects on Physical Correlators

3.1 Motivations

In this section, we introduce the theoretical scheme to calculate in-plane and out-of-plane resistivities according to our spin-charge gauge approach. Our aim here is to relate these quantities to the computation of appropriate correlators starting from the derived low-energy effective action (2.42) for the "Pseudogap phase".

3.1.1 In-plane Resistivity

As emphasized by Anderson [1], the in-plane resistivity might be interpreted in terms of spin-charge separation. The basic inelastic process taking place in the layer is the decay of the electron into holon and spinon. In a gauge approach if the scattering time of spinons or holons by gauge fluctuations is shorter than the lifetime of the electron, then this time scale will dominate the in-plane resistivity ρ. As a result, ρ might exhibit a different temperature dependence than the electron lifetime.

To calculate the in-plane resistivity we use the Ioffe-Larkin rule[38] stating that the physical resistivity, ρ, is a sum of the resistivity due to spinons, ρ_s and the resistivity due to holons, ρ_h:

$$\rho = \rho_s + \rho_h. \tag{3.1}$$

Both ρ_s and ρ_h result from the separate scattering of spinons and holons with the gauge fluctuations. We recall that this gauge field A_μ represents a contraint: since the physical electron is gauge invariant, the holon current must be balanced by the

corresponding spinon anticurrent. Ioffe-Larkin rule then follows from the basic fact that the charge transport is dominated by the slowest particle, i.e. the particle with shorter lifetime.

The formal derivation of this addition rule is based on the following consideration: If we couple the electron to an external electromagnetic (e.m.) field, $A_{e.m}$, it turns out that we can attribute an arbitrary e.m. charge ϵ with $0 \leq \epsilon \leq 1$, to the spinon and a charge $1 - \epsilon$ to the holon, because, in the path integral formalism, ϵ can always be eliminated by the change of variable $A \to A + \epsilon A_{e.m}$. As a consequence, neglecting "photon" drag, the renormalized e.m. current polarization bubble, $\Pi_{e.m.}$, obeys the rule:

$$(\Pi_{e.m.})^{-1} = (\Pi_s)^{-1} + (\Pi_h)^{-1}. \tag{3.2}$$

From (3.2) and Kubo formula, one can derive Ioffe-Larkin rule, provided both conductivities σ_s and σ_h are non-vanishing. A crucial assumption here is the quadratic dependence of the effective action in A which is is valid in the scaling limit beyond the standard perturbation expansion.

Denoting by j^s the spinon current, the spinon resistivity is calculated from the fully renormalized current polarization bubble:

$$\langle j^s(x) j^s(y) \rangle = \Pi_s(x - y) \tag{3.3}$$

via the Kubo formula:

$$
\begin{aligned}
(\rho_s)^{-1} &= \sigma_s = -(\omega^{-1} \mathrm{Im}\Pi_s^R(\omega, \vec{q} = 0))_{|\omega \to 0} \\
&= 2\mathrm{Re} \int_0^\infty dx^0 x^0 \Pi_s(x^0, \vec{q} = 0). \tag{3.4}
\end{aligned}
$$

For holons we have similar equations replacing the index s by h (e.g. j^h denotes the holon current). In eq.(3.3) the expectation value is taken by integration over A, the spinon field, z_α of the continuum NLσ model and the Dirac holon field ψ. The last equality in (3.4) is obtained via Lehmann representation and the superscript R denotes the retarded propagator.

In order to calculate the spinon resistivity ρ_s we need first to compute the effect of gauge fluctuations at finite T on the bare spinon propagator.

The presence of the mass gap implies that at low T we expect the spinon sector to give the dominant contribution to the physical conductivity if $\sigma_s \neq 0$. In particular the observed MIC originates from the competition between the spinon mass term, dominating at low T, with the gauge field dissipation overwhelming at high T.

3.1.2 Out-of-plane Resistivity

A very distinctive feature of the spin-charge approach is the fact that the in-plane electron lifetime might have nothing to do with the in–plane resistivity while it sets the scale for the c–axis resistivity.

In such scheme, in fact, a spinon-holon decomposition of the electron holds only in the CuO_2 layer and *spinons and holons should recombine into electrons to hop between layers and contribute to* ρ_c[1]. The out-of-plane resistivity is then determined by the time scale of electron recombination.

This could explain at once one of the puzzles of the Pseudogap, namely the *co-existence* in underdoped samples at $T > T_{MIC}$ of an insulating $\rho_c(T)$ and a metallic $\rho_{ab}(T)$.

To calculate ρ_c we use the approach proposed by Kumar and Jayannavar (K-J)[39] which is motivated by the experimental observation that the c-axis transport is essentially incoherent, i.e. the mean free path for motion along the c–axis is shorter than the interlayer distance. Since successive hoppings are phase-uncorrelated, one can then consider a system of two layers weakly coupled by an effective tunnelling matrix element $-t_c$, taking into account an averaged momentum dependence of the hopping parameter (this is know to vanish for diagonal momenta).

We assume that the 2D retarded Green function of the electron (holon-spinon) has a quasi-particle pole for small ω and momentum $\vec{k}_F$ on the FS:

$$G^R(\omega, \vec{k}_F) \sim \frac{Z}{\omega + i\Gamma}, \tag{3.5}$$

where Z is the wave function renormalization and Γ the scattering rate.

Taking into account a virtual hopping between two layers induces a shift of the real part of the denominator of (3.5) from ω to $\omega \pm Zt_c$.

Let us denote by $G_\pm^R$ the corresponding Green's functions. The out-of-plane conductivity in the "confined regime" $\Gamma \ll Zt_c$ can be written through the Kubo formula as

$$\sigma_c = -\sum_{\vec{k}} \int \frac{d\omega}{2\pi} 2t_c^2 e^2 \frac{\partial n}{\partial \omega}(\omega) A_+(\vec{k}, \omega) A_-(\vec{k}, \omega), \tag{3.6}$$

where $A_\pm = -\frac{1}{\pi}\mathrm{Im}\,G_\pm^R$ are the spectral functions and $n(\omega)$ the Fermi distribution function. Inserting (3.5) in (3.6) after standard manipulations one obtains

$$\rho_c \sim \frac{1}{\nu}\left(\frac{1}{\Gamma} + \frac{\Gamma}{t_c^2 Z^2}\right), \tag{3.7}$$

with ν the density of states at the FS.

One can already anticipate that the first term causes the insulating behaviour and, being independent of t_c, it is essentially independent of the material, as experimentally observed for underdoped cuprates.

This upturn is a consequence of K-J assumption of conservation of the wavevector parallel to the planes in the tunneling process: we see from (3.7) that the $c-$axis conductivity is proportional to the overlap in energy between the two spectral functions centered at $\omega \pm Zt_c$ and this overlap is small at low temperatures since $\Gamma \ll Zt_c$.

We shall see that the *derived* lifetime of the electron resonance goes as $T^{-1}, T^{-1/2}$ at low and high temperatures in the "Pseudogap phase" and therefore it cannot explain the insulating behavior of the in-plane resistivity at low T, but it indeed sets the scale of the out-of-plane resistivity. In particular the calculated $\rho_c(T)$ has a *rounded knee*, corresponding to the crossover between the high- and low-temperature regimes, in agreement with experiment.

Via eq. (3.7) we have related the behavior of ρ_c to the computation of Γ and Z as a function of T and δ, thus to the low-energy behavior of the electron Green function. This propagator in turn can be expressed at large scales in terms of holon and spinon fields, z_α, ψ_σ and be extracted from a linear combination of terms

$$\langle \psi_\sigma(x) z_\alpha^*(x) \bar{\psi}_\sigma(y) z_\alpha(y) \rangle, \tag{3.8}$$

where σ denotes the pseudospin structure of the Dirac holons, α the component-spin index of the spinons, and the propagator (3.8) is calculated using the low-energy spinon and holon effective actions.

3.2 Spinon Current-Current Correlation Function

In this technical Section we outline the computation of the spinon current-current correlation function $\Pi_s(\omega, \vec{q})$, at small ω and $\vec{q}$; this quantity is needed to compute the spinon resistivity and the spin lattice relaxation rate.

The polarization bubble is evaluated by eikonal methods using a path integral formalism, strictly preserving gauge invariance.

3.2.1 Feynman-Schwinger-Fradkin Representation

We start by noting that the propagator associated to the spinon effective action (2.27) can be written after a suitable rescaling of variables, as a matrix element

$$\langle z(x) z^*(y) \rangle = g v_s \langle x | \frac{1}{\hat{p}^2 + m_s^2} | y \rangle, \tag{3.9}$$

where $\hat{p}$ is the space-time momentum operator. It is convenient to recast (3.9) in the Schwinger representation:

$$G_\alpha(x, y|A) = i g v_s \int_0^\infty ds\, e^{-is(\Delta_A + m_s^2)}(x, y) \tag{3.10}$$

where $x = (v_s x^0, \vec{x})$, $A = (v_s A_0, \vec{A})$ and Δ_A denotes the 3D covariant Dalambertian (or relativistic Laplacian). The propagator has been considered at zero temperature, an approximation justified by the spinon mass gap, provided $T \ll J a m_s \sim J(|\delta \ln \delta|)^{1/2}$.

The kernel appearing in (3.10) has the formal structure of an evolution kernel for a 3D Hamiltonian $H = -\Delta_A + m_s^2$ and time parameter s. It can thus be expanded in terms of Feynman paths starting from y at "time" 0 and reaching x at "time" s.

It is convenient to parametrize these paths through their 3-velocity, ϕ^μ, $\mu = 0, 1, 2$, using a Feynman-Schwinger-Fradkin (FSF) representation (see e.g. Ref. [40]):

$$G_\alpha(x, 0|A) = i g v_s \int_0^\infty ds\, e^{-ism_s^2} \int \mathcal{D}\phi \int d^3p\, e^{ip\left(\int_0^s \phi(t)dt - x\right)} e^{i \int_0^s dt\left[\frac{1}{4}\phi^2(t) + \phi \cdot A\left(x + \int_0^t \phi(t')dt'\right)\right]}. \tag{3.11}$$

Here the p-integration enforces the constraint on the initial and final points of the paths and we use a short-hand notation for the 3D scalar product: e.g.

$$p \cdot x = p_\mu x^\mu. \tag{3.12}$$

For a better understanding of the formula (3.11), notice that formally setting $\phi^\mu(t) = \frac{dx^\mu(t)}{dt}$ the last exponential is i times the Lagrangian of a 3D particle coupled to the

e.m. potential A_μ, corresponding to the previous Hamiltonian H, as one expects in a path-integral formulation. Since under a h/s gauge transformation $\Lambda(x)$, the spinon field $z_\alpha(x)$ changes by the phase factor $e^{i\Lambda(x)}$, it follows that

$$G_\alpha(x, 0|A_\mu + \partial_\mu\Lambda) = e^{i(\Lambda(x) - \Lambda(0))} G_\alpha(x, 0|A_\mu). \qquad (3.13)$$

The gauge dependence of the Green function is already captured by the so-called "Gor'kov approximation"

$$G_\alpha(x, 0|A) = e^{i\int_0^x A_\mu dx^\mu} G_\alpha(x, 0), \qquad (3.14)$$

where $\int_0^x$ denote integration along a straight line from 0 to x and $G_\alpha(x, 0)$ is the free propagator (in the absence of gauge field). The expression (3.11) is useful to go beyond Gor'kov approximation by means of the identity[40]

$$\int_0^s A_\mu\left(x + \int_0^t \phi(t')dt'\right)\phi^\mu(t)dt = \int_0^x A_\mu dx^\mu -$$

$$- \int_0^1 d\lambda\,\lambda \int_0^s dt \int_0^t dt'\, \phi^\mu(t)\phi^\nu(t')F_{\mu\nu}\left(x + \lambda\int_0^t \phi(t'')dt''\right), \qquad (3.15)$$

where $F_{\mu\nu} = \partial_\mu A_\nu - \partial_\nu A_\mu$ is the gauge field strength. A pictorial representation of this important identity is shown in Fig. 3.1: P is a generic path from x to y to which is associated the phase factor $e^{i\int_P A}$; the first term in the r.h.s. corresponds to the Gorkov phase factor while the second represents the gauge flux through the closed region $\Sigma(P)$ and is therefore *gauge invariant*, as it depends only on $F_{\mu\nu}$.

Shifting $\phi^\mu(t)$ by $2p^\mu$ one can rewrite

$$G_\alpha(x, 0|A) = e^{i\int_0^x A_\mu dx^\mu} G_\alpha(x, 0|F), \qquad (3.16)$$

$$G_\alpha(x, 0|F) = igv_s e^{i\int_0^x A(\xi)d\xi} \int_0^\infty ds \int \frac{d^3p}{(2\pi)^3}\, e^{-ipx - i(p^2 + m_s^2)} \int \mathcal{D}\phi\, e^{i\frac{1}{4}\int_0^s dt\,\phi^2(t)}$$

$$e^{-i\int_0^1 d\lambda\,\lambda \int_0^s ds' \int_0^{s'} ds''\,[\phi^\mu(s') - 2p^\mu][\phi^\nu(s'') - 2p^\nu]F_{\mu\nu}\left(\lambda\int_0^{s'}(\phi(s''') - 2p)ds'''\right)}. \qquad (3.17)$$

3.2.2 Gauge Field Strength Correlation Function

Now we turn to the polarization operator Π_s. Expressing it in terms of spinon propagators we find:

$$\Pi_s(x, y) = \langle D_{A(x)} G(x, y|A) D^\dagger_{A(y)} G(y, x|A)\rangle_A = \qquad (3.18)$$

$$\langle(\partial_\mu - \frac{i}{2}\int_y^x F_{\mu\nu}dx^\nu)G(x, y|F)(\partial^\mu - \frac{i}{2}\int_y^x F^{\mu\rho}dx_\rho)G(x, y| - F)\rangle_A,$$

Figure 3.1: Feynman-Schwinger-Fradkin representation

where $\langle \cdot \rangle_A$ denotes the integration over A with the effective action in the scaling limit and D_A the covariant derivative. Notice that the two non-gauge invariant Gor'kov terms of the two spinon propagators *cancel against each other* so that the result is explicitly gauge-invariant as it depends only on F.

We use now the quadratic structure of the scaling action $S_{eff}(A)$ to integrate out the gauge field. The explicit expression for $S_{eff}(A)$ in the Coulomb gauge is:

$$S_{eff}(A) = \frac{1}{2} \int dx^0 d^2x A_\mu \tilde{\Pi}^{\mu\nu} A_\nu.$$

In the scaling limit and for small $\omega/v_F|\vec{q}|$, the non-vanishing polarization components show a leading Reizer singularity, given by[37]

$$\tilde{\Pi}^{\perp}_{ij}(\vec{q}, \omega) = (\delta_{ij} - \frac{q_i q_j}{q^2})[i\kappa\frac{\omega}{|\vec{q}|} - \chi|\vec{q}|^2], \qquad i,j = 1, 2, \tag{3.19}$$

$$\Pi_{00}(\vec{q}, \omega) = \nu + \omega_p. \tag{3.20}$$

In (3.19) and (3.20) $\chi = \chi_s + \chi_h$, where $\chi_{s(h)}$ is the spinon (holon) diamagnetic susceptibility, $\kappa \sim O(\delta)$ the Landau damping, $\nu \propto \delta/t$ the density of states at the holons Fermi Surface and ω_p the plasmon gap. For free holons

$$\chi_h = \frac{1}{12\pi m_h} \sim \frac{t}{6\pi\delta} \tag{3.21}$$

and for free spinons

$$\chi_s \sim m_s^{-1}. \tag{3.22}$$

Hence for low doping we expect $\chi_h \gg \chi_s$.

Due to the dependence on the field strength F in (3.18) only correlator of electric (F_{0i}) and magnetic (F_{ij}) field can appear in the computation. Since the A_0-propagator

is short-ranged whereas the A^T-propagator is long-ranged, the "electric" field contribution at large scales is negligible w.r.t. the "magnetic", and in first approximation we neglect it. However, it might be useful to keep in mind that doing this we neglect a short-range attraction between spinon and antispinon (or holon).

Since A^T is gapless, we consider the effect of finite temperatures using the thermal propagator:

$$\langle F_{ij}(x)F_{rs}(0)\rangle = (\delta_{ir}\delta_{js} - \delta_{is}\delta_{jr}) \int \frac{d\omega}{2\pi} \int \frac{d\vec{k}}{(2\pi)^2} \frac{|\vec{k}|^2 e^{-i\omega\xi^0 + i\vec{k}\cdot\vec{\xi}}}{i\frac{\omega}{|\vec{k}|}\kappa - \chi|\vec{k}|^2} \coth(\frac{\omega}{2T}). \quad (3.23)$$

We want to stress that the bare spinon propagator is evaluated at zero-temperature, as justified by the mass gap m_s, and that temperature enters only via the thermal gauge-field propagator.

Since the typical energy scale for field fluctuations is set by T, in (3.23) the integration over frequency is cut-off at $\omega \lesssim T$ which in turn implies $|\vec{k}| \lesssim Q_0$, where $Q_0 = \left(\frac{\kappa T}{\chi}\right)^{1/3}$ is a momentum cut-off. Following Nagaosa and Lee[41] we interpret Q_0^{-1} as the effective length scale of gauge fluctuations.

In the limit $T\xi^0 \ll 1$ an approximate evaluation of the above integral gives

$$-i\frac{T}{4\pi\chi}Q_0^2 e^{-\frac{Q_0^2|\vec{\xi}|^2}{4}}. \quad (3.24)$$

We also find that for $m_s \gg Q_0$, in the expectation value (3.18) the derivative term dominates over the F-terms at large scales, so that to evaluate Π_s the leading term is obtained by computing

$$\langle G(x,0|F)G(x,0|-F)\rangle_A \quad (3.25)$$

and then taking the spatial derivatives. This can be self-consistently justified *a posteriori*, because (see eq. (3.30)):

$$p \sim m_s \gg \frac{1}{s}\int_0^s ds'\phi(s') \sim s^{-1/2} \sim (x^0/m_s)^{-1/2}. \quad (3.26)$$

Notice that (3.25) coincides with the propagator $\langle\vec{\Omega}(x)\cdot\vec{\Omega}(0)\rangle$, where $\vec{\Omega} = z^*\vec{\sigma}z$ is a "magnon" field.

We denote by ϕ_1^μ and ϕ_2^μ the velocity fields relative to the FSF representation of the two Green functions in (3.25). Integrating over A the product of the two FSF expansions one obtains an effective action, $I(\phi_1, \phi_2)$, which is quartic in the velocity fields.[1]

---

[1]We neglect the ϕ-dependence in F, as justified a posteriori by (3.26).

3.2.3 Eikonal and Saddle Point Approximation

The ϕ-integration is then performed using the eikonal approximation:

$$\int [\mathcal{D}\phi_1][\mathcal{D}\phi_2] \exp\{\frac{i}{4}\int \phi_1^2 + \frac{i}{4}\int \phi_2^2\}e^{I(\phi_1,\phi_2)} \simeq e^{\langle I(\phi_1,\phi_2)\rangle_{\phi_1,\phi_2}}, \qquad (3.27)$$

where $\langle\cdot\rangle_{\phi_1,\phi_2}$ denotes the average w.r.t. the gaussian measure appearing in the l.h.s. of (3.27). This approximation is justified because $I \sim (T/t) \ll 1$.

Then the contribution of the two Green functions factorizes. This factorization in a diagrammatic language means that after the cancellation of self-energy and vertex renormalization (implicitly involved in the cancellation among Gor'kov terms), the remaining leading effect of A-fluctuations is a self-energy renormalization of the gauge-invariant spinon propagator. At this stage the correlator $\langle\vec{\Omega}(x) \cdot \vec{\Omega}(0)\rangle$ can be written as

$$\left[\int d^3p \int_0^\infty ds\, e^{\{-i(p^2+m_s^2-\frac{T}{\chi}f(\alpha))s+ipx-\frac{T}{\chi}Q_0^2s^2g(\alpha)\}}\right]^2, \qquad (3.28)$$

where $\alpha = |\vec{p}|sQ_0$, f and g are functions which summarize the effect of gauge fluctuations. It is important to note that such corrections explicitly break the Lorentz invariance: this should not surprise us because the Reizer propagator (3.19) is not Lorentz invariant.

Explicit integral representations of f and g are:

$$f(\alpha) = \alpha^2 \int_0^1 d\lambda\,\lambda \int_0^1 d\tilde{\lambda}\,\tilde{\lambda} \int_0^1 dv\, v^2 e^{-\alpha^2 v^2(\tilde{\lambda}-\lambda)^2}$$

$$g(\alpha) = \int_0^1 d\lambda\,\lambda \int_0^1 d\tilde{\lambda}\,\tilde{\lambda} \int_0^1 dv\, v e^{-\alpha^2 v^2(\tilde{\lambda}-\lambda)^2}. \qquad (3.29)$$

It is easy to see that $f(\alpha)$ is an increasing function of the argument, vanishing quadratically at $\alpha \to 0$ and growing linearly at large α while $g(\alpha)$ is always decreasing, finite at $\alpha = 0$ and vanishing as α^{-1} at large α.

Finally we evaluate the p and s integrals by saddle point approximation, obtaining for $m_s^2 \gtrsim T/\chi$:

$$p \sim x/2s \qquad s \sim \frac{1}{2}\sqrt{\frac{(x^0)^2 - \vec{x}^2}{m_s^2 - \frac{T}{\chi}f(\alpha)}} \qquad (3.30)$$

and the magnon $\vec{\Omega}$ propagator in x-space becomes

$$\langle\vec{\Omega}(x) \cdot \vec{\Omega}(0)\rangle \sim \frac{1}{(x^0)^2 - |\vec{x}|^2}e^{-2i\sqrt{m_s^2 - \frac{T}{\chi}f(\frac{|\vec{x}|Q_0}{2})}\sqrt{(x^0)^2-\vec{x}^2} - \frac{T}{2\chi}Q_0^2g(\frac{|\vec{x}|Q_0}{2})\frac{(x^0)^2-|\vec{x}|^2}{m_s^2-\frac{T}{\chi}f(\frac{|\vec{x}|Q_0}{2})}}.$$

$$(3.31)$$

which is the key result of this Section. We postpone the final steps of the calculations to derive the spinon resistivity and the spin-lattice relaxation rate to the next chapter where we sistematically compare the derived temperature and doping dependences with experimental data.

3.3 The Electron Green's Function

In this Section we evaluate the continuum limit of the electron Green's function within our approach, extracting, in particular, the wave function renormalization constant, Z, and the inverse lifetime, Γ, needed to compute ρ_c in K-J's approach.

3.3.1 Holon Effective Action

In order to have a more systematic derivation, it is worthwhile to start by writing the hopping Hamiltonian for holons, H_{hopp}, neglecting at first the coupling to the h/s gauge field.

Restricting the holon field H to the two Néel sublattices, labelled by A, to which the origin belongs, and B, we have in momentum space

$$H_{hopp} = \sum_{\vec{k}} \left(H_A^*(\vec{k}) H_B^*(\vec{k}) \right) \begin{pmatrix} 0 & -2t\frac{1}{\sqrt{2}}(\gamma_+ + i\gamma_-) \\ -2t\frac{1}{\sqrt{2}}(\gamma_+ - i\gamma_-) & 0 \end{pmatrix} \begin{pmatrix} H_A(\vec{k}) \\ H_B(\vec{k}). \end{pmatrix}$$

(3.32)

where

$$\gamma_\pm = \cos(k_x a) \pm \cos(k_y a),$$ (3.33)

a being the lattice spacing and the sum over $\vec{k}$ running in the reduced Brillouin zone. The eigenvalues of H_{hopp} are given by:

$$\epsilon_\pm(\vec{k}) = \pm 2t\sqrt{\cos(k_x a)^2 + \cos(k_y a)^2},$$ (3.34)

hence they describe double cones with vertices at $\left(\pm \frac{\pi}{2}, \pm \frac{\pi}{2} \right)$ in the Brillouin zone.

Since the chemical potential for the holes is positive, $\mu \sim 2t\delta$, only the ϵ_+ band of the double cones exhibits a FS. For each of these double cones one can identify a two-component, continuum, Dirac field ψ_α, $\alpha = \uparrow, \downarrow$ describing the low energy physics of the system.
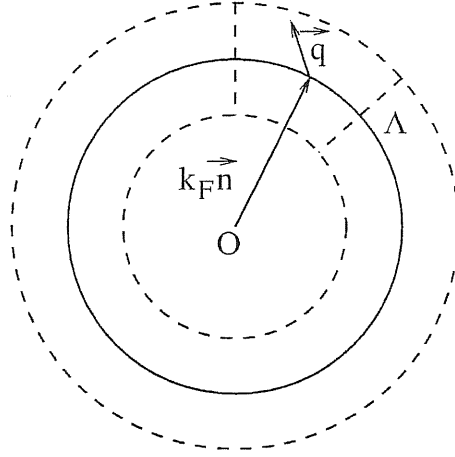
Figure 3.2: Tomographic decomposition of the Fermi Surface patch with square boxes of size Λ.

The relation between ψ, z and the original electron field c_α in the two sublattices is found to be given, e.g. near the $\left(\frac{\pi}{2}, \frac{\pi}{2}\right)$ double cone, by

$$\langle c_\alpha^A(x) c_\alpha^{\dagger A}(0) \rangle \quad \sim \quad e^{i\left(\frac{\pi}{2}, \frac{\pi}{2}\right) \cdot \vec{x}} \langle (\bar{\psi}_\downarrow(x)\psi_\downarrow(0) - \bar{\psi}_\uparrow(x)\psi_\uparrow(0)) z_\alpha(x) z_\alpha^*(0) \rangle \tag{3.35}$$

$$\langle c_\alpha^B(x) c_\alpha^{\dagger A}(0) \rangle \quad \sim \quad e^{i\left(\frac{\pi}{2}, \frac{\pi}{2}\right) \cdot \vec{x}} \langle \left(e^{i\frac{\pi}{4}} \bar{\psi}_\uparrow(x)\psi_\downarrow(0) + e^{-i\frac{\pi}{4}} \bar{\psi}_\downarrow(x)\psi_\uparrow(0)\right) z_\alpha(x) z_\alpha^*(0) \rangle.$$

Analogous relations hold near the other three double cones.

3.3.2 Tomographic Decomposition

In the previous Section we evaluated the effect of gauge fluctuations on the z correlator at large scales, using the FSF path-integral representation. An analogous representation is hard to use for the ψ_α correlator because of the finite density of holons. This representation would in fact contain a series of alternating sign contributions, corresponding to an arbitrary number of closed fermion wordlines, describing the contributions of the particles in the finite-density ground state, besides the path from 0 to x (see e.g. Ref. [27]).

To overcome this difficulty, we apply a dimensional reduction by means of the tomographic decomposition introduced by Luther-Haldane.[42] To treat the low-energy degrees of freedom we choose a slice of thickness $\Lambda = k_F/\lambda$, with $\lambda \gg 1$, in momentum space around the FS of ψ, as shown in Fig. 3.2.

To simplify the description, we assume a circular FS, an approximation reasonable for low δ (the method applies nevertheless to the general case by considering a Fermi

momentum varying along the FS). We decompose the slice in approximately square sectors; each sector corresponds to a quasi-particle field in the sense of Gallavotti-Shankar renormalization[43] (see also Ref. [44]). Each sector is characterized by a unit vector $\vec{n}(\theta)$, pointing from the center of the FS to the centre of the box, labelled by the angle θ between this direction and the k_x axis. The original momentum $\vec{k}$ inside a given sector is written as

$$\vec{k} = k_F \vec{n}(\theta) + \vec{q}, \tag{3.36}$$

where $\vec{q}$ spans the box, therefore $|\vec{q} \cdot \vec{n}(\theta)|$, $|\vec{q} \wedge \vec{n}(\theta)| \leq \Lambda$. Due to the Dirac structure of ψ, to apply the tomographic decomposition to the holon propagator, we first decompose the free ψ correlator as[2]

$$
\begin{aligned}
\langle \bar{\psi}_\alpha(x)\psi_\beta(0) \rangle \;=\;& \int \frac{d^3k}{(2\pi)^3} \left[\frac{e^{-ikx}}{-\gamma_0(k_0 + k_F) + \gamma_\mu k_\mu - i\varepsilon\,\mathrm{sgn}(|\vec{k}| - k_F)} \right]_{\alpha\beta} \\
=\;& \int \frac{d^3k}{(2\pi)^3} e^{-ikx} \frac{1}{k_0 + k_F - |\vec{k}| + i\varepsilon\,\mathrm{sgn}(|\vec{k}| - k_F)} \\
& \times \left[\frac{\gamma_0(k_0 + k_F) - \gamma_\mu k_\mu}{k_0 + k_F + |\vec{k}| - i\varepsilon\,\mathrm{sgn}(|\vec{k}| - k_F)} \right]_{\alpha\beta}.
\end{aligned} \tag{3.37}
$$

In the scaling limit the matrix in square brackets does not have a pole and, for momenta in a box labelled by $\vec{n}(\theta)$, it approaches

$$A(\theta) = \frac{\gamma_0 - \vec{\gamma} \cdot \vec{n}(\theta)}{2}. \tag{3.38}$$

In Ref. [45] it has been shown that the tomographic decomposition is valid at large distances even in the presence of a minimal coupling to a "photon" field. Applying the tomographic decomposition to the holon propagator in the presence of an external h/s gauge field A, in the scaling limit, using (3.37),(3.38), we derive

$$
\begin{aligned}
\langle \bar{\psi}_\alpha(x)\psi_\beta(0) \rangle \;\sim\;& \sum_i A_{\alpha\beta}(\theta_i) \int \frac{dq_0}{2\pi} \int_\Lambda \frac{d^2q}{(2\pi)^2} e^{-ik_F \vec{n}(\theta_i)\cdot \vec{x}} e^{iq_0 x_0 - i\vec{q}\cdot\vec{x}} \\
& \times \left[\frac{1}{q_0 - H_{\theta_i} + i\varepsilon\,\mathrm{sgn}(\tilde{q} \cdot \tilde{n}(\theta))} \right],
\end{aligned} \tag{3.39}
$$

where

$$H_\theta = A_0 + \vec{n}(\theta) \cdot (\vec{q} - \vec{A}) + \frac{1}{2k_F}\left[(\vec{q} - \vec{A}) \wedge \vec{n}(\theta) \right]^2, \tag{3.40}$$

---

[2]Here and below we set $v_F = 1$.

and $\int_\Lambda$ denotes integration over a square box of size Λ. To the Fourier transform of the term in square bracket of (3.39) one can apply the FSF path representation.

Using manipulations analogous to those performed for the evaluation of the spinon bubble, one can rewrite (3.39) as

$$\frac{k_F}{\Lambda}\int d\theta A(\theta)e^{-ik_F\vec{n}(\theta)\vec{x}}e^{i\int_0^x A_\mu dx^\mu}\int\frac{dq_0}{2\pi}[\int_0^\infty du\int_\Lambda\frac{d^2q}{(2\pi)^2}\Theta(q_\|)+$$

$$\int_{-\infty}^0 du\int_\Lambda\frac{d^2q}{(2\pi)^2}\Theta(-q_\|)]e^{iq^0(x^0-u)-i\vec{q}(\vec{x}+\vec{n}(\theta)u)}e^{\frac{iq_\perp^2}{2k_F}v_Fx^0}$$

$$\times\{\int \mathcal{D}\varphi_\perp e^{i\int_0^u\frac{k_F}{2}\varphi_\perp^2(u')du'}e^{-i\int_0^1 d\tau\tau\int_0^u du'\int_0^{u'}du''\varphi^\mu(u')\varphi^\nu(u'')F_{\mu\nu}(\tau\int_0^{u'}\varphi(u''')du''')}\},$$

$$(3.41)$$

where we use the short notation $q_\| = \vec{q}\cdot\vec{n}(\theta)$, $q_\perp = \vec{q}\wedge\vec{n}(\theta)$ and φ is the velocity field of components $\varphi^\mu(t) = (1, 1, \varphi_\perp(t))$. Note that in (3.41) we have replaced the original discrete summation $\sum_i$ with the continuum limit $\frac{k_F}{\Lambda}\int d\theta$. We have checked by explicit computation [46] that the term in curly brackets describing the correction to Gork'ov approximation is irrelevant within the approximation scheme adopted in previous Section and below, so we shall drop it from now on.[3] Then, the u integration can be performed exactly, after the trivial q_0 integration. The $q_\|$ integration gives

$$\int_{-\Lambda}^\Lambda dq_\| e^{iq_\|(x_\|-x^0v_F)}\Theta(q_\|) = \frac{1}{i}\frac{e^{i\Lambda(x_\|-x^0v_F)}-1}{(x_\|-x^0v_F)} \simeq i\frac{1}{x_\|-x^0v_F}, \qquad (3.42)$$

where in the last approximation is valid in the limit $\Lambda v_Fx^0 \gg 1$.[4] Setting $\Lambda(x_0) = \left(\frac{k_F}{v_Fx^0}\right)^{\frac{1}{2}}$, the $q_\perp$ integration gives

$$\int_{-\Lambda}^\Lambda dq_\perp e^{i(q_\perp x_\perp-\frac{v_F}{k_F}q_\perp^2x^0)} = \Lambda(x_0)\int_{-\Lambda/\Lambda(x_0)}^{\Lambda/\Lambda(x_0)} dy\, e^{i\Lambda(x_0)x_\perp y}e^{-i\frac{1}{2}y^2} \sim \Lambda(x_0)\frac{e^{\frac{i}{2}x_\perp^2\Lambda(x_0)}}{\sqrt{i}}.$$

$$(3.43)$$

Collecting all pieces, the holon Green's function in the scaling limit and for $\Lambda x_0 \gg 1$ can be written as:

$$\langle\bar{\psi}_\alpha(x)\psi_\beta(0)\rangle \sim \frac{\Lambda(x_0)k_F}{\Lambda}\int d\theta\frac{e^{\frac{i}{2}x_\perp(\theta)^2\Lambda(x_0)}}{\sqrt{i}}A(\theta)_{\alpha\beta}e^{ik_Fx_\|(\theta)}$$

$$\left[\frac{1}{x_\|(\theta)-x^0v_F}\Theta(x_0) + \frac{1}{x_\|(\theta)+x^0v_F}\Theta(-x_0)\right]e^{i\int_0^x A_\mu dx^\mu}. \qquad (3.44)$$

---

[3]This agrees with the fact that the holon scattering time behaves like $\sim T^{-4/3}$, *a posteriori* a much longer time with respect to the electron scattering time, triggered by gauge fluctuations on spinons.

[4]The neglected term is proportional to a rapidly oscillating phase factor.

3.3.3   Quasi-particle Pole

The electron Green's function in real space is given by the product of the holon propagator (3.44) and the spinon propagator, given by the square root of (3.31), averaged over gauge fluctuations. (3.35). The underlying idea is that gauge fluctuations are sufficiently strong to bind holon and spinon into a resonance at finite temperatures.

The Gor'kov terms in the ψ and the z correlators cancel against each other and the gauge field fluctuations act only on the gauge-invariant spinon correlator.

We perform now the Fourier transform of the electron propagator for momenta close to the Fermi surface, in a sector laballed by the angle η, $G_\alpha(\omega, (\pi/2, \pi/2) + \vec{n}(\eta)k_F + \vec{q})$, for small ω and $\vec{q}$. We integrate over θ using the following:

Lemma: [45] Let $f(\theta, \vec{x})$ be a smooth function, then in the large distance limit $|\vec{x}| \gg \Lambda^{-1}$ we have

$$\int d\theta e^{ik_F(\vec{n}(\eta)-\vec{n}(\theta))\cdot\vec{x}} f(\theta, \vec{x}) \sim \frac{2\pi}{k_F} f(\eta, \vec{x})\delta_{\Lambda^{-1}}(\vec{x} \wedge \vec{n}(\eta)), \qquad (3.45)$$

where $\delta_{\Lambda^{-1}}$ denotes an approximate δ-function of width Λ^{-1}.

Setting $\vec{x} = |\vec{x}|\vec{n}(\phi)$ we approximate

$$\delta_{\Lambda^{-1}}(\vec{x} \wedge \vec{n}(\eta)) \sim \frac{1}{|\vec{x}|}[\delta(\phi - \eta) + \delta(\phi - \eta + \pi)]. \qquad (3.46)$$

One can easily perform the ϕ-integration; the remaining integration over space-time variables is done as in previous Section, namely by saddle point approximation for $|\vec{x}|$ in the limit $x^0 \gg |\vec{x}|$ and by principal part evaluation and scale renormalization for x^0. The final result is

$$G_\alpha\left(\omega, \left(\frac{\pi}{2}, \frac{\pi}{2}\right) + \vec{n}(\eta)k_F + \vec{q}\right) \sim S(\eta)Z\cdot$$

$$\cdot \left[e^{i\vec{q}\cdot\vec{n}(\eta)|x_c(0)|}\frac{1}{\omega + \Sigma - v_F\frac{d|x_c|}{d|x_0|}(0)q_\parallel} + e^{-i\vec{q}\cdot\vec{n}(\eta)|x_c(0)|}\frac{1}{\omega - \Sigma - v_F\frac{d|x_c|}{d|x_0|}(0)q_\parallel}\right],$$
$$(3.47)$$

where $S(\eta)$ is the angle dependent part of the wave function renormalization constant

$$S(\eta) = \frac{1}{2}\left[1 - \frac{1}{\sqrt{2}}(\cos(\eta) + \sin(\eta))\right] \qquad (3.48)$$

whose lattice analogue is shown in Fig. 3.3. We see that the spectral weight is strongly suppressed outside the Reduced Brillouin zone, in qualitative agreement with experiments.
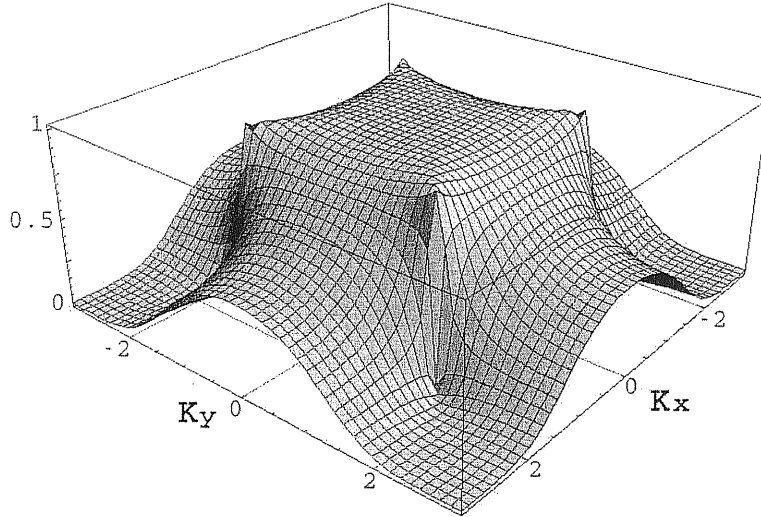
Figure 3.3: Angle-dependent spectral weight of the electron propagator

In (3.47) Z is the wave function renormalization constant averaged over the FS; writing the tomographic momentum cut-off as $\Lambda = \frac{k_F}{\lambda}$, with $\lambda \gg 1$ and taking into account the definition of Q_0 we obtain

$$Z \approx \lambda (\frac{Q_0}{k_F})^{\frac{1}{2}} (\frac{m_s \kappa}{J^2})^{\frac{1}{2}}. \qquad (3.49)$$

The renormalized electron self-energy Σ is given by

$$\Sigma = v_s \sqrt{m_s^2 - ic\frac{T}{\chi}}, \qquad (3.50)$$

where v_s is the spinon velocity previously set equal to 1. From (3.47) we can immediately read off the inverse scattering time Γ for the electron: $\Gamma = -\mathrm{Im}\Sigma$.

We see that $\Gamma(T)$ is an increasing function of temperature changing from T to $T^{1/2}$ as the temperature increases. This damping rate is much bigger than the $T^{4/3}$ estimate for the holon self-energy, which justify *a posteriori* our former approximation to consider only the Gorkov term for holons.

3.3.4 Fermi Surface and Electron Resonance

We now make the following

Assumption FS: the neglected short - range attraction between spinon and holon exactly renormalize $\mathrm{Re}\Sigma$ to 0 at the Fermi surface so that the electron exhibits a Fermi surface.

Under Assumption FS, finally, for $\vec{q} = \vec{0}$ and $\omega > 0$ small we find the structure (3.5) with the replacement $Z \to S(\eta)Z$.

This structure shows that the gauge fluctuations are able to bind together spinon and holon into a resonance for low energies and momenta close to the Fermi momenta, but with a wave function renormalization constant which depends both on the point of the FS, due to $S(\eta)$, and the temperature. In particular $Z \sim T^{1/6}$, so Z vanishes if formally extrapolated[5] to $T = 0$ even if the electron life-time is infinite. A qualitatively similar behaviour is predicted by Marginal Fermi Liquid theory where Z vanishing logarithmically at $T = 0$.[47]

It is important to recall that setting $T = 0$ in our formalism corresponds to neglect the coupling with the gauge field: the convolution of the bare holon and spinon propagators then gives branch cut singularities but no simple poles, so the Green's function is completely incoherent and $Z = 0$.

In principle the thermal and doping dependences of Z could be measured in ARPES experiments. In fact, the measured intensity is proportional to $\mathrm{Im}G(\omega, \vec{k})n(\omega)$. Denoting by $I(\vec{k})$ the integrated intensity along the "electron FS", the electron resonance contributes with a term I_{qp} given by

$$I_{qp}(\vec{n}(\theta)k_F) \sim S(\theta)Z.$$

The factor $S(\theta)$ is peaked around the diagonal in the reduced Brillouin Zone ($\theta = \frac{5\pi}{4}$ for the FS near $(\frac{\pi}{2}, \frac{\pi}{2})$) and it nearly vanishes in the outer zone (see Fig. 3.3). This angular dependence therefore yields a reduction of the electron spectral weight outside the reduced Brillouin Zone, in rough qualitative agreement with experiments.

---

[5]We remind that the $|\vec{x}|$ - saddle point is only dominant for $T \gtrsim \chi m_s Q_0$.

Chapter 4

Pseudogap: Comparison with Experiments

In this chapter we use the results for the spinon-spinon correlator obtained in the previous chapter to evaluate in-plane spinon resistivity, magnetoresistance and spin lattice relaxation rate in a unified frame: the derived temperature and doping dependences reproduce qualitatively the phenomenology discussed in Chapter 1.

We shall discuss in details the findings of a very recent experiment by Dumm et al.[53]. The authors measured the in-plane Far Infrared AC conductivity and the related a-b anisotropy for lightly doped LSCO samples ($x = 0.03, 0.04$). By decreasing the temperature below 80K the simple Drude-like response evolves in a broad peak at finite frequency $\sim 100\text{cm}-1$ bearing very much resemblance to the Metal-Insulator peak in the DC conductivity when plotted against temperature. We extend the theory to account for finite frequency response and present a thorough understanding of these data.

4.1 In-plane Resistivity

As mentioned in Section 3.2.2, the spinon contribution ρ_s to the resistivity can be calculated from the spinon-spinon correlator (2.26) by noting that the current-current propagator is given by $\Pi^s(x) \sim \langle \partial_\mu \vec{\Omega}(x) \cdot \partial^\mu \vec{\Omega}(0) \rangle$.

In order to apply Kubo formula, we need to integrate over $\vec{x}$ to obtain $\Pi^s(x^0, \vec{q} = 0)$. We consider the region $x^0 >> |\vec{x}|$ and evaluate the $|\vec{x}|$-integration via saddle point. Using the form of f and g one finds that the exponent of (3.31) at large x^0 exhibits a complex saddle point at a scale $|\vec{x}|(x^0) \sim (x^0)^{1/2}$, thus verifying the above

assumed inequality with a behavior of a standard diffusion[1], and with argument $\pi/4$.

A numerical extrapolation in the region of small x^0 yields an approximate x^0-dependence of the form:

$$|\vec{x}|(x^0) \sim e^{i\pi/4} x_c(x^0), \quad x_c(x^0) = (C^2 Q_0^{-2} + C'|x^0|/m_s)^{1/2} \qquad (4.1)$$

with C, C' finite positive constant $(C \sim 0.5)$, thus approaching a finite value as $x^0 \to 0$. Setting $\alpha(x^0) = Q_0|\vec{x}|(x^0)$ and

$$I(x^0) = -i\sqrt{m_s^2 - \frac{T}{\chi}f(\alpha(x^0))}x^0 - \frac{T}{4\chi}Q_0^2 g(\alpha(x^0))\frac{(x^0)^2}{m_s^2 - \frac{T}{\chi}f(\alpha(x^0))}, \qquad (4.2)$$

we have:

$$\langle j_\mu j^\mu\rangle(\vec{q}=0, x^0) = \int d^2\vec{x}\langle j_\mu(x^0, \vec{x})j^\mu(0, \vec{0})\rangle$$

$$\sim \frac{x_c^3}{((x^0)^2 - x_c^2)^3}\left(\frac{\partial^2 I(x^0)}{\partial x_c(x^0)^2}\right)^{-1/2} e^{2I(x^0)}. \qquad (4.3)$$

Since f is smooth on the scale $|\vec{x}| \sim Q_0^{-1}$, assuming for x^0 the same scale the dominance of the saddle point requires a lower bound for the temperature, which combined with previous upper bound yields a range of validity given by

$$m_s^2 \gtrsim \frac{T}{\chi} \gtrsim m_s Q_0. \qquad (4.4)$$

For a given doping δ, this gives a range of temperatures between a few tens and a few hundreds of Kelvin. We believe that the bounds above correspond to crossover to different phases, where the derived "Pseudogap" effective action (2.9) is no longer valid. In particular the upper bound gives the crossover T^* to the Strange metal phase.

The real part of the exponential in (4.3) is monotonically decreasing in x^0 at large x^0, therefore we evaluate the x^0 integral appearing in Kubo formula (3.4) by principal part evaluation.

When extrapolated to short time, the correlator (4.3) has a UV divergence, which is clearly unphysical since $x^0 \gg |\vec{x}_c(x_0)|$. Since $|\vec{x}_c(x_0)| \sim Q_0^{-1}$ for vanishing x_0, we introduce an UV cutoff in the integral at λQ_0^{-1} and evaluate the integration assuming λ large. Then we make the conjecture that for small ω the physics is dominated by large

---

[1]The diffusion constant D is proportional to the AF correlation lenght, i.e. $D = v_s/m_s$

scales and the small-scale contribution can be taken into account by removing the UV cutoff after a multiplicative scale renormalization. The result of this approximation is

$$\sigma_s = 2 \operatorname{Im} \int_0^\infty dx^0 x^0 \Pi(x^0, \vec{q} = 0) \sim \operatorname{Im} \left(\frac{Z_j}{\sqrt{m_s^2 - \frac{T}{\chi} f(Ce^{i\pi/4})}} \right), \tag{4.5}$$

where $Z_j = Q_0 Z_\Omega$ with

$$Z_\Omega = (m_s^2 - ic\frac{T}{\chi})^{\frac{1}{4}} (\frac{\chi}{T f''(Ce^{i\pi/4})})^{1/2} Q_0^{\frac{1}{2}}. \tag{4.6}$$

Numerically one finds $f(Ce^{i\pi/4}) \sim 0.2 + i3.3$ and $f''(Ce^{i\pi/4})$ real. For simplicity we set $\operatorname{Im} f(Ce^{i\pi/4}) = c$ and we still denote by m_s^2 the quantity $m_s^2 - \operatorname{Re} f(Ce^{i\pi/4})T/\chi$ which in the range of temperature we are interested is in fact almost equal to m_s^2.

For the spinon resistivity $\rho_s = \sigma_s^{-1}$ we therefore obtain:

$$\rho_s \sim \frac{1}{\sqrt{2\delta}} \frac{|M|^{\frac{1}{2}}}{\sin(\frac{\arg M}{2})} = \frac{1}{\sqrt{\delta}} \frac{\left(m_s^4 + \left(\frac{cT}{\chi}\right)^2 \right)^{\frac{1}{8}}}{\sin\left[\frac{1}{4} \arctan\left(\frac{cT}{\chi m_s^2}\right)\right]}. \tag{4.7}$$

For the holons one can borrow a computation performed diagrammatically in Ref. [41] for a Fermi liquid interacting with a gauge field exhibiting Reizer singularity. Adding, via Matthiessen rule, the contribution of impurities one finds:

$$\rho_h \sim \delta[\frac{1}{\epsilon_F \tau_{imp}} + (\frac{T}{\epsilon_F})^{4/3}]. \tag{4.8}$$

For small δ, $\frac{T}{t}$ we have $\rho_s \gg \rho_h$, so the spinon contribution dominates the physical resistivity in the Ioffe-Larkin rule. For low T, ρ_s is insulating going as $\sim \frac{1}{T}$ while at high temperatures $T \sim \chi m_s^2$, $\rho_s \sim T^{1/4}$, thus showing a metallic behaviour. From formula (4.7) a MIC is thus recovered upon temperature decrease, in agreement with experiments.

This crossover is determined by the interplay between the AF correlation lenght $\xi \sim |\delta \ln \delta|^{-1/2}$ and the thermal de Broglie wave lenght $\lambda_T \sim (\chi/T)^{1/2}$ for holes.

At very low T the mass gap prevails ($\xi \ll \lambda_T$), the spinon configuration is frozen and no spinon current can flow: the system is an insulator. The metallic behaviour is recovered only at high temperatures where $\xi \sim \lambda_T$.

We emphasize that in our interpretation the MIC is *intrinsic* and not driven by impurities effects.

The temperature dependence of ρ_s is controlled by the dimensionless variable y

$$y = \frac{Tc}{\chi m_s^2} \sim \frac{Tc}{t|\ln \delta|} \tag{4.9}$$

which has a weak logaritmic dependence on doping, inherited from the spinon mass m_s. This implies that the calculated MIC temperature T_{MIC} *decreases* slowly upon doping increase, as found in experiments[10].

Our formula for ρ_s has essentially no free parameters except for an overall resistivity scale, which by the way is not universal. The only parameter O(1) used in our numerical calculation is the coefficient r in the parametrization

$$\chi m_s^2 \sim \frac{t}{6\pi \delta}|\delta \ln \delta|r, \tag{4.10}$$

which one can fine-tune by using e.g. the minimum of resistivity for some fixed doping. The entire set of curves $\rho(\delta, T)$ are then completely determined and the agreement with the experimental data is good, as shown in Fig.1 of Ref.[48].

4.2 Universal Normalized Resistivity

We now consider a more subtle prediction following from our theoretical treatment.

As mentioned in Chapter I, an inflection point in the in-plane resistivity has been observed in heavily underdoped cuprates at a temperature T^*, where $d\rho/dT$ has a maximum. We suggest to identify T^* with the pseudogap temperature corresponding to the crossover from the Pseudogap to the Strange Metal in the phase diagram.

Such an inflection point also appears in our derived in-plane resistivity formula ($T^* \simeq \chi m_s^2$, and the "relativistic" structure of the mass term is responsible for it. In particular, the ratio T_{MIC}/T^* is a universal (i.e. doping independent) numerical constant (~ 0.4), suggesting that the two Pseudogap temperatures are related to the same energy scale.

Moreover, if we define the "normalised resistivity" as:

$$\rho_n(T) = \frac{\rho(T) - \rho(T_{MIC})}{\rho(T^*) - \rho(T_{MIC})} \tag{4.11}$$

and neglect ρ_h, this is a universal function of the variable $y = T/T^*$.

This curve has been noticed in the YBCO [12] data and quantitatively similar *universal curves* have been observed also for LSCO,[20] BSLCO, BSCO.[49] [2]. Our formalism explains in a neat way their universality character.

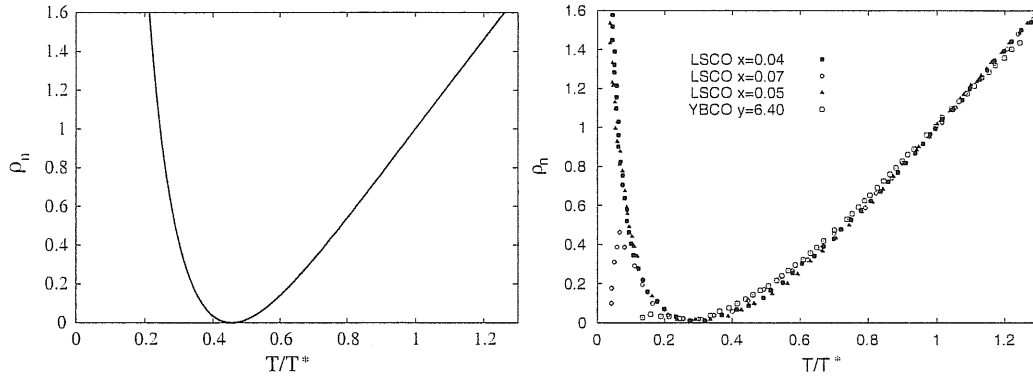[2]In these last references a different definition of T^* was used, based on deviation from linearity

Figure 4.1: *Left:* Calculated "normalised" resistivity ρ_n versus reduced temperature T/T^*. *Right:* Temperature dependence for ρ_n in underdoped LSCO (Extracted from Ref. [10]) and YBCO (Extracted from Ref.[12])

In Fig. 4.1 we plot the calculated normalized resistivity ρ_n to be compared with the experimental curve on LSCO and YBCO that we extracted from data of Takagi et al. [10] and Trappeniers et al.[12]. We did not make any attempts to reconcile the calculated and observed T_{MIC}/T^* ratio which may depend on factors, not included in our considerations, but we remark that the universal character of the normalized resistivity is an explicit prediction of theory in agreement with experiment.

---

of ρ, not directly accessible to our approach, and therefore not permitting a direct comparison with our formula. A rough estimate, however gives for that T^* a value dependent on the material, but approximately twice our definition of T^*

4.3 Hidden MIC in Superconducting Cuprates and Magnetoresistance

The techniques developed in previous sections are useful to compute other observables, like the transverse in-plane magnetoresistance and the ^{63}Cu spin-lattice relaxation rate. The calculation of magnetoresistance is outlined in Ref.[50] and here we review the results for completeness.

The basic underlying hypothesis is that suppressing superconductivity by applying a magnetic field in superconducting underdoped samples, one recovers the normal-state "pseudogap phase".

A magnetic field H perpendicular to the plane then modifies the gauge effective action in two ways:

1. Via a minimal coupling it induces a shift $A \to A - \varepsilon A_{em}$ in the spinon term and $A \to A + (1 - \varepsilon)A_{em}$ in the holon term, where ε is the spinon effective charge and A_{em} is the vector potential corresponding to the applied uniform static magnetic field H. In a mean-field treatment the effective charge is chosen as $\varepsilon \sim \chi_h/\chi$ in order to satisfy the Ioffe-Larkin rule for diamagnetic susceptibility (see Refs. [51, 50]).

2. The presence of H induces a parity-breaking Chern-Simons term in the holon action $(\sigma_h(H)/2\pi)A^0\epsilon_{ij}\partial^i A^j$, where $\sigma_h(H)$ is the holon Hall conductivity. Since A_0 is short-ranged, with a gap $\gamma = \nu + \omega_p$ (see eq.(3.19)), it can be integrated out yielding an effective renormalization of the diamagnetic susceptibility in the transverse action: $\chi \to \chi(H) = \chi + \frac{\sigma_h^2(H)}{4\pi^2\gamma}$ as discussed in Ref. [51]. This effect is however subleading at low T.

Restricting to 1), the presence of A_{em} produces an additional term in the FSF path-representation of $G(x, 0|F)$ discussed in Chapter III:[3]

$$e^{i\varepsilon \int_0^1 d\lambda\lambda \int_0^s ds' \int_0^{s'} ds''(\phi^i(s')-2p^i)(\phi^j(s'')-2p^j)\epsilon_{ij}H}. \qquad (4.12)$$

Evaluating the ϕ integrals in the same gaussian approximation, this term yields a contribution $e^{is^3|\vec{p}|^2 H^2}$ to the $\vec{\Omega}$ correlator in eq.(3.28) which in turn implies a renormalization of the relativistic spinon mass term:

---

[3]This is because the external field H contributes to the total flux penetrating the closed path $\Sigma(P)$ between two given points x and y.

$$M \rightarrow M(H) = \sqrt{m_s^2 - i\left(\frac{cT}{\chi(H)} - \frac{\varepsilon^2 H^2}{3Q_0^2}\right)}. \qquad (4.13)$$

The reduction of the damping $\frac{cT}{\chi}$ makes the thermal de Broglie wavelength λ_T longer, so the MIC occurs at a higher temperature w.r.t. the system at $H = 0$.

Furthermore the shift of the minimum of ρ causes a strong positive transverse magnetoresistance (MR) at low T, as experimentally seen.[66, 17] At higher temperatures, in the region where dissipation dominates, the shift of diamagnetic susceptibility due to the Chern-Simons term induces a reduction of resistivity, a tendency contrasted by the classical cyclotron effect on holons, which can be taken into account in the Boltzmann equation approximation.

One then has two possible types of MR curves: one is always positive but it exhibits a knee below the crossover temperature between the mass gap and the dissipation dominated regions (See Fig. 3 in Ref. [50]). This behavior can be compared with the one observed in LSCO reported in Ref. [66] and one finds a reasonably good agreement.

If, on the contrast, the quantum effects related to $\sigma_h(H)$ are sufficiently strong, a minimum develops, eventually leading to a negative MR in some region around it.

The MR scales quadratically with H (See Fig. 2 in Ref. [50]) in agreement, in particular, with data on LSCO, [17] away from the doping $\delta = 1/8$ where the stripe effects dominate.

Finally we notice that in Zn-doped superconducting samples of BSLCO the MIC become observable upon increase of Zn doping (when a magnetic field suppresses superconductivity) and it shifts to higher temperature as the level of Zn-doping increases.[52] This effect is qualitatively consistent with our picture. In fact, the Zn-doping disturbs the AF background, so making the AF correlation length *shorter*, i.e. shifting the MIC temperature *up*.
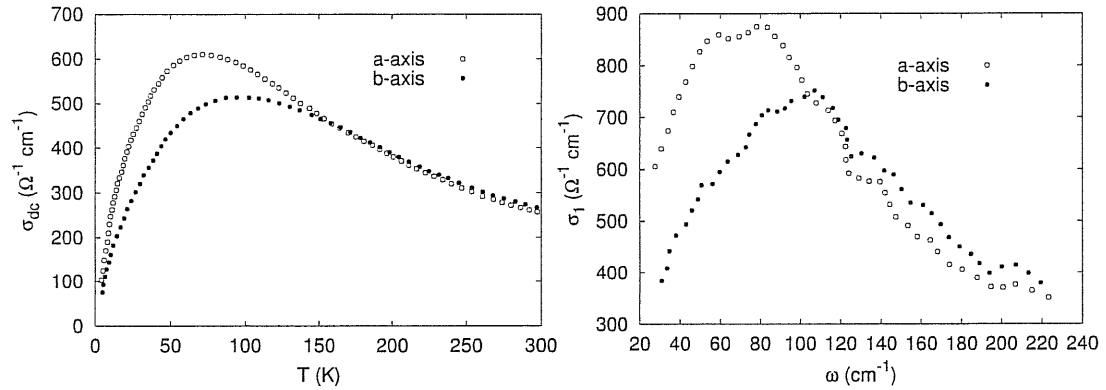
Figure 4.2: Static (left) and dynamical (right) a-b conductivities for a LSCO sample with Sr content $x = 0.03$. From Dumm et al. [53].

4.4 Far Infrared AC Conductivity

Recently, Dumm et al. [53] analysed the in-plane dynamical conductivity of un-twinned $La_{1.7}Sr_{0.3}CuO_4$ crystals. In the Far Infrared region at high temperatures, the data are consistent with a simple Drude model. Below 80 K, a broad resonance appears at finite frequency ($\omega \sim 100$ cm^{-1}) bearing a close resemblance to the peak found in DC conductivity for the same sample; at the same time, a significant a-b resistivity anisotropy is observed in complete analogy with the DC case [54].

The maximal anisotropy $\rho_b/\rho_a - 1$ reaches 50% for 3% doped LSCO which is far too big compared with the orthorhombicity (up to 1.7%).[54] A "natural" explanation of this unusual behavior would be the "self-organized" charge stripe structure, proposed by a number of authors.[55] The conductivity is indeed higher in the stripe direction (along the a-axis)[56] as further confirmed by the AC data of Dumm et al.[53].

However, this intuitive "rivers of charge" interpretation suffers from two main difficulties:

- The mean-field theory predicts the statically charge-ordered state is an insulator,[55] while experimentally these lightly doped cuprates show metallic behavior at high temperatures [54].

- The observed anisotropy ratio is too small compared with quasi-one-dimensional (Q1D) conductors, usually showing order-of-magnitude bigger conductivity along the chain direction.

To avoid these problems, the "electronic liquid crystal" scenario of meandering stripes[58, 57] is invoked to induce metallic conductivity and to reduce the expected

anisotropy. This picture, however, seems not consistent with experimets: a closer examination of the data[54, 53] reveals that the anisotropy effect is most pronounced in the limit $\omega, T \to 0$. If the effect is mainly *static*, why one needs to invoke *dynamical* stripe fluctuations? This was also pointed out in Ref.[53].

In Section 4.3 we have shown that the large positive in plane magnetoresistance found in underdoped cuprates at low T is due to a shift of the MIC temperature as a function of the applied magnetic field. It is evident from the experimental curves[54, 53] that *the major source of the in-plane conductivity anisotropy is also due to the shift of the MIC energy-scale.*

Motivated by these qualitative arguments, below we generalize the spin-charge formalism to frequency-dependent phenomena and show the AC-conductivity exhibits a maximum as function of frequency in an exact analogy with the DC conductivity maximum due to MIC.

In presence of an external field of frequency Ω, the propagator for the gauge field has a natural cut-off energy scale $\Lambda = \max(\Omega, T)$. The spinon-gauge sector dominates the low energy physics of the system and the spinon conductivity is due to scattering against thermal gauge fluctuations, so the entire $T-$dependence comes from $\Lambda = T$.

For small but finite frequencies $\Omega \ll m_s$ and $T = 0$, we have $\Lambda = \Omega$, so we expect that the dynamical conductivity $\sigma_1(\Omega)$ shows a broad peak which is the AC analogue of T_{MIC}.

Let us now consider the theory in more details[60]. The effect of Reizer singularity on gapless fermions is subdominant; it has been analyzed in Ref.[41] and at finite T it gives an inverse scattering rate for the holon of order $T^{4/3}$ instead of the usual Fermi liquid result $\sim T^2$.

In order to include, non-perturbatively, the effect of gauge fluctuations in the spinon current-current correlator, in Sect. 3.2 we first expanded the spinon propagator in Feynman paths, as justified by the mass gap, and we integrated over velocity fields in eikonal approximation. Being *gauge invariant*, the correlator of the spinon current depends only on the gauge field strength F.

As mentioned above, Λ enters as a frequency cut-off in the large scale propagator for the magnetic component F_{ij} of the gauge field, see (3.23). For the sake of clarity, we first summarize the DC calculations ($\Lambda = T$) presented in Sect. 3.2, 4.1 leading to the explicit formula (4.7) for the in-plane resistivity.

As $\omega < T$, we approximate $\coth \frac{\omega}{2T} \simeq \frac{2T}{\omega}$, then the ω-integration in (3.23) be-

comes

$$\int_0^T \frac{d\omega}{2\pi} \frac{2T}{(\omega)^2 + (\frac{\chi|\vec{k}|^3}{\kappa})^2}, \tag{4.14}$$

eventually leading to an evaluation of the large-scale "magnetic" propagator:

$$-i\frac{T}{4\pi\chi} Q_0^2 e^{\frac{-Q_0^2|\vec{x}|^2}{4}}, \tag{4.15}$$

where $Q_0 = (\frac{T\kappa}{\chi})^{1/3}$ is the typical momentum scale for gauge fluctuations. The effects of thermal gauge fluctuations on the massive spinon propagator are described by the functions f, g: at low T they introduce a dissipative term in the spin gap:

$$m_s \rightarrow M_T = (m_s^2 - icT/\chi)^{1/2}, \tag{4.16}$$

where $ic = f(Ce^{i\pi/4})$ is a numerical constant. This leads to the following thermal behaviour for the DC spinon conductivity [see (4.7)]:

$$\sigma(T) \sim \left(\frac{\delta}{f''(Ce^{i\pi/4})|M_T|}\right)^{1/2} \sin(\arg\frac{M_T}{2}). \tag{4.17}$$

The competition between the gap term m_s^2 and the dissipation T/χ causes a MIC upon decrease of temperature.

We turn now to the AC conductivity at $T = 0$ and set $\Lambda = \Omega$. In this case $\coth\frac{\omega}{2T}$ is replaced by $\text{sgn}\omega$ and the ω-integration in (3.23) becomes:

$$\int_0^\Omega \frac{d\omega}{2\pi} \frac{\omega}{(\omega)^2 + (\frac{\chi|\vec{k}|^3}{\kappa})^2}. \tag{4.18}$$

Up to logarithmic accuracy, one finds for the magnetic propagator at large scales:

$$-i\frac{\Omega}{4\pi\chi} Q_\Omega^2 \lambda e^{\frac{-Q_\Omega^2|\vec{x}|^2}{4}}, \tag{4.19}$$

where $Q_\Omega = (\frac{\Omega\kappa}{\chi})^{1/3}$ and λ is a positive constant, with $\lambda \lesssim 1/2$, as follows from comparing (4.18) and (4.14).

Repeating the steps of the DC calculations with this parameter λ included, we find as the analog of (4.16):

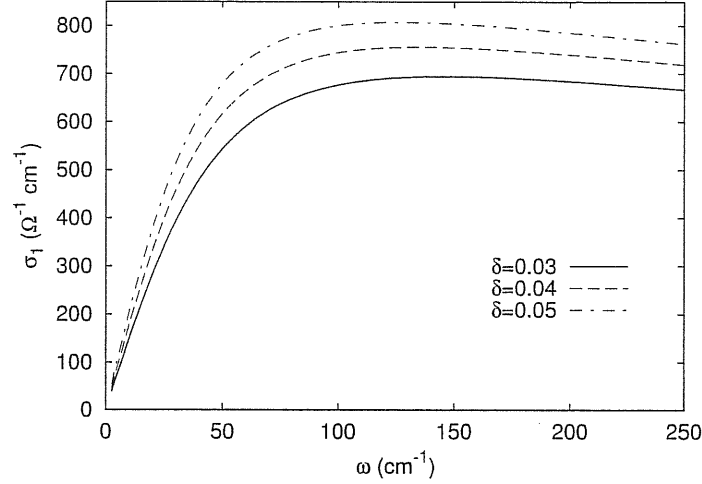$$m_s \rightarrow M_\Omega = (m_s^2 - ic\lambda\Omega/\chi)^{1/2}. \tag{4.20}$$

Figure 4.3: Predicted frequency dependence of the AC conductivity for different hole contents δ.

For $\Omega \ll 2m_s$, one easily obtains for the AC conductivity:

$$\sigma_1(\Omega) \sim \left(\frac{\delta}{\lambda f''(Ce^{i\pi/4})|M_\Omega|} \right)^{1/2} \sin(\arg \frac{M_\Omega}{2}). \qquad (4.21)$$

We see that the behavior of the AC conductivity at $T = 0$ is rather similar to that of the DC conductivity, with a broad peak corresponding to a MIC, hardening and shifting to lower temperature upon doping increase, see Fig. 4.3.

The main differences are that the peak in the AC conductivity appears magnified and shifted to higher frequency with respect to the DC counterpart due to the factor λ, see Fig. 4.4, in qualitative agreement with experimental data[53].

We next consider finite temperature effects for the dynamical conductivity $sigma_1(\Omega)$.

For $T \ll \Omega$, the leading correction is a renormalization of M_Ω in 4.20. A perturbative calculation gives $M_\Omega^2 \to M_\Omega^2 + C(T)$, with the small correction $C(T)$ given by

$$C(T) = -\frac{T}{\chi} f \left((\frac{T}{\Omega})^{1/3} e^{i\frac{\pi}{4}} \right). \qquad (4.22)$$

Since for small α, $f(\alpha) \sim \alpha^2$, $C(T)$ is purely imaginary and of order $(T/\Omega)^{5/3}$. Its leading effect is to increase the damping rate inducing a shift of Ω_{MIC} to lower frequency. This effect would be more pronounced for higher doping concentrations but the peak rapidly disappears because of the intervening superconducting transition
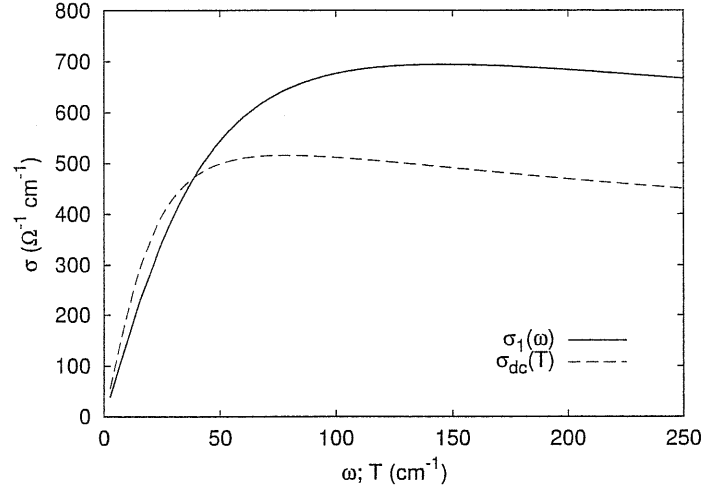
Figure 4.4: Calculated frequency dependence of the AC conductivity for $\delta = 0.03$. The corresponding DC conductivity as a function of temperature is shown with dashed line in the same units (cm^{-1}).

at $T_c \sim \Omega_{MIC}$. Experimentally, the peak in AC conductivity is indeed not seen for $\delta \gtrsim 0.06$[61].

For $\Omega \lesssim T$, instead, the $\Omega = 0$ result applies and the conductivity will be frequency independent and equal to the DC value.

Therefore upon temperature increase, the MIC peak is expected to *shrink asymmetrically* and eventually disappear from the spectrum.

The limits of validity of the approximations involved in the calculation of the spinon bubble are given by (4.4) with T replaced by Ω. We recall that the above calculations does not take into account the holon contribution to the physical conductivity, but this is of order $\Lambda^{4/3}$, hence negligeable for small cutoff Λ.

We close this section by suggesting a feasible experiment which can further support our interpretation of the far-infrared AC data: to repeat the experiment using underdoped superconducting samples in the presence of a strong magnetic field suppressing superconductivity. On the basis of the results found in the previous sections, our predictions are rather tight:

- at very low temperatures a broad peak does emerge from the Drude response;

- the peak shifts to higher frequency by further increasing the magnetic field.

Such an experiment is already in progress [61].

4.5 In-plane $a - b$ Resistivity Anisotropy

Let us discuss how the $a - b$ resistivity anisotropy found [54, 53] in untwinned single crystals of $La_{2-x}Sr_xCuO_4$ ($x = 0.02 - 0.04$) can fit into our scheme.[60]

The neutron scattering experiments have revealed incommensurate magnetic structure in lightly doped LSCO samples ($\delta \leq 0.05$).[62] Unlike the superconducting LSCO compounds where the deviation of the elastic magnetic scattering peaks from (π, π) is along the a, b directions in the tetragonal basis,[63] these peaks are rotated by 45 degrees around (π, π), *i.e.*, they are located along the b^* axis in the orthorhombic basis, or along the diagonal of the tetragonal basis.

Moreover, from the half-width of the elastic peaks one can determine the magnetic correlation length in different directions. As a big surprise, one finds the correlation length strongly anisotropic. In particular, for $\delta = 0.024, \xi'_{a*} = 94.9A, \xi'_{b*} = 39.9A$.[56] The authors of Ref. [56] interpreted this result as due to stripe formation along a-axis, although no quantitative argument was given.

We do not have a quantitative microscopic theory to consider the anisotropy of the AF correlation length, but we take this experimental fact as our starting point to explore its consequences. Since the spinon mass m_s is inversely proportional to the correlation length, we assume $m_{s,a} < m_{s,b}$. This anisotropy is not due to the orthorhombicity which is much smaller, up to 1.7%.[54] Similarly, the diamagnetic susceptibility χ which is inversely proportional to the holon effective mass, should be also anisotropic.

As discussed in Section 4.1, the combination $\chi m_s^2 = \frac{t}{6\pi}|\ln \delta|r$ is crucial in determining the MIC point. If we assume that the basic results of our theory developed for the 2D isotropic model survives the generalization to anisotropic case, one would anticipate the parameter r to be also anisotropic. In view of the above discussion we expect $r_a/r_b < 1$. As a consequence, the peak in σ_a will be shifted to lower temperature with respect to σ_b, as follows from Eq.(4.16); the anisotropy ratio σ_a/σ_b will show a sharp increase near the MIC and saturates as $T \to 0$, in agreement with experiments. [54]

The same phenomenon occurs for the AC conductivity at low temperatures, where the factor λ makes the anisotropy ratio even bigger. To estimate this enhancement, we extract the ratio r_a/r_b by fitting the DC data (the extracted value $r_a/r_b = 0.725$). We can then use (4.21) to evaluate the corresponding anisotropy ratio for AC conductivity without introducing any additional parameters; a comparison with the experimental curve is shown in Fig. 4.5.
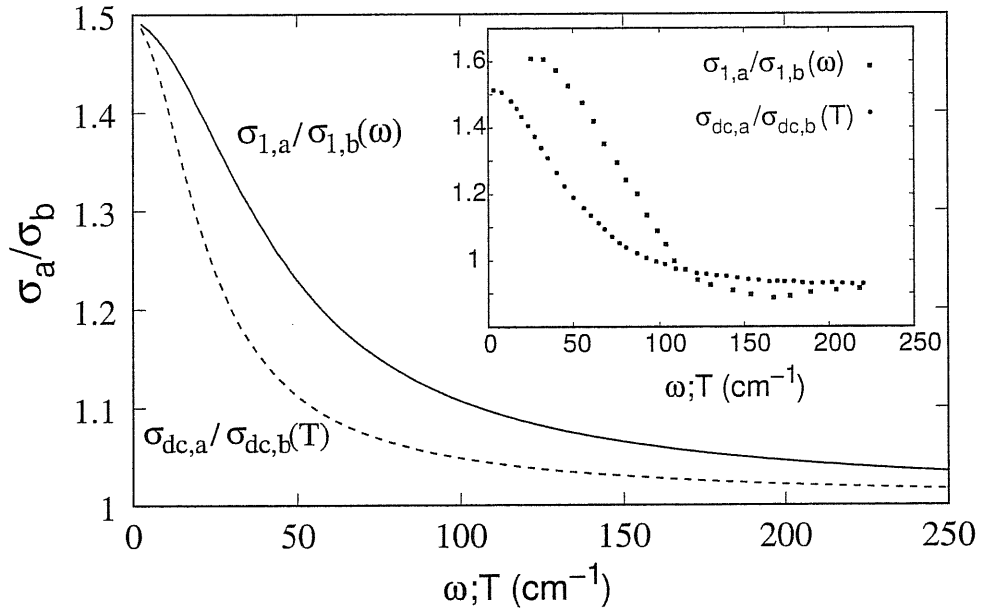
Figure 4.5: Calculated AC anisotropy ratio versus ω and DC anisotropy ratio versus T for hole content $\delta = 0.03$. Inset: AC and DC anisotropy ratio for a $La_{1.7}Sr_{0.3}CuO_4$ sample. From Dumm et al. [53]

This anisotropy is less pronounced than the experimentally observed value for AF correlation length, as quoted above for $\delta = 0.024$, but we should bear in mind that part of the anisotropy effect in the combination χm_s^2 has already been cancelled since presumably $m_{h,a} < m_{h,b}$.

4.6 Spin-Lattice Relaxation Rate

The spin-lattice relaxation rate for the Cu-sites has been computed within our approach in Ref. [48]. The hyperfine field $\vec{A}(\vec{q})$ is peaked around $Q_{AF} = (\pi, \pi)$, thus probing the AF spin fluctuations.

Since the electron spin field $\vec{S}(x) = c^\dagger \frac{\vec{\sigma}}{2} c(x)$ is related to the spinon and holon fields by

$$\vec{S}(x) \sim (1 - H^* H(x)) e^{i\vec{Q}_{AF}\cdot\vec{x}} \vec{\Omega}(x).$$

we find:[4]

$$\lim_{\omega\to 0} \frac{\mathrm{Im}\chi_s(\mathcal{Q}_{AF} + \vec{q}, \omega)}{\omega} \sim \mathrm{Im} \int_0^\infty dx_0 i x_0 \int d^2 x \cdot (1 - \delta)^2 < \vec{\Omega}(x) \cdot \vec{\Omega}(0) > e^{i\vec{q}\cdot\vec{x}}.$$

(4.23)

The retarded magnon correlator in momentum space is obtained from the Fourier transform of (3.31); for positive ω we get:

$$\langle \vec{\Omega} \cdot \vec{\Omega} \rangle(\omega, \vec{q}) \sim \frac{Z_\Omega}{\omega - 2\sqrt{m_s^2 - ic\frac{T}{\chi}}} J_0(|\vec{q}| C Q_0^{-1} e^{i\pi/4}),$$

(4.24)

where J_0 is the Bessel function and Z_Ω is defined in (4.6).

Using a cutoff $|\vec{q}| \lesssim Q_0$ for the integration over momentum in (1.4) and assuming that $\vec{A}(\vec{q})$ is smooth at this scale we derive

$$\int d\theta \int_{|\vec{q}|<Q_0} d|\vec{q}||\vec{q}| \quad |\vec{A}(\vec{q})|^2 e^{i\vec{q}\cdot|\vec{x}|(0)\cos\theta} \sim Q_0^2 J_0(C e^{i\pi/4}).$$

(4.25)

Numerically one finds $\mathrm{Re} J_0(ce^{i\pi/4}) \equiv a$ and $\mathrm{Im}\ J_0(ce^{i\pi/4}) \equiv b$ with $a/b \sim 0.1$. Plugging (4.25) and (4.24) in (4.23) one obtains from (1.4)

$$\frac{1}{T_1 T} \sim (1 - \delta)^2 \sqrt{\delta} |M|^{-\frac{1}{2}} (a \cos(\frac{\arg M}{2}) + b \sin(\frac{\arg M}{2})).$$

(4.26)

For low T, $\frac{1}{T_1 T} \sim a + bT$ and for higher T one finds $\frac{1}{T_1 T} \sim T^{-1/4}$; therefore the spin lattice relaxation rate ($\frac{1}{T_1 T}$) on Cu- sites exhibits a maximum and an inflection point at higher temperature, as observed in YBCO underdoped samples.[65]

If a would be 0, then $\frac{1}{T_1 T}$ would be proportional to the spinon conductivity σ_s. However, due to the a term in (4.26) the minimum and the inflection points are shifted w.r.t. their analogues in σ_s.

---

[4]As usual, we approximate $H^* H$ by its mean field value δ.

In particular, the inflection point is at a lower temperature T_0, in qualitative agreement with the fact that experimentally the pseudogap temperature deduced from spin-lattice relaxation rate is lower than that derived from resistivity measurements.[67]

4.7 Out-of-plane Resistivity

Let us summarize the results of Sect. 3.3 needed to compute ρ_c using the K-J's approach.

In the temperature range $m_s^2 \leq \frac{T}{\chi} \leq m_s Q_0$, the gauge fluctuations couple spinon and holon close to the FS into an "electron" resonance with scattering rate Γ proportional to the inverse life-time of the magnon, hence from (3.50) we get

$$\Gamma = -\text{Im} \sqrt{m_s^2 - ic\frac{T}{\chi}} \sim \begin{cases} \frac{JT}{t}\left(\frac{\delta}{|\ln\delta|}\right)^{\frac{1}{2}}, & \frac{T}{\chi m_s^2} \ll 1 \\ J\left(\frac{T\delta}{t}\right)^{\frac{1}{2}}, & \frac{T}{\chi m_s^2} \sim 1. \end{cases} \tag{4.27}$$

The wave function renormalization constant (3.49) shows a weak temperature dependence $Z \sim \sqrt{q_0}m_s \propto T^{1/6}$ due to the fact that the binding of holon and spinon is induced by *thermal* gauge fluctuations.

To compute ρ_c we average the angular dependence of $S(\theta)$ and insert (4.27) and (3.49) in K-J's formula eq.(3.7).

In the "confined regime", relevant for the Pseudogap phase, we have $\rho_c \sim \frac{1}{\Gamma}$ with a coefficient independent of t_c. From (4.27) we see that for low T, $\rho_c \sim T^{-1}$ and for higher temperatures it decreases more slowly as $\rho_c \sim T^{-1/2}$. These features reproduce qualitatively the behavior observed experimentally in several materials (LSCO,YBCO...) in the "pseudogap phase", included the *rounded knee* mentioned in Chapter 1 which corresponds to the above change of temperature dependence.

As a consequence of K-J's approach, the c–axis resistivity $\rho_c(T)$ at low T gives a direct test for the thermal behaviour of the electron scattering rate in the pseudogap phase.

The "metallic" contribution of the second term is important only at relatively high temperature ($T > 300$ K), where it scales as $T^{1/6}$, causing a further flattening of the $\rho_c(T)$ curves or possibly a minimum.

Apart from an overall scale, having already fixed with ρ_{ab} the variable χm_s^2, our formula has only one free parameter, the scale of Z, i.e. essentially the scale λ controlling the cutoff on momenta perpendicular to the FS, $\Lambda = k_F/\lambda$ and weighting the "metallic" contribution. This parameter should be a somewhat large number and might be roughly estimated by fitting ρ_c for one doping concentration.
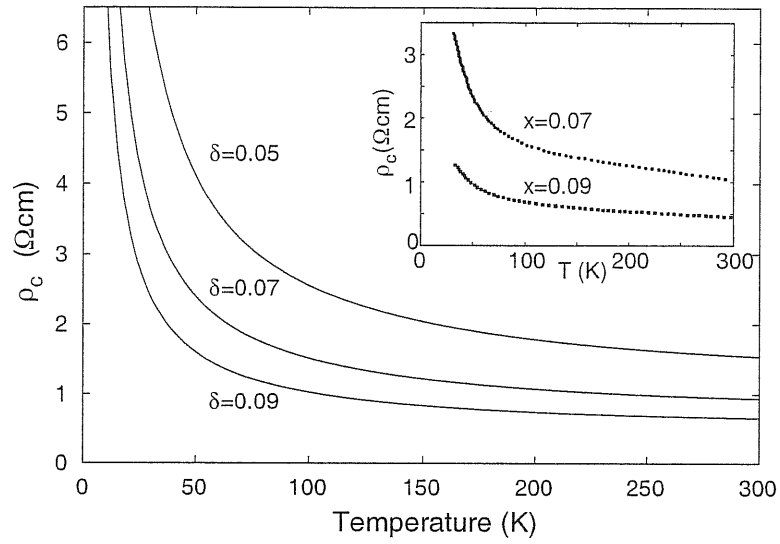
Figure 4.6: Calculated temperature dependence of the out-of-plane resistivity (in arbitrary units) for different doping concentrations: δ=0.05 (full line), δ=0.07 (dashed) and δ=0.09 (dotted). Inset shows experimental data on LSCO, extracted from Ref. [17]

For *other* dopings the T-dependence behavior of ρ_c is then derived and as one can see from Fig. 4.6, the theoretical results are in quite good agreement with experimental data.[68]
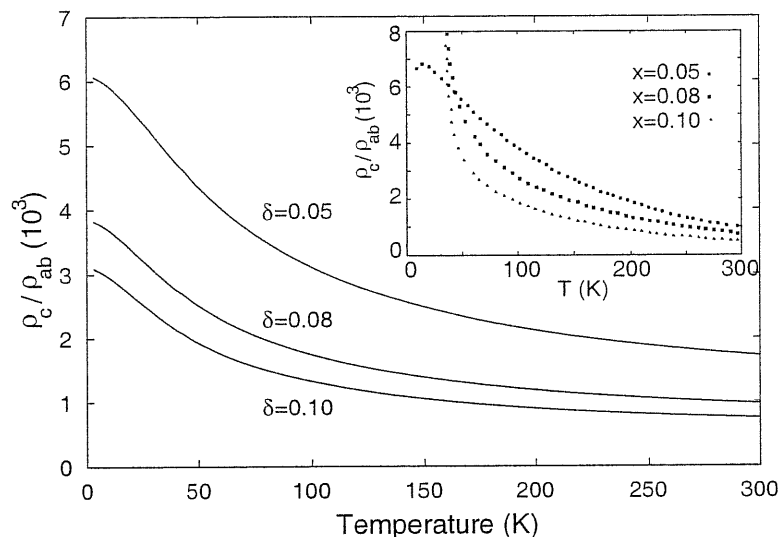
Figure 4.7: Calculated temperature dependence of the resistivity anisotropy ratio as a function of temperature for different doping concentration: δ=0.05 (full line), δ =0.07 (dashed) and δ=0.09 (dotted). Inset shows corresponding experimental data on LSCO, extracted from Ref. [18]

4.8 Resisitivity Anisotropy Ratio

Having an explicit theoretical dependence on δ and T for both ρ_c and ρ_{ab} one can further analyze the anisotropy ratio $\frac{\rho_c}{\rho_{ab}}$.

The derived temperature dependence of this ratio for different hole contents is shown in Fig. 4.7.

This ratio clearly saturates at low T, since both ρ_c and ρ scale as $\frac{1}{T}$ but at higher temperatures, in the "metallic" region for in-plane resistivity, the ratio decreases like $T^{-1/4}$.

Again this behavior is qualitatively consistent with the experimental data in the "pseudogap phase"[1, 15], as shown in the inset of the same figure. The drastic upturn at low T for Sr content $x = 0.08, 0.10$ is due to proximity to the superconducting transition: by applying a strong pulsed magnetic field suppressing superconductivity, the anisotropy ratio is indeed known to saturate at low temperatures. [16]

Chapter 5

Strange Metal

5.1 Introduction

Our spin-charge gauge theory was originally formulated to describe the MIC in ρ_{ab} and related phenomena taking place in the Pseudogap; its range of applicability was therefore limited to underdoped systems and low temperatures where the spin correlation lenght ξ is smaller or of the order of the thermal De Broglie wavelenght, i.e. $\xi \lesssim \lambda_T$. At higher temperatures $T \sim T^*$, underdoped cuprates cross over a new "phase" called Strange Metal. Overdoped cuprates, also, reach this phase at relatively high T but presumably from an ordinary Fermi Liquid.

The Strange Metal phase is *metallic* in nature with anomalous yet very simple temperature dependences of physical observables such as the celebrated $T-$linearity of both in-plane and out-of-plane resistivities. In optimally doped samples this simple law extends from just above T_c to temperatures of order J ($\sim 1000K$)[10].

Experimentally, the "Strange Metal" shares with the "Pseudogap" a fairly robust short range antiferromagnetism (SRAF) which in our approach originates from the gapping of spin waves due to scattering against the vortices attached to the moving holes. In the following we will assume that the low energy effective action S_s for spinons is still given by (2.36) with $m_s^2 \approx |\delta \ln \delta|$. We emphasize that our derivation makes sense only if the AF correlation length is larger than the lattice spacing, i.e. $\xi = m_s^{-1} \gtrsim a$, and therefore fails when the density of holes is very large.

There are strong indications, in particular from ARPES experiments[69], that charge degrees of freedom undergo instead a radical rearrengement near the crossover temperature T^*: the excitations far from the zone diagonals, i.e. located near $(\pi, 0)$ of the Brillouin zone, become gapless and lead to a *large* closed Fermi surface. This means that the density of *effective* charge carriers has grown from δ to $1 - \delta$, the value

expected from band structure calculations.

The increase of the electron density of states at the (new) Fermi surface leads to a renormalization of the parameters (diamagnetic susceptibility χ, Landau damping κ) that appear in the Reizer propagator (2.43) for the transverse gauge field.

As a result, gauge fluctuations in the spinon sector strengthen and dominate over the spin gap at all temperatures down to T^* for the underdoped samples, thus driving the thermal behaviour of many physical properties. In particular we shall recover some of the distinctive features of the Strange Metal, namely the $T-$linearity of in-plane and out-of-plane resistivities and the T^{-1} behaviour for $\frac{1}{T_1 T}$.

Our theoretical understanding of the Strange Metal is however less clear near optimal doping and very low temperatures where the inequality $\xi \gtrsim \lambda_T = (\chi/T)^{\frac{1}{2}}$ ceases to be valid.[1] This is indeed the realm of superconductivity and we do not have a theory for it.

In this chapter we go through the same analisys as for the Pseudogap: we first find the optimal spinon configuration leading to a new low energy effective action for holons, then we compute the effects of gauge fluctuations on the spinon-spinon and spinon-holon correlation functions and finally we apply the obtained results to evaluate thermal and doping dependences for the in-plane and out-of-plane resistivities and the spin-lattice relaxation rate.

5.2 Optimization

In our approach, the increase in the density of state at the Fermi energy ε_F reflects a change in the dispersion relation. The $\pi-$ flux statistical field that minimizes the ground state energy near half filling was responsible for the small Fermi surface in the Pseudogap phase.

Since the Strange Metal is metallic in nature, we expect that in this phase there are no magnetic fields to frustrate the charge motion and therefore we assume

$$arg(U_{\partial p}) = 0, \qquad (5.1)$$

where $arg(U_{\partial p})$ denotes the statistical magnetic flux per plaquette.

The corresponding optimal spinon configuration is found by fixing explicitly the variables $\tilde{g}_j$. We defer the details to the Appendix quoting here the main results.

---

[1] A related problem is the behaviour of the pseudogap temperature T^* near optimal doping. Loram et al.[20] claimed that an extrapolation of their experimental estimate for T^* is only consistent with a vanishing T^* at the presumed critical point $\delta_c \simeq 0.19$ but this issue is still under strong debate.

Writing $\tilde{g}_j = e^{i\vec{\sigma}\cdot\vec{n}_j}$, we find n_j of the form $n_j = (\cos\phi_j, \sin\phi_j, 0)$ with ϕ_j given by:

$$\phi_j = \begin{cases} \frac{\pi}{4}(-1)^{|j|} & \text{if } H_j^* H_j = 1 \\ -\frac{\pi}{2}(-1)^{|j|} & \text{if } H_j^* H_j = 0. \end{cases}$$

In view of a Mean Field Approximation (MFA), it is convenient to introduce new spin variables R_j measuring fluctuations around the optimal configuration:

$$g_j = \bar{g}_j R_j \tilde{g}_j = e^{-\frac{i}{2}\sum_{\ell \neq j}(-1)^\ell \sigma_z \arg(\ell-j)} R_j \tilde{g}_j. \tag{5.2}$$

The key point is that we self-consistently expect the variable R_j to be slowly varying at the lattice scale so that it makes sense to take the continuum limit by expanding $R_j := R(j)$ in powers of the lattice constant a.

Plugging (5.2) into (2.19),(2.20) we get a new exact version for the $t - J$ model effective action $S = S_h + S_s$:

$$S_h = \int_0^\beta dx^0 \Big\{ \sum_j H_j^* [\partial_0 - (\sigma_x^{|j|} \tilde{g}_j^\dagger R_j^\dagger \partial_0 R_j \tilde{g}_j \sigma_x^{|j|})_{11} - \mu] H_j$$

$$+ \sum_{<ij>} [-t H_j^* e^{-i\int_{<ij>} \delta B} H_i (\sigma_x^{|i|} \tilde{g}_i^\dagger R_i^\dagger P e^{i\int_{<ij>}(\bar{V}+\delta V)} R_j \tilde{g}_j \sigma_x^{|j|})_{11} + h.c.] \Big\} \tag{5.3}$$

$$S_s = \int_0^\beta dx^0 \Big\{ \sum_j (\sigma_x^{|j|} \tilde{g}_j^\dagger R_j^\dagger \partial_0 R_j \tilde{g}_j \sigma_x^{|j|})_{11}$$

$$+ \sum_{<ij>} \frac{J}{2}(1 - H_i^* H_i)(1 - H_j^* H_j) \left[|(\sigma_x^{|i|} \tilde{g}_i^\dagger R_i^\dagger P e^{i\int_{<ij>}(\bar{V}+\delta V)} R_j \tilde{g}_j \sigma_x^{|j|})_{11}|^2 - \frac{1}{2} \right] \Big\}. \tag{5.4}$$

The remarks below (2.27) apply here as well. We note that the statistical field $\bar{B}$ has disappeared in S_h, cancelled by an appropriate choice for the phase factors θ_j, as explained in the Appendix.

The field $V^{(c)}$ carries $0-$flux per plaquette and its Mean Field value $\bar{V} = V^c(g^m)$ is the same as for the Pseudogap[2] and given by (5.50). The fields $\delta B, \delta V$ will again be neglected in the subsequent analysis while the variables $\tilde{g}_j$ are replaced by their istantaneous values in terms of ϕ_j. Once this is done, we obtain the following simplified actions:

---

[2]Note that the field $V^{(c)}$ defined in (2.18) has contributions only from non empty sites and therefore its mean field value does not depend on the variables $\tilde{g}_j$.

$$S_h = \int_0^\beta dx^0 \left\{ \sum_j H_j^* [\partial_0 - (\sigma_x^{|j|} R_j^\dagger \partial_0 R_j \sigma_x^{|j|})_{11} - \mu] H_j \right.$$

$$\left. + \sum_{<ij>} [-t H_j^* H_i (\sigma_x^{|i|} R_i^\dagger P e^{i \int_{<ij>} \vec{V}} R_j \sigma_x^{|i|})_{11} + h.c.] \right\} \qquad (5.5)$$

$$S_s = \int_0^\beta dx^0 \left\{ \sum_j (\sigma_x^{|j|} R_j^\dagger \partial_0 R_j \sigma_x^{|j|})_{11} \right.$$

$$\left. + \sum_{<ij>} \frac{J}{2} (1 - H_i^* H_i)(1 - H_j^* H_j) \left[|(\sigma_x^{|i|} R_i^\dagger P e^{i \int_{<ij>} \vec{V}} R_j \sigma_x^{|j|})_{11}|^2 - \frac{1}{2} \right] \right\}. \qquad (5.6)$$

Note in particular that the spinon action (5.6) is formally identical to that considered for the Pseudogap case [see (2.27)], thus leading to the same low energy effective action (2.36).

Since $\bar{B} = 0$, the dispersion relation for bare holons has changed from the $\pi-$flux phase spectrum $\epsilon^{PG}(\vec{p}) = \pm 2t \sqrt{\cos(p_x a)^2 + \cos(p_y a)^2}$ restricted to the magnetic Brillouin zone to the more conventional tight binding spectrum $\epsilon^{SM}(\vec{p}) = 2t(\cos(p_x a) + \cos(p_y a))$ defined in the entire Brillouin zone.

5.3   Holon Effective Action

In this section we derive the low energy effective action for holons. The matrix element in the hopping term is expanded in powers of the lattice constant a. Using the usual CP^1 representation for R_j, see (2.28), and the fact that $z_{j\alpha}$ are slowly varying at the lattice scale a, we find

$$(\sigma_x^{|i|} R_i^\dagger P e^{i \int_{<ij>} \vec{V}} R_j \sigma_x^{|j|})_{11} \simeq 1 + ia\bar{V}_z (z_{i\alpha}^* \sigma_z^{\alpha,\beta} z_{i\beta}) + (-1)^{|i|} a z_{i\alpha}^* \partial_\mu z_{i\alpha} + O(a^2). \quad (5.7)$$

The term proportional to $\bar{V}_z$ is purely imaginary and it is cancelled by the $H.c.$. To the same degree of accuracy, for the temporal component we obtain:

$$\sum_j (\sigma_x^{|j|} R_j^\dagger \partial_0 R_j \sigma_x^{|j|})_{11} = \sum_j [(-1)^{|j|} z_{j\alpha}^* \partial_0 z_{j\alpha} - i\frac{a}{2}\vec{L}_j \cdot (\vec{\Omega}_j \wedge \partial_0 \vec{\Omega}_j) + O(a^2).] \quad (5.8)$$

thus leading to the low effective action (2.36) for spinons once the ferromagnetic variables L_j are integrated over.

Introducing the self-generated gauge field A_μ as in (2.37) and collecting all pieces, the holon effective action takes the simple form

$$S_h(H, H^*, A) = \int_0^\beta d^2x H_j^*(\partial_0 - \mu - iA_0)H_j + \sum_{<ij>}(tH_i^* H_j e^{i\int_{<ij>} A} + h.c.). \quad (5.9)$$

Neglecting gauge fluctuations, the Fermi surface is obtained by filling all the states up to $\mu := \epsilon_F \sim 2t\delta$ obtaining a large closed Fermi surface, contained in the reduced Brillouin zone. Note that the bottom of the band for the holes is at the corners of the Brillouin zone and we have to account for $1 + \delta$ empty states.

Since the chemical potential is near the center of the band, the density of states $\nu(\epsilon_F)$ at the Fermi surface is basically flat, independent of ϵ_F. A direct consequence is that in the Strange Metal the Landau damping $\kappa \propto \nu(\epsilon_F)v_F$ is almost doping independent.

Writing a continuum limit for the holon action is of course rather cumbersome because the Fermi momentum varies along the Fermi surface. As a crude approximation, we substitute the FS with a sphere having the same volume and make a *particle/hole* conjugation. The tight binding action defined on the square lattice is then replaced by a continuum action describing free particles ($\epsilon_k = k^2/2m$) with an effective chemical potential $\epsilon_F \sim 4t(1 - \delta)$, where $-4t$ corresponds to the bottom of the tight binding band.

The continuum low energy action describing "filled" states near the Fermi surface is given by

$$S^{free} = \int d\tau d^2x \left[\bar\psi(\tau, \vec{x})(\partial_\tau - \epsilon_F - iA_0 - \frac{1}{2m^*}(\nabla - i\vec{A})^2)\psi(\tau, \vec{x}) \right]. \quad (5.10)$$

Using the above simplified action, the Landau damping and diamagnetic susceptibility can be easily evaluated and have a weak dependence on doping in the relevant limit $\delta \lesssim 0.3$ as required. First note that $v_F \sim 2ta$ is doping independent, $k_F a \propto (1 - \delta)$ and therefore $m^* = k_F/v_F = (1 - \delta)/2ta^2$. The parameters entering the Reizer propagator (3.19) are then given by

$$\kappa \sim O(1 - \delta) \quad (5.11)$$

$$\chi = 1/12\pi m^* = \frac{ta^2}{6\pi(1 - \delta)}. \quad (5.12)$$

The main difference with respect to the Pseudogap estimates in Sect. 3.2.2 is that δ is now replaced by $(1-\delta)$ so that, roughly speaking, both quantities vary by a factor of order 5-10.

The decrease of the diamagnetic susceptibility implies that the thermal De Broglie wavelenght for holons is shorter w.r.t. the Pseudogap analogue and therefore spin-gap effects ($\xi^2 < \lambda_T^2$) are confined to very low temperatures (though they do not disappear, see below).

5.4 Gauge Effects in the Spinon Sector

The h/s gauge field renormalizes the massive spinons in a non trivial way. The expression (3.31) obtained for the *dressed* spinon-spinon correlator in the Pseudogap applies here as well:

$$\langle \vec{\Omega}(x) \cdot \vec{\Omega}(0) \rangle \sim \frac{1}{(x^0)^2 - |\vec{x}|^2} e^{-2i\sqrt{m_s^2 - \frac{T}{\chi}f(\frac{|\vec{x}|Q_0}{2})}\sqrt{(x^0)^2 - \vec{x}^2} - \frac{T}{2\chi}Q_0^2 g(\frac{|\vec{x}|Q_0}{2})\frac{(x^0)^2 - |\vec{x}|^2}{m_s^2 - \frac{T}{\chi}f(\frac{|\vec{x}|Q_0}{2})}}.$$

$$(5.13)$$

provided the new estimates for κ and χ are used.

It is important to note that, in contrast to the Pseudogap estimate (3.23), the new typical momentum scale $Q_0 = \frac{(1-\delta)^{(2/3)}}{a}\left(\frac{6\pi T}{t}\right)^{1/3}$ for gauge fluctuations is almost doping independent.

The spinon contribution ρ_s to the resistivity is calculated below. It may be useful, however, to give a rough estimate of the spinon mean free path. This can be done by noting that, since $\frac{T}{\chi} \geq m_s^2$ (or, equivalently, $\lambda_T^2 \leq \xi^2$), the damping rate in the exponent of (5.13) diverges when $f(\frac{|\vec{x}|Q_0}{2})$ is of order 1 or larger. Since $f(\alpha) \sim \alpha$ at large α, we find that the spinon travels at most a distance ℓ_{max} with $\ell_{max}Q_0 \sim \frac{\chi m_s^2}{T}$, so that $\ell_{max} \propto T^{-4/3}$.

We shall see below that ℓ_{max} sets the scale of the mean scattering rate Γ of the electron at the Fermi surface, i.e. $\Gamma(T) \sim v_s \ell_{max}^{-1} \propto T^{4/3}$. This result is used in Sect. 5.8 to derive the temperature dependence of the c-axis resistivity via Kumar's formula (3.7).

5.5 In-plane Resistivity

In order to apply Ioffe-Larkin rule, we need to evaluate the contribution of both sectors to the in-plane resistivity.

It is known, since Nagaosa and Lee[41], that for a 2D Fermi gas scattering against a U(1) gauge field with Reizer-like singularity, the inverse scattering time at the Fermi surface is proportional to $T^{4/3}$. This power law follows simply by scaling analisys and does not depend on the details of the dispersion relations. The contribution ρ_h from our gas of spinless holons is of the form

$$\rho_h \sim \left(\frac{1}{\tau_{imp}} + \epsilon_F (\frac{T}{\epsilon_F})^{4/3} \right) , \tag{5.14}$$

where we also added the contribution of impurities via Matthiessen rule. Since ϵ_F is of order t in the Strange Metal, ρ_h contains the small factor $(T/t)^{4/3}$ and we therefore expect it to be subleading w.r.t. the spinon contribution.

We now turn to spinons. In order to apply Kubo formula (3.4), we need to integrate over $|\vec{x}|$ to obtain $\langle \vec{j} \cdot \vec{j} \rangle (x^0, \vec{q} = 0)$. We again consider the region $x^0 \gg |\vec{x}|$. Since the propagator is non-vanishing only at short distances, the largest contribution comes from $|\vec{x}|Q_0 \lesssim 1$. We expand the functions $f(\alpha), g(\alpha)$ defined in (3.29) to the lowest significant order around $\alpha = 0$:

$$f(\alpha) \simeq \frac{f''(0)}{2}\alpha^2 = \frac{Q_0^2 |\vec{x}|^2}{24} \tag{5.15}$$

$$g(\alpha) \simeq g(0) = 1/8. \tag{5.16}$$

The spinon-spinon correlator (5.13), to the same accuracy, is given by

$$\langle \vec{\Omega}(x) \cdot \vec{\Omega}(0) \rangle \simeq \frac{1}{x^{0^2}} e^{-2im_s x^0 + i\frac{T}{\chi m_s}\frac{|\vec{x}|^2 Q_0^2}{24}} e^{-\frac{T}{2\chi}Q_0^2 g(0)\frac{x^{0^2}}{m_s^2}\left(1+\frac{T}{\chi m_s^2}\frac{|\vec{x}|^2 Q_0^2}{24}\right)}, \tag{5.17}$$

valid in the limit $x^0 \gg |\vec{x}|$ and $|\vec{x}| \lesssim Q_0^{-1}$. The current-current correlator $\Pi_s(x)$ is then given by

$$\Pi_s(x) \simeq \frac{4}{x^{0^2}}ba^2 e^{-a|\vec{x}|^2}, \tag{5.18}$$

where

$$b = e^{-2im_s x^0 - \frac{T}{2\chi m_s^2}g(0)Q_0^2 x^{0^2}} \tag{5.19}$$

$$a = \frac{T}{\chi m_s^2}\frac{Q_0^2}{24}\left(\frac{T}{2\chi m_s^2}g(0)Q_0^2 x^{0^2} - im_s x^0\right). \tag{5.20}$$

The integration over $|\vec{x}|$ is simply gaussian; assuming $\mathrm{Re}(a) \gg Q_0^2$, we are allowed to remove the cut-off:

$$\Pi_s(x^0, \vec{q} = 0) \simeq \frac{4b}{x^{0^2}} a^2 \int_{|\vec{x}|Q_0 \lesssim 1} e^{-a|\vec{x}|^2} |\vec{x}|^2 d^2 |\vec{x}| = \frac{4\pi b}{x^{0^2}}. \tag{5.21}$$

For the Kubo formula we obtain the following expression:

$$\frac{\Pi_s}{\omega}(\omega, \vec{q} = 0)\Big|_{\omega \to 0} \simeq \int dx^0 i x^0 \frac{4\pi}{x^{0^2}} e^{-2im_s x^0 - \frac{T}{2\chi m_s^2} g(0)Q_0^2 x^{0^2}}. \tag{5.22}$$

We note that the above integral is logarithmic divergent at short times: this is due to the fact that our working assumptions

$$x^{0^2} \mathrm{Re}(a) \gg 1, \quad \mathrm{Re}(a) \gg Q_0^2, \tag{5.23}$$

require x^0 sufficiently large (note that $\mathrm{Re}(a) \propto (x^0)^2$).

We may cure this unphysical divergence by introducing a UV cut-off for the integration over x^0 in (5.22). Since $|\vec{x}|Q_0 \lesssim 1$, we see that a natural cut-off is given by $x^0_{min} \sim \lambda Q_0^{-1}$ with $\lambda \gg 1$.

Integration via principal part evaluation then gives

$$\frac{\Pi_s}{\omega}(\omega, \vec{q} = 0)\Big|_{\omega \to 0} \simeq \frac{4\pi}{x^0} \frac{1}{-2m_s + i\frac{T}{2\chi m_s^2} g(0)Q_0^2 2x^0} b(x^0)\Big|_{x^0 = \lambda Q_0^{-1}}. \tag{5.24}$$

Requiring that $b(\lambda Q_0^{-1})$ is slowly varying and of order 1, we find for the spinon conductivity:

$$\sigma_s \simeq -\mathrm{Im} \frac{4\pi Q^0}{\lambda} \frac{1}{(-2m_s + i\frac{T}{\chi m_s^2} g(0)\lambda Q_0)}. \tag{5.25}$$

In the high temperature limit $Q_0 \gg m_s$, the damping rate in (5.25) dominates over the spin gap $2m_s$ and the spinon resistivity $\rho_s = \sigma_s^{-1}$ is linear in T:

$$\rho_s \simeq \frac{T}{\chi m_s^2} g(0)\lambda^2. \tag{5.26}$$

Moreover, the doping dependence of the slope coefficient $\alpha = \rho_s / T$ is found to be

$$\alpha(\delta) \propto \frac{1}{\chi m_s^2} \sim \frac{1 - \delta}{\delta |\ln \delta|}. \tag{5.27}$$

Neglecting the holon contribution (5.14), subleading for $T \ll t$, the above results reproduce qualitatively the T–linearity of the in-plane resistivity in the Strange Metal, *included the decrease of the slope upon doping increase*.
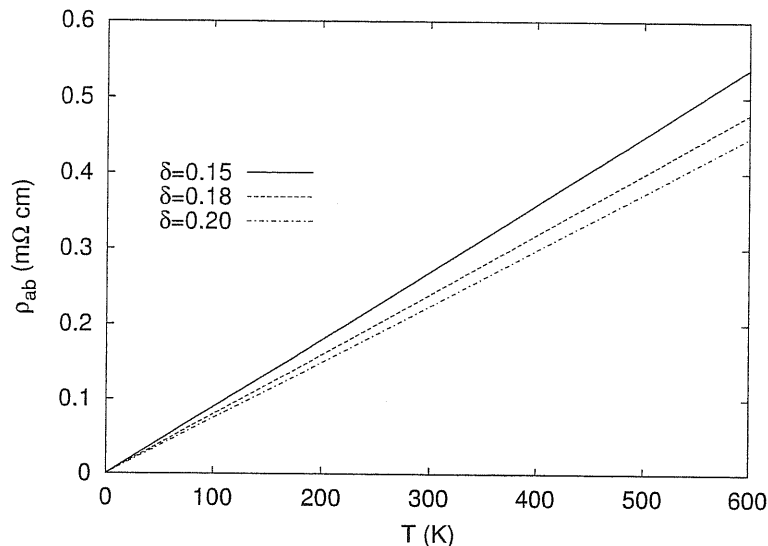
Figure 5.1: Calculated temperature dependence of the in plane resistivity for different dopings δ.

A very similar result is also predicted by the gauge field theory by Nagaosa and Lee[41] for the uniform RVB state. In slave boson theory holes are bosons and filled states are fermions. The resistivity is determined by the bosons and one finds

$$\rho \approx \rho_B \approx \frac{m_B}{\delta} T, \tag{5.28}$$

where m_B and δ are the mass and the density of bosons (holes).

In Fig. 5.1 we plot Eq.(5.26) versus temperature for different dopings; the arbitrariness in the slope coefficient due to the factor λ is eliminated by fitting it to the experimental data of Takagi et al.[10] for LSCO for $x = 0.15$, see Fig. 5.2. For other doping concentrations there are no free parameters in Eq.(5.26) and the agreement with experiments is reasonably good.

We remind that the derived formula applies only at high temperatures, while at low temperatures $\rho_s(T)$ has an unphysical upturn, due to spin gap effects. This is actually the most serious drawback of the present theory when applied to optimally doped cuprates where the linear-in-T behaviour of the in-plane resistivity extends at all temperatures down to T_c.
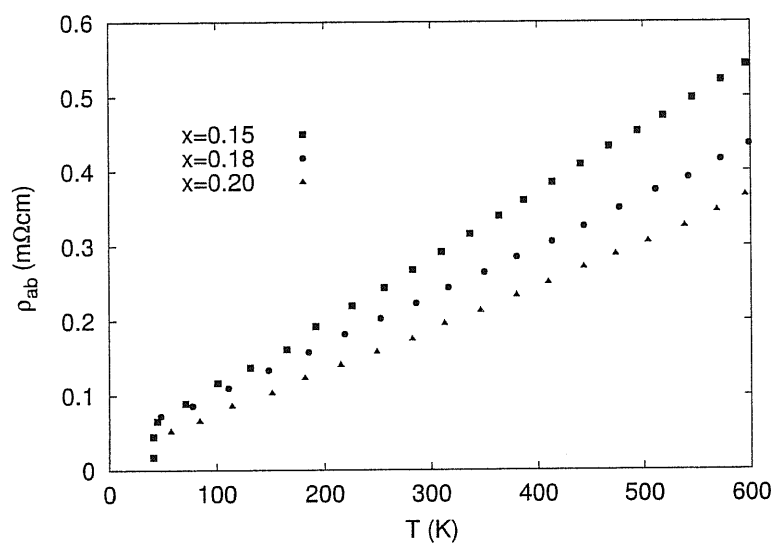
Figure 5.2: Temperature dependence of the in plane resistivity for LSCO single crystals with different Sr content. From [10]

5.6 Spin-lattice Relaxation Rate

From the experimental point of view, one of the hallmark of the Strange Metal is the very simple law for the Spin-lattice relaxation rate at the Cu-sites:

$$\frac{1}{T_1 T} \sim A^2 \lim_{\omega \to 0} \sum_{\vec{q}} \frac{\text{Im}\chi_s(\omega, \vec{q})}{\omega} F(\vec{q}) \sim \frac{1}{T}. \tag{5.29}$$

While in optimally doped samples the above relation is valid over a wide range of temperatures above T_c, in overdoped samples $\frac{1}{T_1 T}$ saturates to a constant (i.e. T-independent) value at low temperatures, suggesting a possible crossover to a Fermi liquid phase.

The formalism necessary to compute this important observable has been described in Sect. 4.6. There, it was shown that the imaginary part of the spin susceptibility $\chi_s(\omega, Q_{AF} + \vec{q})$ is related, for small $\vec{q}$ and ω, to the spinon-spinon correlator by the following formula:

$$\lim_{\omega \to 0} \frac{\text{Im}\chi_s(Q_{AF} + \vec{q}, \omega)}{\omega} \sim \text{Im} \int_0^\infty dx_0 i x_0 \int d^2x \cdot (1 - \delta)^2 < \vec{\Omega}(x) \cdot \vec{\Omega}(0) > e^{i\vec{q}\cdot\vec{x}}. \tag{5.30}$$

We again neglect $|\vec{x}|$ w.r.t. x^0 and expand the correlator as in the previous section. The integration over $|\vec{x}|$ then gives:

$$\int d^2|\vec{x}| e^{i\vec{q}\cdot\vec{x}} e^{-a|\vec{x}|^2} = \frac{\pi}{a} e^{-\frac{|\vec{q}|^2}{2a}}, \tag{5.31}$$

where a is defined in (5.20).

Replacing the summation over $\vec{q}$ with an integration, we get

$$\int \frac{d^2|\vec{q}|}{(2\pi)^2} e^{-\frac{|\vec{q}|^2}{2a}} = \frac{a}{\pi}. \tag{5.32}$$

Collecting the results, we remain with the following integral:

$$\frac{1}{T_1 T} \sim (1 - \delta)^2 \int dx^0 i x^0 \frac{1}{x^{0\,2}} e^{-2im_s x^0 - \frac{T}{2\chi m_s^2} g(0) Q_0^2 x^{0\,2}}. \tag{5.33}$$

Up to the factor $(1 - \delta)^2$, the above integral is equal to (5.22) for the evaluation of the spinon conductivity. This result is a consequence of the gaussian expansion of the correlator and of the fact that the dominant contribution to the in-plane resistivity comes from the spinon sector.

In the high temperature limit we have

$$\frac{1}{T_1 T} \approx \frac{(1-\delta)^2}{g(0)\lambda^2} \frac{\chi m_s^2}{T}.$$ (5.34)

Also in this case, the predicted temperature dependence is in agreement with the experimental data.

5.7   Electron Green's Function: Quasiparticle Pole

The Green's function for the 2D electron is given in real space by the product of the holon (G^h) and the spinon (G^s) propagators, averaged over gauge fluctuations:

$$G^e(x,y) = \frac{\int DA_\mu G^h(x,y|-A)G^s(x,y|A)e^{iS_{eff}(A)}}{\int DA_\mu e^{iS_{eff}(A)}}.$$ (5.35)

We are interested here in the quasi-particle pole, in particular in the thermal and doping dependences of the wave function renormalization constant Z and the damping rate Γ as defined in (3.5).

Since the final result depend weakly on the details of the Fermi surface, we assume for simplicity a circular Fermi surface. The holon propagator follows immediately from the low energy action (5.10) under the tomographic decomposition described in Section 3.3.2. Within Gor'kov approximation we have (see also (3.44):

$$G_h(x^0, \vec{x}) = \langle \bar{\psi}_\alpha(x)\psi_\beta(0) \rangle \sim \frac{\Lambda(x_0)k_F}{\Lambda} \int d\theta \frac{e^{\frac{i}{2}x_\perp(\theta)^2 \Lambda(x_0)}}{\sqrt{i}} e^{ik_F x_\parallel(\theta)}$$

$$\left[\frac{1}{x_\parallel(\theta) - x^0 v_F}\Theta(x_0) + \frac{1}{x_\parallel(\theta) + x^0 v_F}\Theta(-x_0) \right] e^{i\int_0^x A_\mu dx^\mu}.$$ (5.36)

where $\Lambda(x_0) = \left(\frac{k_F}{v_F x^0}\right)^{\frac{1}{2}} \gg 1$ and $\vec{n}(\theta)$ labels the $\vec{k}$-state at the Fermi surface: $\vec{k} = k_F \vec{n}(\theta)$.

The spinon propagator $G_s(x, 0|A)$ is written as in (3.16):

$$G_s(x, 0|A) = e^{i\int_0^x A_\mu dx^\mu} G_s(x, 0|F).$$ (5.37)

The Gor'kov phase factors in (5.36) and (5.37) cancel against each other and the gauge invariant correlator $G_s(x, 0|F)$, averaged over gauge fluctuations, is given by the square root of (5.13).

We again consider the region $x^0 \gg |\vec{x}|$ and expand $G_s(x^0, |\vec{x}|)$ to quadratic order in $|\vec{x}|Q_0$. We find:

$$G_{el}(x^0 > 0, \vec{x}) \simeq -\frac{\Lambda(x_0)k_F}{\Lambda x^0 v_F} \int d\theta \frac{e^{\frac{i}{2}x_\perp(\theta)^2\Lambda(x_0)}}{\sqrt{i}} e^{ik_F x_\parallel(\theta)} \cdot \frac{b}{2} e^{-\frac{a}{2}|\vec{x}|^2}. \qquad (5.38)$$

where $a = a(x^0)$ and $b = b(x^0)$ are defined in (5.20) and (5.19) respectively.

We finally perform the Fourier transform of (5.38) to obtain the Retarded electron Green's function $G^R(\omega, \vec{q})$ for states near the Fermi surface.

Writing $\vec{x} = |\vec{x}|\vec{n}(\phi)$, the integration over ϕ, i.e. along the Fermi surface, is done via Lemma (3.45) and the $|\vec{x}|$ and x^0 integrations exactly as in Sections 5.5 and 5.6. We find

$$G^R(\omega, \vec{k} = k_F\vec{n}) = Z\frac{1}{(-m_s + i\frac{T}{4\chi m_s^2}g(0)Q_0^2 2x^0)}b(x^0)_{|x^0=\lambda Q_0^{-1}}, \qquad (5.39)$$

where the wave function renormalization constant Z is given by

$$Z \approx \lambda_1 \left(\frac{Q_0}{k_F}\right)^{\frac{1}{2}} \left(\frac{m_s\kappa}{J^2}\right)^{\frac{1}{2}} \qquad (5.40)$$

with λ_1 related to the tomographic momentum cut-off Λ by $\Lambda = \frac{k_F}{\lambda_1}$. We see that Z has the same thermal behaviour $Z \propto T^{1/6}$ as in the Pseudogap but the doping dependence is rather different since in the Strange Metal k_F, Q_0, κ all depend weakly on doping. We shall see below that the above estimate for Z is crucial to reproduce the correct linear-in-T behaviour for the c-axis resistivity.

From (5.39) we can read-off the electron damping rate Γ at the Fermi surface:

$$\Gamma = \frac{T}{2\chi m_s^2}Q_0 g(0)\lambda \propto T^{4/3}\frac{(1-\delta)^{5/3}}{\delta|\ln \delta|}. \qquad (5.41)$$

We see that Γ is inversely proportional to the doping concentration. This is acceptable in the Strange Metal where the magnetic frustration disappears: if more empty sites are added, the electrons can take profit to delocalize so the Gutzwiller projector becomes less effective and the scattering with the associated gauge field is weaker. We therefore expect that for very *high dopings*, our underlying assumption that the gauge field is the main source of scattering among excitations is no longer acceptable and a more conventional Fermi liquid picture should emerge.

Note that both electrons and holons have scattering rate proportional to $T^{4/3}$ but their respective doping dependences suggest $\Gamma \gg \Gamma_{hol}$ which again justifies the Gor'kov approximation for holons.

5.8 Out-of-plane Resistivity

Conductivity along the c-axis in cuprates occurs by interplanar tunneling processes. Since presumably there is no measurable Fermi velocity along this axis, we can use Kumar-Jayannavar approach described in sect. 3.1.2 to calculate $\rho_c(T)$. According to the authors, the out-of-plane motion in cuprates is incoherent and governed by the strong in-plane scattering via the quantum blocking effect. At high temperature $\Gamma \gg t_c$ the interlayer tunnelling rate is reduced by in-plane scattering just as thermal fluctuations limit tunneling by repeatedly "observing" a two level system. Under these assumptions, $\rho_c(T)$ is controlled by the second term in Kumar's formula:

$$\rho_c \sim \frac{1}{\nu}\left(\frac{1}{\Gamma} + \frac{\Gamma}{t_c^2 Z^2}\right). \tag{5.42}$$

We have already seen in the previous Chapter that the first term in (5.42) describes correctly the insulating behaviour of $\rho_c(T)$ in the Pseudogap, included the *rounded knee* observed in many underdoped samples.

Analogously, we expect that the metallic contribution in (5.42) yields a qualitatively correct estimate for $\rho_c(T)$ in the Strange Metal.

Substituting Γ and Z with the corresponding estimates (5.41) and (5.40) in (5.42), we recover the $T-$linearity in the "incoherent regime" $\Gamma \gg t_c Z$:

$$\rho_c \simeq \frac{J^2}{t_c^2} \frac{k_F}{m_s \nu(\epsilon_F)\kappa} \frac{T}{2\chi m_s^2} \frac{g(0)\lambda}{\lambda_1^2}. \tag{5.43}$$

Taking into account that $\nu(\epsilon_F) = \pi m_h$, $\chi = 1/6\pi m_h$ and $\kappa, k_F \propto (1 - \delta)$, the doping dependence in (5.43) comes entirely from m_s and therefore we find

$$\rho_c \simeq \frac{T}{(\delta|\ln\delta|)^{3/2}} \frac{J^2}{t_c^2}. \tag{5.44}$$

We see from (5.44) that the slope coefficient $\rho_c(T)/T$ decreases upon doping increase.

Unfortunately, we don't have a clean method to estimate the (extrapolated) $T = 0$ intercept of $\rho_c(T)$ which is large when compared to the corresponding $ab-$plane intercept, see Fig 5.3, so we cannot extract the anisotropy ratio $\rho_c(T)/\rho_{ab}(T)$.
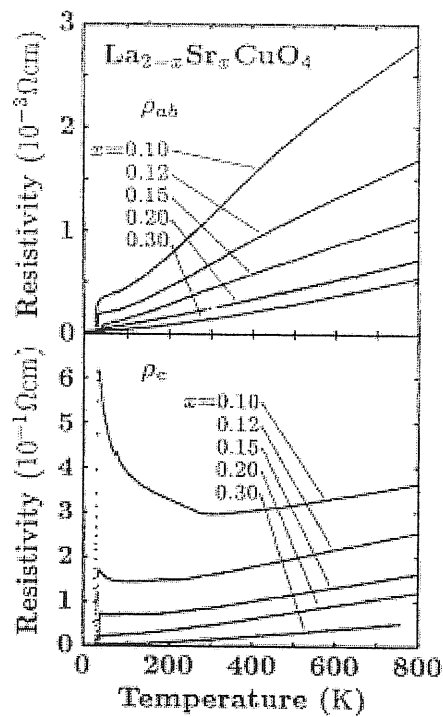
Figure 5.3: Temperature dependence of the in-plane (upper panel) and out-of-plane (lower panel) resistivity for LSCO single crystals with various compositions in the metallic phase. From [70]

Conclusions

We briefly review the main results achieved in this thesis. The spin-charge gauge theory was originally introduced to describe the Metal Insulator Crossover (MIC) in underdoped, non superconducting cuprates as temperature decreases. The MIC originates from the competition of a *spin* lengthscale, the antiferromagnetic correlation length $\xi \approx (\delta| \ln \delta|)^{-1/2}$, where δ is the doping concentration, and a *charge* lengthscale, the thermal De Broglie wavelength for the holes $\lambda_T \approx (T\delta/t)^{-1/2}$, where T is the temperature, t the hopping integral.

We believe that most of the experimental crossovers appearing in the temperature dependence of transport phenomena in the Pseudogap can be explained by the existence of these two factors.

Motivated by a very recent experiment [53], in this work we have generalized the gauge approach to frequency dependent phenomena and calculated the (Far Infrared) dynamical in-plane conductivity for strongly underdoped cuprates. We have shown that at low temperatures the Drude response disappears and a broad peak emerges at finite frequencies ($\omega \sim 100$ cm^{-1}) which is the analogue of the peak found in temperature dependent DC conductivity for the same sample. We expect that an analogous peak should appear also in underdoped superconducting cuprates once a strong magnetic field is used to suppress superconductivity.

The anisotropy in the MIC temperatures along the a and b plane directions found in both the DC [54] and AC [53] conductivities data, is almost certainly related to a corresponding anisotropy in the antiferromagnetic correlation lengths. Neutron scattering experiments[56] have indeed revealed that the magnetic correlation lengths are strongly anisotropic, with $\xi_a > \xi_b$.

We have shown that the $a - b$ anisotropy in the MIC temperatures is the key to understand the *large $a - b$* resistivity anisotropy found in both the experiments in the limit $T \to 0$ and $\omega \to 0$, respectively.

Another important result following from our calculations is that, near the Fermi level, holon and spinon bind together into a weak resonance with the quantum num-

bers of the physical electron. This binding is entirely provided by thermal gauge fluctuations and disappears as $T \rightarrow 0$. We have calculated the wave function renormalization constant and the scattering rate at the Fermi surface as a function of the relevant parameters T, δ. The spectral weigth varies along the Fermi surface and is strongly suppressed outside the Reduced Brillouin zone.

We have applied these results to calculate the temperature dependence for the out-of-plane resistivity, following the approach of Kumar et al.[39] The calculated ρ_c as well as the anisotropy ratio ρ_c/ρ_{ab} are in fairly good agreement with experiments[17, 18].

Finally, we have extended our analysis to describe optimally doped cuprates and underdoped samples at $T > T^*$, where T^* is the pseudogap crossover temperature (Strange Metal "phase"). Here we reproduced qualitatively the expected T−linearity of the in-plane and out-of-plane resistivities[10, 70] and of the inverse spin lattice relaxation $(T_1 T)^{63}$ at high temperatures as well as the tendency to evolve to a superlinear behaviour at lower temperatures for high doping levels, in agreement with experimental data.

Let us finally spend few words for future directions of work.

Since the spin-charge gauge approach relies on strong assumptions and it is higly non trivial, only the strict comparison with the huge amount of experimental information can ascertain the relevance of this method to the understanding of the puzzling phenomena in these strongly correlated systems.

Preliminary calculations are giving encouraging results, when compared with the experimental data, for the the Knight shift in both the "Pseudogap" and the "Strange Metal" phases.

An interesting open problem is to study the normal to superconducting phase transition in cuprate compounds within the *holon − spinon* scenario.

Appendix

We outline here the procedure followed to find the istantaneous optimal spinon configuration g_j^m for a given holon distribution. We recall that g_j^m is defined as the configuration at which $\Xi(g)$ reaches its maximum [see (2.23)].

The starting point is to write an equivalent path-integral first-quantized expression for Ξ:

$$\Xi(g) = e^{i \sum_j \int_0^\beta dx^0 A_j} \sum_{N=0}^{\infty} \frac{e^{\beta \mu N}}{N!} Z_N(g), \qquad (5.45)$$

where the canonical partition function $Z_N(g)$ of N holes is given by

$$Z_N(g) = \sum_{\pi \in P_N} (-1)^{\sigma(\pi)} \sum_{j_1 \ldots j_n} \prod_{r=1}^{N} \int_{\substack{\omega_r(0)=j_r \\ \omega_r(\beta)=j_{\pi(r)}}} d\mu(\omega_r)$$
$$\cdot \prod_{<ij> \in \underline{\omega}^\perp} t U_{<ij>} e^{-i \int_{\underline{\omega}^{\parallel}} dx^0 A} e^{-\sum_{<ij> \cap \underline{\omega} = \emptyset} \frac{J}{2} \int_0^\beta dx^0 (|U_{<ij>}|^2 - \frac{1}{2})}. \qquad (5.46)$$

Here P_N is the group of permutations of N elements, $\sigma(\pi)$ is the sign of the permutation π and $\underline{\omega} = \{\omega_1, ..., \omega_N\}$ denote the worldlines of holon particles, $\underline{\omega}^\perp$ the components of $\underline{\omega}$ perpendicular and $\underline{\omega}^{\parallel}$ parallel to the time axis, respectively.

The above expression is written as a complicated product of terms defined at all links $< i, j >$ and sites (through $\underline{\omega}^{\parallel}$) of the lattice. The optimal configuration g_j^m is then found by requiring that any single term in the product (5.46) gives the largest possible contribution. From now on we drop the m index.

To start with, we kill the on-site fluctuating phase in (5.46) by imposing

$$iA_j = (\sigma_x^{|j|} g_j^\dagger \partial_0 g_j \sigma_x^{|j|})_{11} = 0, \quad j \in \underline{\omega}^{\parallel}. \qquad (5.47)$$

Eq. (5.47) is satisfied choosing g_j constant during the period when no particle hops.

Imposing $U_{<ij>} = 0$ in S_2 (see (2.20)) corresponds in the first quantized formalism to setting:

$$(\sigma_x^{|i|} g_i^\dagger P e^{i \int_{<ij>} V^{(c)}} g_j \sigma_x^{|j|})_{11} = 0, \quad < ij > \cap \underline{\omega} = \emptyset. \qquad (5.48)$$

In physical terms this means that the $s + id$ RVB order parameter[71] is very small.

We notice that if

$$g_j = \cos \theta_j + i \sin \theta_j \sigma_z, \quad j \notin \underline{\omega} \tag{5.49}$$

for some angle $\theta_j \in [0, 2\pi)$, (5.48) is then satisfied. In fact, since $V^{(c)}$ depends only on sites where there are no holes (see (2.18)), from (5.49) it follows that correspondingly

$$V^{(c)}(x) = \sum_j (1 - H_j^* H_j) \frac{(-1)^{|j|}}{2} \partial_\mu \arg (x - j) \sigma_z, \tag{5.50}$$

so that $g_i^\dagger P e^{i \int_{<ij>} V^{(c)}} g_j$ has only diagonal components.

The condition $|\hat{U}_{<ij>}| = 1$ in S_1 (see (5.46)) corresponds to imposing:

$$|(\sigma_x^{|i|} g_i^\dagger P e^{i \int_{<ij>} V^{(c)}} g_j \sigma_x^{|j|})_{11}| = 1, \quad < ij > \in \underline{\omega}^\perp \tag{5.51}$$

which means in physical terms that the AM order parameter[72] is of order 1.

To discuss (5.51) we note that if $< ij > \in \underline{\omega}^\perp$, at a given time either site i is empty ($i \notin \underline{\omega}$) and site j is occupied ($j \in \underline{\omega}$) or viceversa. Suppose for instance $j \in \underline{\omega}$. Then we can write

$$g_i^\dagger P e^{i \int_{<ij>} V^{(c)}} = \cos \theta_{<ij>} + i \sin \theta_{<ij>} \sigma_z, \tag{5.52}$$

for some angle $\theta_{<ij>} \in [0, 2\pi)$.[3]

Representing g_j as

$$g_j = \cos \varphi_j + i \vec{\sigma} \cdot \vec{n}_j \sin \varphi_j, \tag{5.53}$$

we immediately find from (5.51) that

$$\varphi_j = \frac{\pi}{2}, \quad n_{jz} = 0. \tag{5.54}$$

So far the optimization process was independent of the density δ of holes. In particular we have found that the optimal spinon configuration must satisfy $A_j = 0$ and $|U_{<ij>}| = 1, 0$ in S_1 and S_2 respectively. There still remain undefined variables corresponding to the phase of $\hat{U}_{<ij>}$ whenever a hole hops along the link $< ij >$.

We recall that $arg(U_{<ij>})$ is not invariant under h/s symmetry, the gauge invariant variable being the magnetic flux $arg(U_{\partial p})$ penetrating a given plaquette p. Assuming traslational invariance, the optimal configuration g_j^m is a function of the mean magnetic flux per plaquette $< arg(U_{\partial p}) >$.

---

[3]This is because the l.h.s. of (5.52) is a diagonal SU(2) matrix.

Pseudogap

Numerical simulations at $T = 0$ and near half filling [73] have shown that the stable state is realized when

$$\arg\left(\hat{U}_{\partial p}\right) = \pi(1 - \delta), \quad \delta \ll 1 \tag{5.55}$$

We shall use (5.55) as ansatz for the Pseudogap phase.

Since the B-dependent part of $\arg\left(\hat{U}_{\partial p}\right)$ has a translation invariant mean satisfying condition (5.55), it is natural to impose (on average)

$$\left(\sigma_x^{|i|} g_i^\dagger e^{i \int_{<ij>} V^{(c)}} g_j \sigma_x^{|j|}\right)_{11} \simeq 1, \quad < ij > \in \underline{\omega}^\perp. \tag{5.56}$$

Defining

$$\bar{g}_j = e^{-\frac{i}{2} \sum_{\ell \neq j} (-1)^\ell \sigma_z \arg\,(\ell - j)}, \tag{5.57}$$

and choosing

$$g_j = \begin{cases} \bar{g}_j, & j \notin \underline{\omega} \\ \bar{g}_j \tilde{g}_j, & j \in \underline{\omega} \end{cases} \tag{5.58}$$

where $\tilde{g}_j$ is to be found, we can kill the fast fluctuating first term in (5.50). The remaining term, denoted by

$$\bar{V} = -\sum_j H_j^* H_j \frac{(-1)^{|j|}}{2} \partial_\mu \arg\,(x - j)\sigma_z, \tag{5.59}$$

depends only on the holes distribution and yields a contribution $O(\delta)$ to $\arg(U_{<ij>})$, with zero translational average. Finally, using (5.54), (5.57), (5.58) we find

$$g_i^\dagger e^{i \int_{<ij>} V^{(c)}} g_j = e^{i \int_{<ij>} \bar{V}} \tilde{g}_j \simeq \tilde{g}_j. \tag{5.60}$$

Since the left hand side of (5.60) has to satisfy (5.54), we write

$$\tilde{g}_j = e^{i \frac{\pi}{2} (\sigma_x n_{jx} + \sigma_y n_{jy})} \quad j \in \underline{\omega} \tag{5.61}$$

and we immediately derive from (5.60) the conditions $n_{jx} = 0, n_{jy} = (-1)^{|j|}$. The "optimal" spinon configuration defined in (5.58) is now completely fixed:

$$g_j^m = \bar{g}_j \tilde{g}_j = e^{-\frac{i}{2} \sum_{\ell \neq j} (-1)^\ell \sigma_z \arg(\ell - j)} e^{i \frac{\pi}{2} (-1)^{|j|} \sigma_y H_j^* H_j}. \tag{5.62}$$
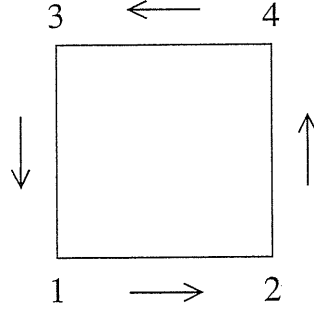
Figure 5.4: Circuitation of a plaquette.

Strange Metal

It is not difficult to see that the statistical field V^c defined in (2.18)does not carry magnetic flux per plaquette, so strictly speaking the constraint $\arg(\hat{U}_{\partial p}) = 0$ cannot be satisfied. However, it is sufficent for our pourposes that whenever a hole make a closed loop on the lattice, it acquires a trivial phase factor $(2\pi n)$.

We recall that, at the lattice level, the particle can either stay at rest at a given site or jump to a nearest neighbor.

Without loss of generality, we consider a holon going around a given plaquette p counterclockwise as shown in Fig. 5.4.

Now assume that the particle hops from site i to site j. Defining $\bar{g}_j$, $\tilde{g}_j$ and $\bar{V}$ as in (5.57)-(5.59), we see from (5.60) that

$$\left(\sigma_x^{|i|} g_i^\dagger e^{i \int_{<ij>} V^{(c)}} g_j \sigma_x^{|j|}\right)_{11} \simeq \left(\sigma_x^{|i|} \tilde{g}_i^\dagger \tilde{g}_j \sigma_x^{|j|}\right)_{11}. \tag{5.63}$$

The SU(2) variables $\tilde{g}_i$, $\tilde{g}_j$ are as in (5.49) and (5.54):

$$\tilde{g}_i = e^{i\theta_i \sigma_z}, \quad i \notin \underline{\omega} \tag{5.64}$$

$$\tilde{g}_j = i(\vec{\sigma} \cdot \vec{n}_j), \quad n_j = (\cos\phi_j, \sin\phi_j, 0), \quad j \in \underline{\omega} \tag{5.65}$$

with θ_j and ϕ_j so far arbitrary.

These degrees of freedom will be fixed in order to cancel the π−magnetic flux per plaquette generated by $\bar{B}$. We need to impose:

$$\prod_{<ij>\in\partial p} \left(\sigma_x^{|i|} \tilde{g}_i^\dagger \tilde{g}_j \sigma_x^{|j|}\right)_{11} = e^{i\pi}. \tag{5.66}$$

Writing out explicitely the left-hand side of (5.66), we find

$$e^{i(\theta_1+\phi_2)} e^{-i(\theta_2+\phi_4)} e^{i(\theta_4+\phi_3)} e^{-i(\theta_4+\phi_1)} \tag{5.67}$$

which is satisfied by the choice $\phi_j = \frac{\pi}{4}(-1)^{|j|}$ irrespective of the θ_j phases, provided the latter contribute with a trivial phase factor.

We can be even more demanding by requiring that the field $\bar{B}$ is exactly cancelled link by link. For instance, imposing

$$\theta_j = -\frac{\pi}{2}(-1)^{|j|},$$

we cancel the distribution of phase factors for $\bar{B}$ chosen in Sect. 2.8.

The optimal spinon configuration is then completely fixed.

Bibliography

[1] P.W. Anderson, Science **235**, 1196 (1987); P.W. Anderson "The Theory of Super-conductivity in the High-Tc Cuprates" Princeton University Press 1997.

[2] T. Timusk and B. Statt, Rep. Progr. Phys. **62**, 61 (1999); cond-mat/9905219.

[3] Y.J. Uemura et al., Phys. Rev. Lett. **62**, 2317 (1989); M. Randeria et al., **62**, 981 (1989); S. Doniach and M. Inui, Phys. Rev. B **41**, 6668 (1990).

[4] V. Emery and S. Kivelson, Nature (London) **374**, 434 (1995).

[5] G. Baskaran, Z. Zou, and P.W. Anderson, Solid State Commun. **63**, 973 (1987); G. Kotliar and J. Liu, Phys. Rev. B **38**, 5142 (1988); H. Fukuyama, Progr. Theor. Phys. Suppl. **108**, 287 (1992).

[6] G. Baskaran and P.W. Anderson, Phys. Rev. B **37**, 580 (1988).

[7] C. Castellani et al. Z. Phys. B **103**, 137 (1997).

[8] J. Zaanen cond-mat/0103255; S. Chakravarty et al., Phys. Rev. B **63**, 094503 (2001).

[9] T. Senthil and M.P.A. Fisher, Phys. Rev. B **62**, 7850 (2000); cond-mat/0008082.

[10] H. Takagi et al., Phys. Rev. Lett. **69**, 2975 (1992).

[11] A.T. Fiory et al., Phys. Rev. B **41**, 2627 (1990).

[12] B. Wuyts et al., Phys. Rev. B **53**, 9418 (1996); L. Trappeniers et al., J. Low Temp. Phys. **117**, 681 (1999).

[13] Y. Ando et al., Phys. Rev. Lett. **83**, 2813 (1999).

[14] S. Ono and Y. Ando, Cond-mat/0205305.

[15] Y. Ando et al., Phys. Rev. Lett. **75**, 4662 (1995); Y. Ando et al. J. Low Temp. Phys. **105**, 867 (1996).

[16] G.S. Boebinger et al., Phys. Rev. Lett. **77**, 5417 (1996).

[17] T. Kimura et al., Phys. Rev. B **53**, 8733 (1996); Y. Abe et al., Phys. Rev. B **59**, 14753 (1999).

[18] S. Komiya et al. Phys. Rev. B **65**, 214535 (2002).

[19] H. Alloul, Phys. Rev. Lett. **63** (1989)

[20] J.L. Tallon et al., cond-matt/9911157

[21] W.W. Warren,Jr. et al.,Phys. Rev. Lett. **62**, 1193 (1989);

[22] J.W. Loram et al., Phys. Rev. Lett. **71**, 1740 (1993)

[23] J.W. Loram et al. J. Phys. Chem. Solid **59**, 2091 (1998).

[24] D.S. Marshall et al., Phys. Rev. Lett. **76**, 4841 (1996)

[25] M.R. Norman et al., Nature (London) **392**, 157 (1998)

[26] For a simple introduction see the book *Quantum Field Theory in Condensed Matter Physics* (chapter 5), by N. Nagaosa, Springer (1999).

[27] J. Fröhlich and P.A. Marchetti, Phys. Rev. B **46**, 6535 (1992).

[28] P.A. Marchetti, Z.B. Su, L. Yu, Phys. Rev. B **58**, 5808 (1998).

[29] P.A. Marchetti, Z.B. Su, L. Yu, Nucl. Phys. B **482**, 731 (1996).

[30] A.O. Gogolin, A.A. Nersesyan and A.M. Tsvelik, *Bosonization and Strongly Correlated Systems*, Cambridge University Press, 1998.

[31] S. Sachdev, *Quantum Phase Transitions*, Cambridge University Press, 1999.

[32] E. Fradkin, *Field Theories of Condensed Matter Systems* (Addison–Wesley, New York, 1991).

[33] J. Fröhlich, Commun. Math. Phys. **47**, 233 (1976).

[34] R. T. Birgenau et al., Phys. Rev. B **38**, 6614 (1988).

[35] X.G. Wen and P.A. Lee, Phys. Rev. Lett. **76**, 503); P. A. Lee et al., Phys. Rev. B **57**, 6003 (1998).

[36] J. Fröhlich and U. Studer, Rev. Mod. Phys. **65**, 733 (1993); J. Fröhlich, R. Götschmann and P.A. Marchetti, J. Phys. A **28**, 1169 (1995).

[37] M. Reizer, Phys. Rev. B **39**, 1602 (1989); **40**, 11571 (1989).

[38] L. Ioffe and A. Larkin, Phys. Rev. B **39**, 8988 (1989).

[39] N. Kumar and A.M. Jayannavar, Phys. Rev. B **45**, 5001 (1992); N. Kumar et al., Mod. Phys. Lett. B **11**, 347 (1997);Phys. Rev. B **57**, 13399 (1998)

[40] H.M. Fried and Y. M. Gabellini, Phys. Rev. D **51**, 890 (1995).

[41] P.A. Lee and N. Nagaosa, Phys. Rev. Lett. **65**, 2450 (1990); Phys. Rev. B **46**, 5621(1992); L.B. Ioffe and P.B. Wiegmann, Phys. Rev. Lett. **65**, 653 (1990).

[42] A. Luther, Phys. Rev. B **19**, 320 (1979); F.D.M. Haldane, Varenna Lectures 1992.

[43] G. Benfatto, G. Gallavotti, J. Stat. Phys. **59**, 541 (1990); R. Shankar, Rev. Mod. Phys. **66**, 129 (1994).

[44] J. Fröhlich et al., in Proceedings of Les Houches 1994 "Fluctuating Geometries in Statistical Mechanics and Field Theory".

[45] J. Fröhlich, R. Götschmann and P.A. Marchetti, Commun. Math. Phys. **173**, 417 (1995).

[46] L. De Leo, Laurea Thesis , University of Padova 2000

[47] P.B. Littlewood in "Strongly interacting fermions and High T_c superconductivity", Proceedings of Les Houches 1991.

[48] P.A. Marchetti, J.H. Dai, Z.B. Su and L. Yu, J. Phys. Condens. Matt. **12**, L329 (2000).

[49] Z. Konstantinovic et al., Physica C **351**, 163 (2001).

[50] P.A. Marchetti, Z.B. Su and L. Yu, Phys. Rev. Lett. **86**, 3831 (2001).

[51] L. Ioffe and G. Kotliar, Phys. Rev. B **42**, 10348 (1990); L. Ioffe and P. Wiegmann, Phys. Rev. B **45**, 519 (1992).

[52] Y. Fukuzumi et al., Phys. Rev. Lett. **76**, 684 (1996); K. Segawa and Y. Ando, Phys. Rev. B **59**, P3948 (1999); Y. Hanaki et al., Phys. Rev. B **64**, 172514 (2001).

[53] M. Dumm, D. N. Basov, S. Komiya and Y. Ando, Phys. Rev. Lett. **91**, 077004 (2003).

[54] Y. Ando et al., Phys. Rev. Lett. **88**,137005 (2002)

[55] J. Zaanen and O. Gunnarson, Phys. Rev. B **40**, 7391 (1989); H.J. Schulz, J. Phys. (Paris) **50**,2833 (1989); D. Poilblanc and T..M. Rice, Phys. Rev. B **39**, 9749 (1989); M.Cato and K. Machida, J. Phys. Soc. Jpn **59**, 1047 (1990); S.A. Kivelson and V.J. Emery, in *Strongly Correlated Electronic Materials: The Los Alamos Symposium 1993*, (eds K. Bedell *et al.*)p. 619 (Addison-Wesley, Maine, 1994).

[56] M. Matsuda *et al.*, Phys. Rev. B **62**,9148 (2000).

[57] J. Zaanen, Science **286**, 251 (1999).

[58] V.J. Emery, S.A. Kivelson, and O. Zachar, Phys. Rev. B **56**, 6120 (1997); S.A. Kivelson, E. Fradkin, and V. Emery, Nature (London) **393**, 550 (1998).

[59] P.A. Marchetti, L. De Leo, G.Orso, Z.B. Su, L. Yu, cond-mat/0304408, *submitted to* Phys. Rev. B.

[60] P.A. Marchetti, G. Orso, Z.B. Su and L. Yu, *submitted to* Phys. Rev. Lett.

[61] D.N. Basov, private communication.

[62] S. Wakimoto *et al.* Phys. Rev. B **60**, R769 (1999); *ibid*, Phys. Rev. B **61**, 3699 (2000).

[63] K. Yamada *et al.*, Phys. Rev. B **57**, 6165 (1998).

[64] A.N. Lavrov, Y. Ando, S. Komiya, and I. Tsukada, Phys. Rev. Lett. **87**, 017007 (2001).

[65] C. Berthier et al., Physica C **235-240**, 67 (1994).

[66] A. Lacerda et al., Phys. Rev. B **49**, 9097 (1994).

[67] M. Imada, A. Fujimori and Y. Tokura, Rev. Mod. Phys. **70**, 1039 (1998).

[68] T.Ito et al., Nature (London) **350** (1991) 596; Y.F. Yan et al., Phys. Rev. B **52**, R751 (1995).

[69] A. Damascelli, Z. Hussain, and Z.X. Shen, Rev. Mod. Phys. **75**, 473 (2003)

[70] Y. Nakamura and S. Uchida, Phys. Rev. B **47**, 8369 (1993)

[71] G. Kotliar, Phys. Rev. B **37**, 3664 (1988).

[72] J. Affleck and J.B. Marston, Phys. Rev. B **37**, 3774 (1988).

[73] J. Bellissard and R. Rammal, Europhys. Lett. **13**, 205 (1990).

Acknowledgements